ORNL
DATE ISSUED: AUG 6 1969

ORNL-4429
UC-25 – Metals, Ceramics, and Materials

STATUS AND PROGRESS REPORT FOR THORIUM FUEL CYCLE DEVELOPMENT FOR 1967 AND 1968

Compiled by
R. G. Wymer and A. L. Lotts

OAK RIDGE NATIONAL LABORATORY
operated by
UNION CARBIDE CORPORATION
for the
U.S. ATOMIC ENERGY COMMISSION

Printed in the United States of America. Available from Clearinghouse for Federal Scientific and Technical Information, National Bureau of Standards, U.S. Department of Commerce, Springfield, Virginia 22151
Price: Printed Copy $3.00; Microfiche $0.65

LEGAL NOTICE

This report was prepared as an account of Government sponsored work. Neither the United States, nor the Commission, nor any person acting on behalf of the Commission:

A. Makes any warranty or representation, expressed or implied, with respect to the accuracy, completeness, or usefulness of the information contained in this report, or that the use of any information, apparatus, method, or process disclosed in this report may not infringe privately owned rights; or

B. Assumes any liabilities with respect to the use of, or for damages resulting from the use of any information, apparatus, method, or process disclosed in this report.

As used in the above, "person acting on behalf of the Commission" includes any employee or contractor of the Commission, or employee of such contractor, to the extent that such employee or contractor of the Commission, or employee of such contractor prepares, disseminates, or provides access to, any information pursuant to his employment or contract with the Commission, or his employment with such contractor.

ORNL-4429

Contract No. W-7405-eng-26

CHEMICAL TECHNOLOGY DIVISION

METALS AND CERAMICS DIVISION

STATUS AND PROGRESS REPORT FOR THORIUM FUEL CYCLE DEVELOPMENT FOR 1967 AND 1968

Compiled by
R. G. Wymer and A. L. Lotts

Edited by
Sigfred Peterson

AUGUST 1969

OAK RIDGE NATIONAL LABORATORY
Oak Ridge, Tennessee
operated by
UNION CARBIDE CORPORATION
for the
U.S. ATOMIC ENERGY COMMISSION

CONTENTS

Page

1. Process Demonstration and ^{233}U Distribution 1
   Storage and Distribution Facility. 1
   Distribution Activities Summary. 1
   Fuel Preparation for High-Temperature Lattice Test Reactor 3
      Solex Development Laboratory. 3
      Sphere Forming. 6
      Particle Coating. 7
2. Thorium-Uranium Recycle Facility. 11
   TURF Building Construction and Procurement 11
   Design of Sol-Gel Microsphere Equipment. 15
   Design of Fueled-Graphite Refabrication Equipment. 18
3. Sol-Gel Process Development 22
   Sol Preparation by Amine Solvent Extraction. 22
      Equipment 23
      Preparation of ThO_2-UO_3 Sol 25
      Preparation of UO_2 Sol. 27
   Preparation of Urania Sols by Precipitation-Peptization. . . 30
      Continuous Equipment for Preparation of Precipitation UO_2 Sols. 31
      Batch Preparation of Precipitation UO_2 Sols 33
   Microsphere Preparation Process Development. 36
      Feeding and Dispersion of Sol 36
      Fluidization. 40
      Mass Transfer During Gelation 42
      Control of Alcohol Compositions 45
      Preparation of Small (< 100-μ-diam) Spheres 53
      Optimization of Process Equipment 57
   Chemistry of Microsphere Forming Column. 59
   Sol-Gel Process and Equipment Demonstration. 62
   Material Preparation 68

4. Fueled-Graphite Fabrication Development 70
Particle Handling. 70
Particle Coating 71
The 5-in.-ID Coater 72
Coating Process Development 75
Remote Coater 79
Particle Inspection. 79
Measurement of Coating Anisotropy 79
Measurement of Coating Density. 80
Particle Counting and Size Analysis 80
Bonding of Coated Fuel Particles in Fuel Elements. 83
Blending. 84
Bonding 84
Preparation of Fuel Sticks. 85
Resin Curing. 86
Effects of Bonding Matrix on Coatings 86
Characterization of the Carbonization Process 88
Evaluation of Fuel Sticks and Bonding Matrices. 91
Fuel Stick Fabrication. 92
5. Irradiation of Coated-Particle Fuels. 95
Comparison of Test Results with Model Predictions. 96
Comparison of Sol Gel with Sintered Spheroids. 100
Summary of Irradiation Tests on Sol-Gel-Derived Fuels as Coated Particles. 106
6. Bulk Oxide Process Development. 109
Low-Energy Microsphere Packing (Sphere-Pac). 109
Pelletizing of Sol-Gel Oxides. 115
7. Characterization of Oxide Fuels 121
Thermal Conductivity 121
Sintered Specimens. 121
Sphere-Pac Bed Microspheres 123
ThO_2, 93.7% Dense, Measured to 1400°K 126
Thermal Analysis with ThO_2. 129
LiF Thermal Conductivity. 129
Mechanical Properties of Sol-Gel-Derived Fuel Bodies 132

8. Irradiation of Bulk Oxide Fuels 137

Effect of Intermediate Heat Rating at High Burnup Levels. 140

Effects of Extended Burnup 143

Performance of Sphere-Pac ThO_2–5% PuO_2 Fuel Rods 148

9. Advanced Studies. 152

Conversion of Oxide-Carbon Gels to Carbides and to Porous Oxides 152

Preparation and Properties of Oxide-Carbon Sols 153

Conversion of Oxide-Carbon Gels to Carbides and Carbonitrides 155

Conversion of Oxide Gels to Porous Oxides 159

Kinetics of the Graphite-UO_2 Reaction. 160

Drying and Sintering Studies on Urania Gel Microspheres. . . 160

1. PROCESS DEMONSTRATION AND ^{233}U DISTRIBUTION

R. E. Brooksbank

Storage and Distribution Facility

J. R. Parrott R. G. Shannon
R. G. Nicol W. A. Shannon

Oak Ridge National Laboratory serves as a national distribution center for ^{233}U. The facility includes shielded wells for storing up to 120 kg of ^{233}U in solid form and tanks (containing borosilicate glass for neutron poisoning) that can store 500 kg of ^{233}U in uranyl nitrate solutions at ^{233}U concentrations up to 250 g/liter. In addition, during the reporting period an existing building was converted to a shielded vault and approved for the storage of 70 kg of ^{233}U or ^{239}Pu in shipping containers.

The facility accepts ^{233}U as uranyl nitrate solution or as properly packaged solids. The solids can be uranium metal or uranium compounds that can be dissolved easily and safely in stainless steel equipment.

The purification facilities in the center include a single-cycle solvent extraction system capable of purifying ^{233}U at the rate of 25 kg/week. All ^{233}U processed in the facility is shipped as nitrate solution.

Distribution Activities Summary

J. R. Parrott R. G. Shannon
R. G. Nicol W. A. Shannon

During the past two years 42 shipments containing 171 kg of ^{233}U were received by the facility. There were 45 shipments from the facility, amounting to 112 kg of ^{233}U. The largest single receipt was 71 kg of ^{233}U (as nitrate solution) from criticality experiments in the ORNL Neutron Physics Division. The largest disbursement was 36 kg of ^{233}U (as UO_2) to the Thorium-Uranium Fuel Cycle Development Facility for conversion to the LiF_4-UF_4 eutectic salt, which is being used in the

Molten Salt Reactor Experiment. The activity of the facility for each year from 1960 through 1968 is shown in Fig. 1.1. The present inventory of ^{233}U in the facility, showing the form, isotopic purity, and ^{232}U content, is shown in Table 1.1.

The TRUST (Thorium Reactor Uranium Storage Tank) facility was built to receive, transfer, and store 1100 kg of highly enriched uranium (75% ^{235}U, 11% ^{233}U) in the form of a uranyl nitrate solution.[1] This material, which is the uranium product from the Indian Point Reactor fuel,

[1]Chem. Technol. Div. Ann. Progr. Rept. May 31, 1968, ORNL-4272, pp. 138–141.

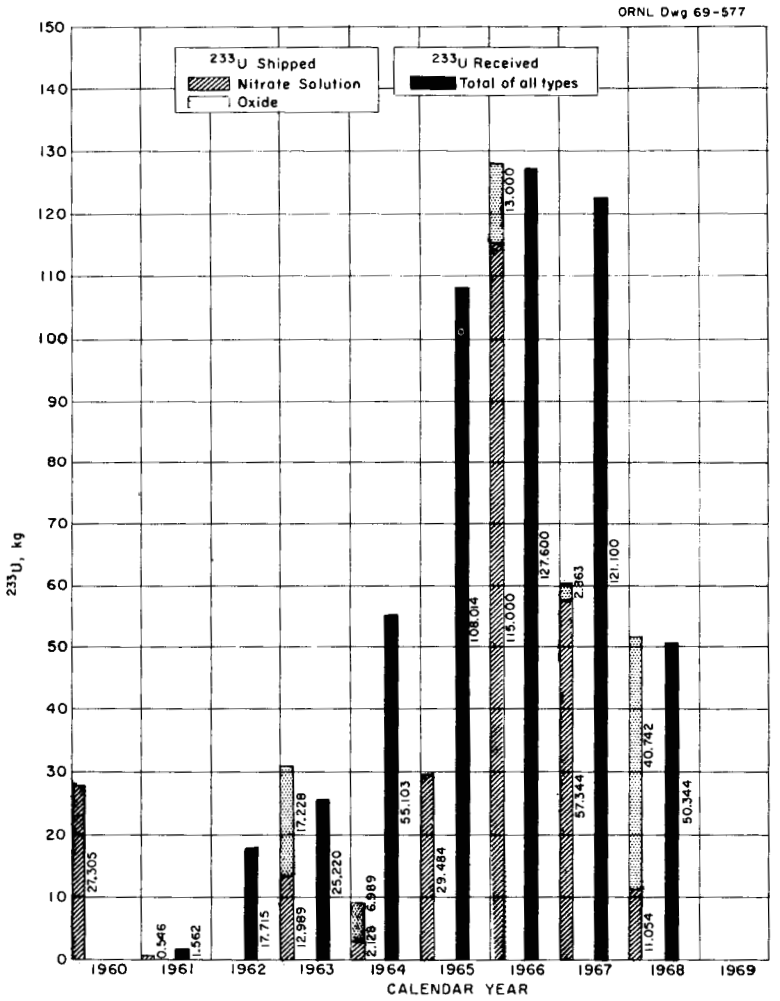

Fig. 1.1. Receipts and Shipments of ^{233}U at Bldg. 3019 Dispensing Facility.

Table 1.1. ^{233}U Inventory – December 31, 1968

Form	Isotopic Purity (at. %)	^{233}U Content (ppm)	Quantity (kg)
Nitrate	91	13	24.1
	97	5–9	67.0
	97	34	14.7
Oxide	84	6	7.6
	91	250	61.7
	97	5–6	28.4
	97	50	13.6
	98	5	12.1
Fluoride	91	250	1.9
Metal	97	42	5.6
Slag	97	6	0.7
Total			237.4

was purified by solvent extraction at the Nuclear Fuels Services plant in West Valley, New York. The uranium solution will be stored indefinitely; the ^{232}U content (120 ppm) prohibits direct refabrication into fuel elements, and the low ^{233}U content makes it uninteresting for reactors demonstrating the thorium fuel cycle. Seven shipments of uranyl nitrate solution (in 152 "safe" 10-liter plastic bottles) were received in December 1968. These shipments contained 305.7 kg of uranium, including 34.4 kg of ^{233}U and 226.5 kg of ^{235}U.

Fuel Preparation for High-Temperature Lattice Test Reactor

Solex Development Laboratory (J. W. Snider, F. L. Daley)

We are preparing about 32 kg of $(Th,^{233}U)O_2$ microspheres for use in reactor physics tests as part of a national effort in support of high-temperature gas-cooled reactors (HTGR's). The microspheres are being coated with pyrolytically deposited carbon and will be used as fuel in the High-Temperature Lattice Test Reactor (HTLTR).

The Solex Development Laboratory (in Building 3019) is being used to prepare $^{232}ThO_2$–25% $^{233}UO_2$ as a concentrated hydrosol. The process consists of solvent extraction of nitric acid from aqueous solutions of thorium nitrate and uranyl nitrate with a solution of a long-chain secondary amine in a hydrocarbon. The aqueous solutions hydrolyze to form colloidal dispersions (sols). The process equipment consists of three contactors and two digesters for hydrosol formation and three contactors for amine (organic phase) regeneration. The nitrate solution feed stream, which is approximately 0.3 M in total metal, is processed through the following sequence when the cocurrent flowsheet is used (differences between the cocurrent and countercurrent flowsheets will be described).

1. The aqueous and organic phases are contacted cocurrently in the first contactor. About 85% of the nitrate in the aqueous stream is extracted into the organic phase.

2. Following phase separation, the aqueous phase is digested for 30 min in the first digester.

3. Aqueous and organic phases are then contacted cocurrently in the second contactor. The organic phase used in this extraction step may or may not be the same as that used in the first step. About 75% of the nitrate entering this contactor is extracted into the organic phase.

4. After phase separation the aqueous phase is digested for 30 min in the second digester.

5. The aqueous and organic phases are contacted cocurrently in the third contactor. About 10% (50% for the countercurrent flowsheet) of the nitrate entering this contactor is extracted into the organic phase.

6. The hydrosol from the third contactor is evaporated to approximately 2 M total heavy metal (1 M for countercurrent operation).

In the cocurrent flowsheet 70% of the organic phase is fed to the first contactor; the remaining 30% is fed into the second contactor along with the effluent organic from the first contactor. This mixed organic phase is also used in the third contactor before being sent to

the amine regeneration portion of the process. The total amount of amine in the organic phase is 75% excess over that required for stoichiometric extraction of nitrate in the feed stream.

In the countercurrent flowsheet all of the organic phase is fed to the third contactor, then to the first contactor, and finally to the second contactor. The total amount of amine in the organic phase is 45% excess over that required for stoichiometric extraction of the nitrate in the feed stream.

The spent organic phase is contacted with water in an amine regeneration contactor to remove any entrained aqueous phase (this water is returned to become a part of the feed stream) before being contacted with a 1 M Na_2CO_3 and 1 M NaOH mixture for neutralization of the amine. Following neutralization, the organic phase is contacted with water again; this removes any entrained neutralization solution from the organic phase before its reuse in the extraction cycle.

Before process use, the organic phase was pretreated by cycling three batches (50 liters per batch) through seven complete cycles, using nitric acid and water as feed. This removed trace quantities of low-molecular-weight material from the organic phase. A brownish-black crud formed at the interface in the first contactor during the first few cycles and disappeared as the cycles progressed. With the disappearance of the crud, there was an improvement in phase separation and a diminished propensity to foam. A sample of the seventh-cycle organic phase was compared with the organic phase that had been used in earlier studies. The organic-aqueous break times with water, carbonate solution, and nitric acid were almost identical for the two samples. Two of the 50-liter batches of organic were stored for later use, and one was left in the process equipment for use in the ^{233}U-thorium hydrosol production.

We prepared 33 batches of hydrosol (~ 1 kg of metal per batch). The first eight were made according to the cocurrent flowsheet. The nitrate-to-metal mole ratio in these runs was between 0.14 and 0.15. The hydrosol from these runs was concentrated to 2 M; however, difficulty was encountered in preparing microspheres from this (high-nitrate) product. The remaining 25 batches were made according to the countercurrent flowsheet. The nitrate-to-metal mole ratio in these runs was

0.10 ± 0.01, the electrical conductivity was 2.20 ± 0.02 milliohms/cm, and the pH was 5.52 ± 0.53.

Equipment has operated very well. The only difficulty has been with pumps; the seal on the original pump used with the evaporator failed, but a replacement pump is performing satisfactorily. Two metering pumps have been replaced; one replacement was necessitated by a pump failure, and the second was required to reach the design flow rate.

Sphere Forming (J. R. Parrott, R. G. Shannon)

The remotely operated, neutron-shielded facility in cell 4, Building 3019 was used to form 250–350-μ-diam spheres from the hydrosol ThO_2–25% $^{233}UO_2$ prepared in the Solex Development Laboratory. The cell 4 facility was originally constructed to demonstrate the ^{238}Pu microsphere preparation flowsheet;[2] to provide flexibility it included two parallel sphere-forming columns, two dryers, and one calcining furnace for preparing microspheres from hydrosols prepared elsewhere.

After completing the plutonium program, we started to convert thoria-urania hydrosol into microspheres that were suitable for coating with pyrolytic carbon. Initial operation of the system was unsuccessful because of (1) insufficient upflow velocity to maintain the spheres in the column for sufficient drying time, and (2) cracking of the spheres in the column when formed from sols having a nitrate-to-metal mole ratio greater than 0.12. Characterization of the spheres formed in the column was further complicated by temperature excursions in the dryer, which resulted from insufficient removal of residual organic during steam stripping.

We then made six runs using ^{238}U (instead of ^{233}U) to establish operating conditions. The column throat diameter was decreased from 1 3/4 to 1 1/2 in. by remotely removing the top of the column and dropping in a machined stainless steel insert. The sphere dryer was

---

[2] Chem. Technol. Div. Ann. Progr. Rept. May 31, 1968, ORNL-4772, pp. 168–170.

redesigned to give better distribution of steam through the bed; this change eliminated the previously mentioned temperature excursions. With these improvements and with the availability of sols with lower nitrate-to-metal ratios, the system began to produce microspheres meeting the specifications. Following operation with ThO_2–25% $^{238}UO_2$, we returned to ThO_2–25% $^{233}UO_2$ and began operating on a 16-hr day, 5-day week basis. Spheres were formed at the rate of 0.5 kg/day of metal (U + Th). Drying and calcining are batch operations, with batch sizes of 0.5 and 2 kg of metal, respectively.

Spheres are formed in a tapered glass column. The 1 M (U + Th) sol is introduced into the two-fluid nozzle at 3 cm^3/min. A 2-ethyl-1-hexanol (2EH) stream is introduced into the periphery of the nozzle at 169 cm^3/min. The spheres, formed at the nozzle tip, are suspended in 2EH by a total upflow of 6800 cm^3/min. The water content is controlled by a side stream (470 cm^3/min) of 2EH to a still, which is operated at 160°C.

The wet spheres are transferred onto a glass frit in 500-g batches and dried by heating to 105°C in argon and then feeding in superheated steam. During steam purging, the temperature is slowly increased to 200°C and held until 5 g of steam has been purged through the spheres for each gram of oxide present.

The spheres are calcined in 2-kg (U + Th) batches by heating in argon (at 250°C/hr) to 1150°C and purging with Ar–4% H_2 for 4 hr and then cooled in argon. The calcined microspheres are then transferred to the Coated Particle Development Laboratory (CPDL) for testing and coating.

During the report period, approximately 18.8 kg of oxide was successfully processed through the facility. Preliminary screening (to remove spheres outside the 200- to 500-μ-diam range) reduced the quantity transferred to 17 kg.

Particle Coating (F. J. Furman, Jr., R. A. Bowman)

The oxide microspheres are coated with pyrolytic carbon to limit the spread of contamination and thereby facilitate reactor operation and subsequent handling of the fuel. The coating must withstand moderate mechanical shock, as would occur during pouring, and also withstand the thermal stress that would be developed on heating to 1300°C, the upper

limit expected in the HTLTR experiments. A 5-in.-diam cone furnace, described in Chapter 4 of this report, was selected to perform this coating operation because of our extensive operating experience with it.

Propylene was selected as the coating gas because of the consistent results that are obtained at the comparatively low pyrolytic carbon deposition temperature of 1250°C. Typical coating properties that can be obtained with propylene are shown in Chapter 4 of this report.

The major activities associated with coating the microspheres are material transfer, precoating treatment, coating, postcoating treatment, and inspection. Material transfer involves the procedures and equipment required to safely transfer the large amounts of ^{233}U-containing material. These operations will not be described here but are mentioned to emphasize the effort involved in transferring fissionable materials safely and keeping records for accountability.

The precoating treatment consists of breakage testing, screening, separating the nonspherical microspheres, sampling, and weighing. The coating operation includes loading the particles into the coating furnace, coating, and unloading. The postcoating treatment consists of initial weighing, screening, alpha monitoring, sampling, and weighing. Inspection includes size and density determinations on both the uncoated microspheres and the coatings. The coated microspheres are analyzed for uranium and thorium contents.

In the precoating operation the microspheres are first tested for breakage resistance. They are loaded into a particle singularizer,[3] which accelerates them in single file at a high velocity at a glass wall. Any weak microspheres crack and can be separated later. Next the particles are screened to obtain the desired coating size ranges. Most particles fall in a 250- to 350-μ-diam range. Also saved are 350- to 420-μ-diam particles, which are grouped into another coating range. After sizing, the particles are shape separated,[3] to remove nonspherical

---

[3]R. B. Pratt and S. E. Bolt, "Particle Coating," Status and Progress Report for Thorium Fuel Cycle Development Dec. 31, 1966, ORNL-4275, pp. 61–87.

particles by vibration and gravity. Next the particles are sampled, weighed, and placed in 1000-g batches for coating.

The particles are coated in a 5-in.-diam cone furnace. The cone, surrounded by an argon blanket, is heated to 1250°C. The batches are pneumatically injected into the top of the cone and levitated by argon passing through the apex of the cone. Once the temperature is stabilized, the argon flow is stopped, and propylene is injected. The propylene is cracked, carbon is deposited on the particles, and the by-product hydrogen and soot are exhausted. After approximately 100 μ of coating is deposited (this takes approximately 60 min) the propylene is replaced by argon and the coated particles are unloaded through the bottom of the furnace. A photomicrograph of some typical coated ^{233}U-thorium oxide microspheres is shown in Fig. 1.2.

Postcoating treatment begins with initial weighing to ensure that all particles have been unloaded from the furnace. Then the particles

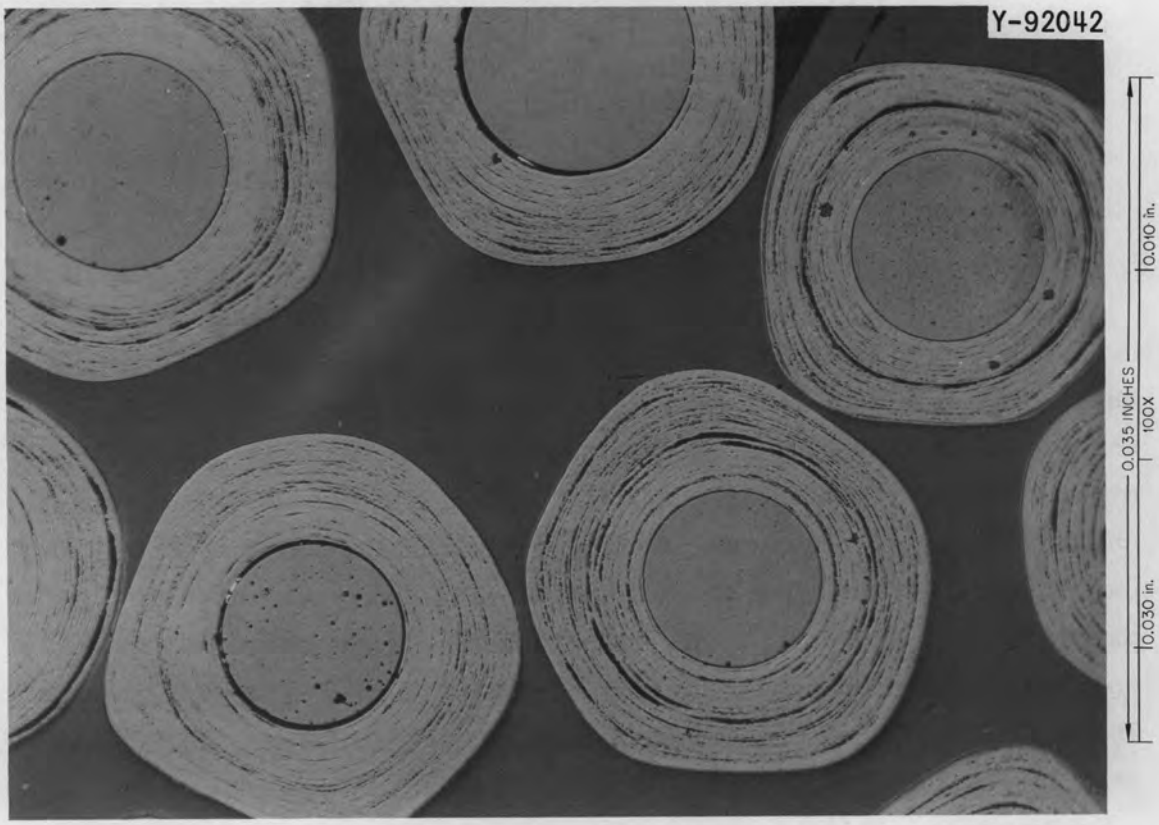

Fig. 1.2. Typical Pyrolytic-Carbon-Coated $(Th,^{233}U)O_2$ Microspheres.

are screened to eliminate large carbon chunks and undercoated particles. Next the microspheres are checked for alpha radiation by passing them across a monolayer feed plate (see Fig. 1.3) over which an alpha monitor is suspended. This feed plate distributes the particles in a 6-in.-wide highly dense single layer. Finally the particles are sampled and weighed.

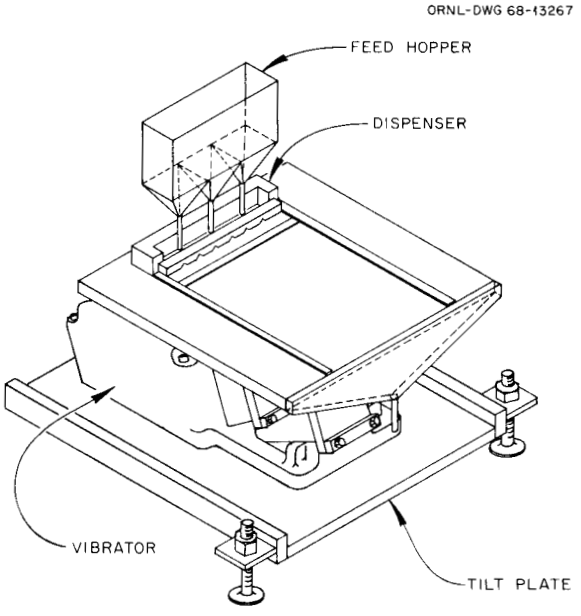

Fig. 1.3. Monolayer Feed Plate.

Inspection includes analyzing for density, size distribution, and chemical composition. The density is determined on both the coated and uncoated particles by the mercury pycnometer method. Carbon is determined by burning the coating off the oxide particles and measuring the change in weight. From the percent carbon and the coated particle and oxide particle densities the coating density can be calculated. The oxide particle and coated particle diameters are measured individually on radiographs of a number of particles with a split-image microscope. The particles are also analyzed for uranium and thorium. An isotopic analysis is done on the uranium.

This preparation program will be completed in the spring of 1969, and a detailed report will then be prepared.

2. THORIUM-URANIUM RECYCLE FACILITY

TURF Building Construction and Procurement

J. W. Anderson
J. M. Chandler
S. Mann
S. E. Bolt
J. P. Jarvis
D. M. Shepherd

A portion of the Thorium-Uranium Recycle Facility, shown in Fig. 2.1, was completed by Blount Brothers Construction Company of Montgomery, Alabama, on September 15, 1967, and accepted by the Laboratory for occupancy. This permitted acceptance of the facility before total completion to expedite the installation of processing equipment in cell G for the MSRE ^{233}U fuel preparation experiment. The remainder of the facility was completed and accepted for occupancy on October 2, 1967.

During the last several months of construction an intensive effort was made to test performance of the major utility service systems and the operational equipment in the facility. To realize the maximum effectiveness from this testing program, we prepared detailed test procedures to be used by the contractor in testing the following plant systems: water, steam and condensate, compressed air, electrical power distribution, waste, gas, fire protection, heating, ventilating and air conditioning,

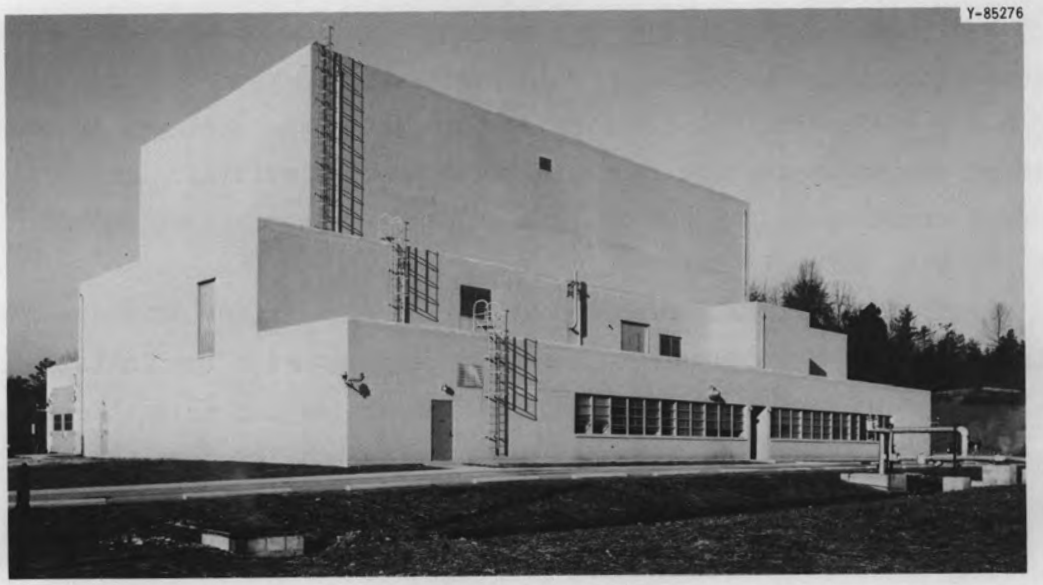

Fig. 2.1. The Thorium-Uranium Recycle Facility.

and electromechanical systems. These test procedures were accepted by the contractor and performed by him. The tests were witnessed jointly by the architect-engineer and ORNL personnel.

Immediately upon our occupancy, Rust Engineering Company began installing the out-of-cell processing equipment for cell G, in-cell crane and manipulator systems, various service plugs in service sleeves throughout the cell bank, viewing windows at cell operating modules, and the equipment mounting pad on the floor in cells C and D (shown in Fig. 2.2). This portion of the construction program, authorized as cost-plus-fixed-fee participation, was completed on January 15, 1968, at approximately 15% less than the estimated cost. Painting was completed on March 9, 1968.

The installation of special equipment in the facility by the Laboratory began November 1, 1967, and was completed on March 15, 1968. This work consisted primarily of installation of master-slave manipulators, special sampling equipment for the liquid waste tanks, a pneumatic-tube solid sample conveyor system for cells C, D, and E, and the facility radiation and contamination monitoring and control equipment. Also, we cleaned and filled the zinc bromide window tanks in cells G and F. The filling of the remainder of the window tanks has been deferred until facility operations require shielded viewing windows in other cells. The Laboratory's participation in the construction project has included the procurement and installation of special-purpose equipment costing $1,753,000. This participation was concluded on March 15, 1968, within the estimated time and cost. Sol-gel sphere-forming equipment and the remaining zinc bromide shielding media have been deferred until the end of 1969. The fuel fabrication equipment has not yet been authorized.

Problems previously reported with the screw drives of radiation shielding doors 2 and 3 were apparently resolved with the installation in December 1967 of ball screw and nut assemblies replacing the modified square thread mechanical screw jacks. The assemblies were tested in January 1968 and found satisfactory.

The cleaning of the copper lining inside the viewing window tanks has been the object of some limited experimentation for the past three

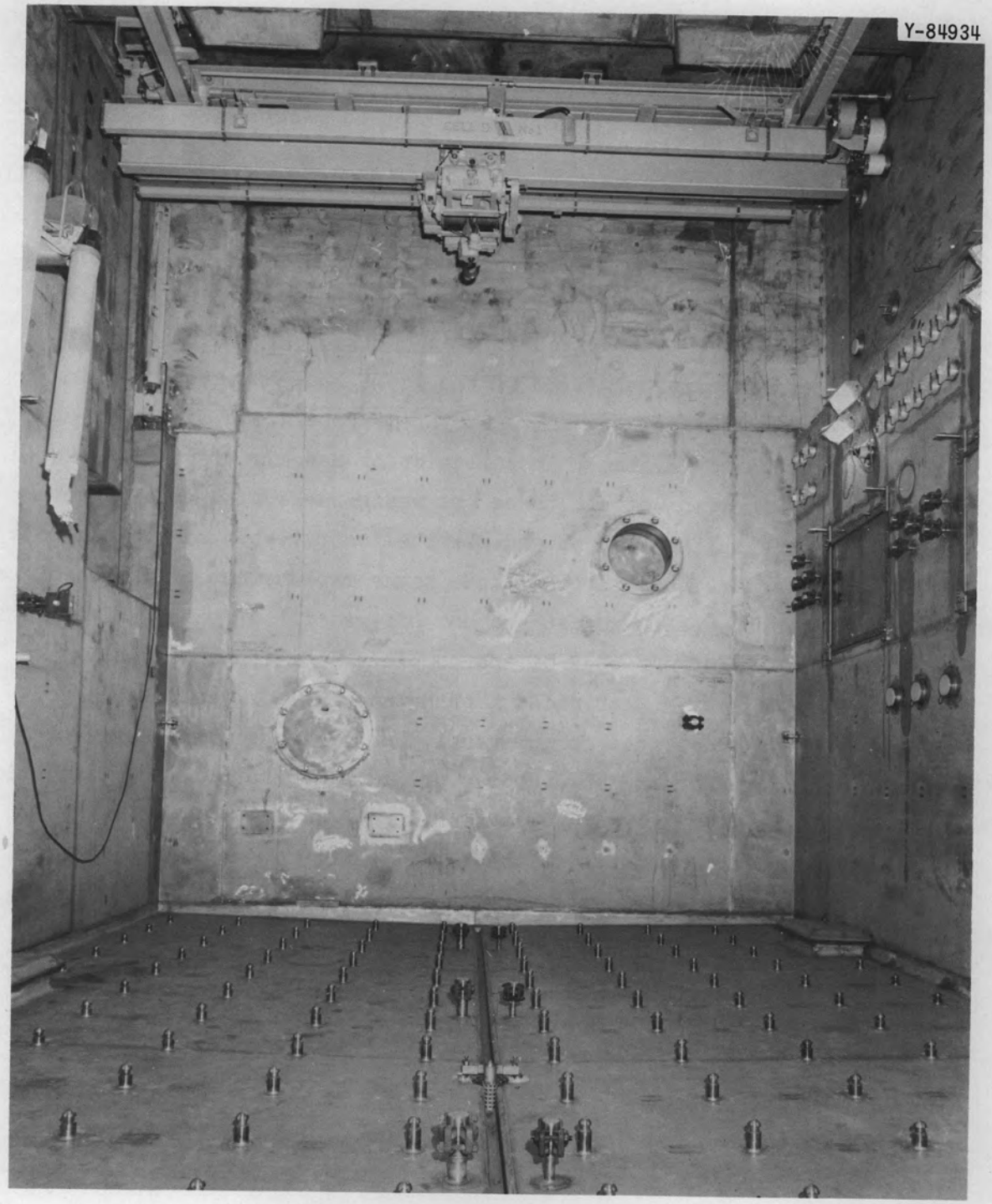

Fig. 2.2. Cell D, Showing Equipment-Mounting Pad Installed.

years. We developed a cleaning procedure with the following major steps: (1) degreasing with alcohol; (2) washing with a solution of acetic acid, sodium chloride, and demineralized water; (3) rinsing and drying with alcohol; (4) washing with a solution of 10% zinc bromide and demineralized water; (5) finally rinsing with demineralized water inhibited with hydroxylamine. This procedure appeared to result in a satisfactorily clean window tank, ready for filling with zinc bromide.

Concurrent with the construction operations by Rust Engineering Company and the Laboratory, the TURF operating staff prepared and executed procedures whereby the facility was checked out and placed into normal operating condition. Some of the items were operator training and rechecking of the utility service systems, operation of the in-cell crane and manipulator systems, installation of Raschig rings in a liquid waste tank, calibration of all three hot waste tanks with checkout of the waste tank sampling station and all the instrumentation and controls for operating and maintaining the waste tanks, replacement of the absolute filters in both the cell exhaust and hot off-gas filter pits, and testing of the filter pit and checkout of the complete facility ventilating and air conditioning system with dioctyl phthalate. Plans were also developed and placed into effect for preventive maintenance on all operating equipment and for coordinating various programs for testing and inspection of equipment essential to safe operation.

A number of improvements to the facility were made. These include landscaping of the site, identification of equipment and service lines within the facility, installation of an argon supply system for maintaining a purge and blanket on shielded viewing windows, installation of neutron threshold detector instruments on both the first and third floor levels of the facility, and the installation of an additional constant alpha air monitor.

An emergency manual for the facility was prepared, and assembly of data for the facility operating manual was completed. Manuals were prepared for all the facility utility service systems.

The in-cell fire protection system was charged with carbon dioxide liquid and preliminary tests of the system were conducted. These tests

indicated problem areas remained in this system. The master carbon dioxide flow control valve is being redesigned, and minor piping changes are being made in the pilot valve piping at each cell selector valve station. Also, piping changes are being made in the carbon dioxide storage tank charging system. The system is scheduled to be made operational early in 1969.

The safety analysis was prepared for the facility during the latter part of 1967, and the facility received preoperational review by the AEC on January 21, 1968. These efforts resulted in approval of the facility to carry out the MSRE ^{233}U fuel preparation experiment[1] and a December 27, 1968, approval of operation of the facility for the broad spectrum of research activities for which it was designed and constructed.

The TURF is being maintained in operational readiness for recycle development work.

Design of Sol-Gel Microsphere Equipment

P. A. Haas C. C. Haws

Microsphere forming equipment typically consists of a nozzle to make spherical droplets of a closely controlled, predetermined size, a long column containing flowing alcohol to fluidize the droplets until they gel, and alcohol regeneration equipment. Earlier reports[2] have dealt with many aspects of this equipment. This report emphasizes column geometry. The correct column configuration will improve microsphere droplet fluidization and reduce microsphere sticking and clustering. While the fluidization flow rates and the alcohol compositions are probably more important variables, a good column configuration should

---

[1]J. M. Chandler and S. E. Bolt, Preparation of Enriching Salt ^{7}LiF-$^{233}UF_4$ for Refueling the Molten Salt Reactor, ORNL-4371 (March 1969).

[2]A. R. Irvine, J. M. Chandler, F. L. Hannon, and J. W. Snider, Status and Progress Report for Thorium Fuel Cycle Development Dec. 31, 1966, ORNL-4275, pp. 8-10.

also be used. This is simple to achieve since it does not require control of operating variables and involves few compromises of conflicting requirements.

A tapered column is required to produce a superficial velocity that decreases up the column and thus causes a separation of particles according to settling velocity. The settling velocity of the gel sphere is about 1.4 times that of the sol droplet fed to the column. For a given product sphere diameter, the settling velocity of a droplet of sol less concentrated than 2 M varies little with molarity. The effects of decreasing diameter and increasing density on the settling velocity as water is extracted from the sol approximately cancel.

For a given microsphere forming capacity, the column size can be minimized by having a tapered section of sufficient volume to hold particles more concentrated than 4.0 M, topped by a cylindrical section to hold the sol drops of lower concentration. When such a column is lightly loaded, the fluidized bed will all be in the taper. As the sol feed rate is increased, the bed will build up into the cylindrical section without an excessive loading at any level. If the taper is continued without any cylindrical section, the loading increases as the superficial fluidizing velocity decreases. Then as the sol feed rate is increased, the top of the bed will be higher and more heavily loaded until excessive sticking or clustering occurs.

The column taper can be specified by two ratios. One is the ratio of radii at the top and bottom of the taper (r_{max}/r_{min}). The other is the degree of taper, dr/dL, where r is radius and L is length.

A radius ratio of 2.0 or slightly higher gives good loadings of the cylindrical section. Lower ratios give lighter loadings in the cylindrical section and give excessive streaming of particles out of the cylindrical section unless the drop size and fluidization are very uniform. This ratio gives an area ratio of 4 (or a superficial velocity ratio of 1/4), which is much higher than the maximum ratio, 1.4, of gel sphere to sol drop settling velocities. The higher ratio gives a lower bed density at the bottom of the bed and restricts the discharge rate while allowing a higher bed density in the upper part of the column and

thus a greater column capacity. As mentioned earlier, if the column is loaded to give a fluidized bed over an excessive range of superficial velocities, the top of the bed will be overloaded with sol drops, and they are more likely to coalesce or stick. Beds of droplets and spheres where $(r_{top}/r_{bottom}) > 2.5$ are used only when the drop size distribution, the fluidization, the loading, or some combination of these is poor.

We have obtained satisfactory operation with dr/dL from 1/96 to 1/24, or wall-to-center line angles of 0.6 to 2.5°. The only disadvantage of decreasing amounts of taper appears to be inconvenient lengths of column. As the amount of taper is increased, more droplets stick to the wall and the tendency increases for higher loadings to accumulate at the wall, with channeling at the wall caused by the higher bed density. Therefore, we prefer to use $dr/dL \leq 0.03$ (1.8°), but there are no clear-cut limits. Tapers of $dr/dL = 1/24$ (2.5°) have been used in glove boxes with severe headroom limitations.

Geometrically similar columns with the general configurations suggested can be characterized by a single dimension. We use the minimum column inside diameter; namely, the diameter at the bottom of the fluidized bed. Then a standard column might have:

D_B as the minimum diameter,
$2D_B$ as the diameter at the top of the taper,
$15D_B$ as the length of taper,
$10D_B$ as a reasonable length of the cylindrical section of diameter $2D_B$.

Then the volume of the taper is approximately $27D_B^3$ and the volume of the cylinder is $31D_B^3$. The total volume would be $58D_B^3$. This is 950, 3200, 7600, and 25,000 cm^3 for 1-, 1 1/2-, 2-, and 3-in. columns, respectively.

Average bed loadings of 10 to 20 vol % seem reasonable. Lower loadings must be used for small spheres to reduce clustering and sticking, and the higher loadings are possible for large, uniform drops. Most of the volume loading is from gelling drops; the gel spheres have volumes 1/6 to 1/16 of the sol droplet volumes. From these criteria, the estimated capacities for several sol molarities and drop sizes can be

calculated (Table 2.1). About half the bed volume is in the cylindrical section, so columns without this feature would have correspondingly smaller capacities.

The column capacities increase with the cube of the diameter. The capacities in sol volume per unit time vary little with sol molarity or drop size; the more rapid gelation of smaller drops is offset by the smaller bed loadings recommended for the smaller spheres. The capacities in weight of product per unit time increase more than in proportion to the sol molarity; the more concentrated sols gel more rapidly. Columns of 2- and probably 3-in. minimum diameter could be made critically safe by boron-loaded baffles in the wider top sections. The allowable column sizes for low-enrichment fuels would depend on the compositions.

The capacities listed in Table 2.1 can be bracketed by upper and lower limits about half and double those listed. The 1 1/2- and 2-in. columns were operated for long periods at about half the Table 2.1 capacities without any visible signs of overloading. Higher capacities have been demonstrated only for short periods. The top and bottom of the bed show lower loadings than the middle. Capacities double those of Table 2.1 would require the most heavily loaded parts of the bed to approach volume loadings that correspond to fixed-bed loadings without fluidizing. Operating problems are almost certain at such high loadings. Thus the capacities listed are unlikely to be in error by factors of two.

Design of Fueled-Graphite Refabrication Equipment

J. D. Sease

We plan to design, construct, and install in the TURF a pilot-scale remote fueled-graphite refabrication line to demonstrate the refabrication technology needed for the development of high-temperature gas-cooled reactors. The original plan for the fueled-graphite line called for operation in 1970; however, delay in the overall HTGR program plan has postponed cold operation of the refabrication plant to January 1974 and hot operation to early 1975. Therefore, very little design effort has been expended since the middle of 1967. Design activity will increase in mid-1969.

Table 2.1. Estimated Microsphere Forming Column Capacities for Three Product Diameters and Two Starting Sol Molarities[a]

Product diameter, μ	200	200	400	400	500	500
Sol molarity	1.0	2.4	1.0	2.4	1.0	2.4
Sol drop diameter, μ	675	500	1350	1000	1700	1250
Gelation time, min	19	10	38	19	48	23
Bed loading, vol %	10	10	20	20	20	20
Holdup volume/sol feed rate, min						
during gelation	10	6	20	11	25	13
as gel spheres	4	5	7	10	10	12
Volume ratio capacities or sol feed rate/bed volume, hr^{-1}	0.43	0.55	0.44	0.57	0.34	0.48
g gel cm^{-3} hr^{-1}	0.11	0.35	0.12	0.36	0.09	0.30
Column capacity, cm^3 sol/hr						
1-in. column	410	520	420	540	320	460
1.5-in. column	1400	1800	1400	1800	1100	1500
2-in. column	3300	4200	3300	4300	2600	3600
3-in. column	11,000	14,000	11,000	14,000	8500	12,000
Column capacity, g gel/hr						
1-in. column	100	330	110	340	90	280
1.5-in. column	350	1100	380	1100	290	1000
2-in. column	850	2700	900	2700	700	2300
3-in. column	2700	9000	3000	9000	2300	7500

[a]Basis: arithmetic average volume for gelation time, θ_G. Additional average holdup equivalent to $3\theta_G$ as gel spheres; 10 vol % loading for 200-μ product and 20 vol % for 400- or 500-μ product.

For the design of the fabrication line, the reference fuel element is the Public Service of Colorado Company, Fort St. Vrain Reactor (PSC) fuel element, which consists of a 14-in. hexagonal graphite block 31 in. long. A cross section of the reference fuel element is shown in Fig. 2.3. The fuel holes are filled with fuel sticks composed of pyrolytic-carbon-coated microspheres of thorium and uranium oxide or carbide in a carbonaceous matrix. The design production rate for the coated particle portion of the line has been established at 10 kg/day of ^{233}U-bearing particles. In fuel stick fabrication, the design will permit handling and fabricating any combination of ^{235}U, ^{233}U, and Th, as either the oxide or carbide, that may be selected for the optimum fuel cycle. The production capacity of the present design in a 24-hr day, with a 70% plant factor, is two PSC elements. The limiting step is fuel stick fabrication.

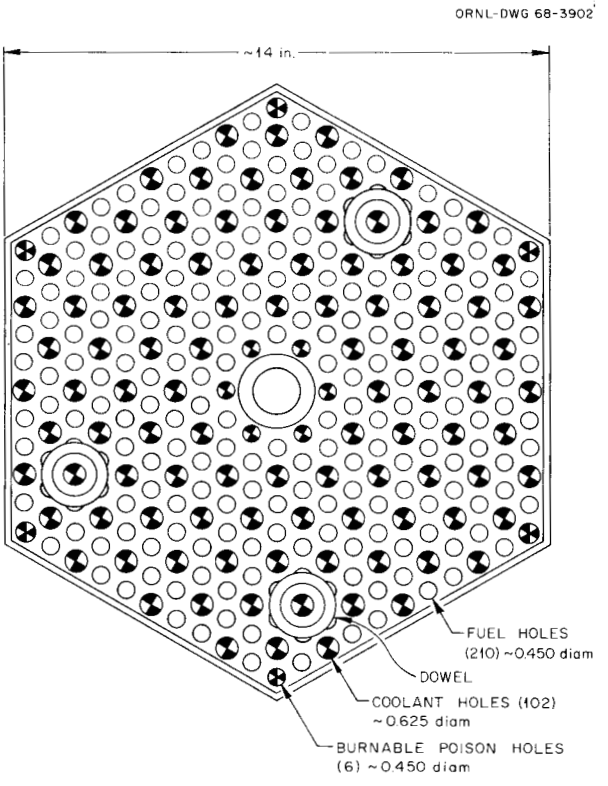

Fig. 2.3. Cross Section of PSC Fuel Element. Dimensions are in inches.

The process flowsheet[3] has remained essentially unchanged. The essential steps consist of coating the fuel microspheres with carbon by cracking a hydrocarbon gas at high temperature, blending the various types of particles into desired ratios, cementing these together into a fuel stick with resin and carbon, and finally loading the stick into the graphite block and sealing the blocks.

For the fueled-graphite line a flowsheet has been established, a critical path schedule has been developed, and a conceptual design of all of the process equipment has been made. The major contributions during the report period were the completion of the conceptual design of the process equipment and an analysis of the data collection and control requirements of the refabrication line. A computer-based system for data collection and process control was indicated from this analysis. The work completed represents less than 10% of the design requirement of the line. A detailed description of the development work in support of the TURF fueled-graphite fabrication line is contained in Chapter 4.

---

[3] J. D. Sease, "Fueled-Graphite Refabrication Equipment," Status and Progress Report for Thorium Fuel Cycle Development Dec. 31, 1966, ORNL-4275, pp. 11–14.

3. SOL-GEL PROCESS DEVELOPMENT

W. D. Bond P. A. Haas J. P. McBride

The sol-gel process development studies have been concerned primarily with the preparation of thoria, urania, and plutonia (and their binary mixtures), although many other oxide sols were also prepared in laboratory studies. A primary current objective is to develop procedures and equipment useful for remotely operated fuel preparation in the Thorium-Uranium Recycle Facility (TURF). Results are presented for our studies of three operations common to our sol-gel processes: (1) preparation of an aqueous sol, (2) removal of water to give gel particles, and (3) firing at controlled conditions to remove volatiles, to sinter to a high density, and to effect any necessary reduction or chemical conversion.

Sol Preparation by Amine Solvent Extraction

B. C. Finney A. D. Ryon

A new method for preparing ThO_2-UO_3 and UO_2 sols was developed,[1,2] in which an aqueous nitrate solution is denitrated by extracting nitric acid with a long-chain aliphatic amine. The nitrate-deficient solution is digested to produce the sol, releasing additional nitrate, which is removed in a subsequent amine extraction. The amine nitrate is regenerated for recycle by contact with 1 M Na_2CO_3. Two advantages this method has over the old sol-forming method of dispersing solids in dilute nitric acid are (1) it avoids remote handling of solids, and (2) it is amenable to continuous operation.

On the basis of batch laboratory data, we designed and built an engineering test unit for the continuous production of sols at rates that are full scale for TURF (1 kg/hr of ThO_2-UO_3 or 0.33 kg/hr of UO_2). The

---

[1]J. G. Moore, A Sol-Gel Process for Preparing ThO_2-UO_3 Sols from Nitrate Solutions by Solvent Extraction with Amines, ORNL-4095 (October 1967).

[2]J. P. McBride, Laboratory Studies of Sol-Gel Processes at the Oak Ridge National Laboratory, ORNL-TM-1980 (September 1967), pp. 32–36.

purposes of the engineering tests are: (1) to demonstrate the feasibility of making both ThO_2-UO_3 and UO_2 sols continuously, (2) to measure the effects of operating parameters, (3) to provide information for designing remote equipment, and (4) to supply sols for use in development of subsequent steps in the sol-gel process.

Equipment

Mixer-settlers were the contacting devices selected for the engineering studies. Use of glass pipe permitted observation of the process streams. The geometries of all components are criticality-safe. Only a few piping changes adapt the same equipment to make either a mixed ThO_2-UO_3 sol or a pure UO_2 sol.[3,4] All components are vented to a common header so that an inert atmosphere can be maintained over the UO_2 sol.

Details of the mixer-settler show in Fig. 3.1. The mixer, which is made of 3-in.-diam glass pipe, is divided into six compartments, each of which has a mixing impeller; the impellers are mounted on a common shaft. The aqueous and organic phases enter at the top and flow cocurrently through the six compartments to give the effect of mixing vessels in series; this arrangement ensures good stage efficiency. The mixer is designed so that the aqueous phase is dispersed into the organic phase to minimize emulsification. At shutdown, the aqueous phase is drained from the mixer; thus, at subsequent startup only the organic phase is present. In this manner the aqueous stream is easily dispersed as it enters the mixer.

Phase separation occurs in the section below the mixer. The position of the interface is controlled by adjustable weirs on both the aqueous and organic overflow lines. The nominal volume of the mixing section is 2.0 liters, while that of the settler is 2.8 liters of organic phase and 1.5 liters of aqueous phase.

---

[3]J. W. Snider, The Design of Engineering-Scale Solex Equipment, ORNL-4256 (April 1969).

[4]Drawings of the mixer-settler equipment are available under the number CAPE-1692 from Clearinghouse for Federal Scientific and Technical Information, National Bureau of Standards, U.S. Department of Commerce, Springfield, Virginia 22151.

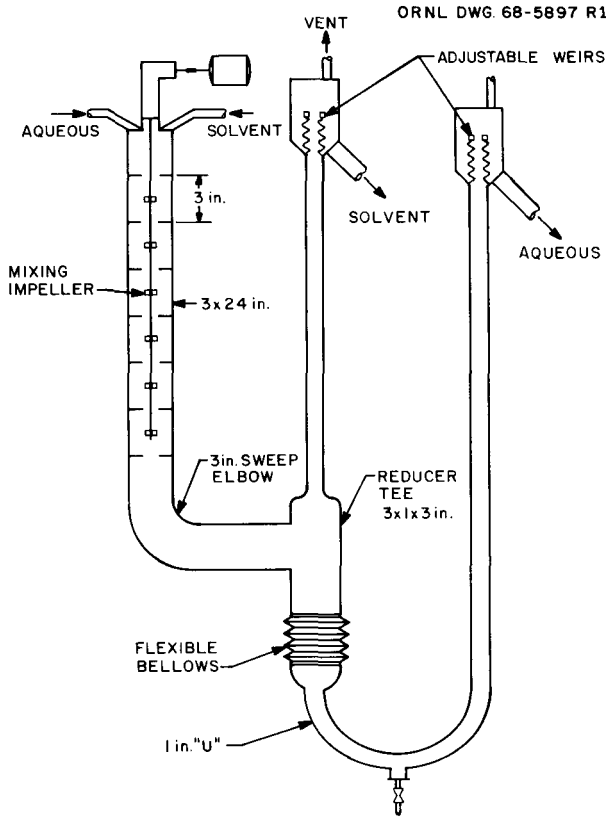

Fig. 3.1. Mixer-Settler Stage.

The digester forms a part of the aqueous-phase jackleg of the first nitrate extraction stage. It is a 2-ft length of 3-in.-diam glass pipe with an internal heating coil made of 3/8-in.-diam stainless steel tubing. Heat is supplied by pressurized hot water circulating through the coil. The sol flows upward to minimize longitudinal mixing. A reflux condenser is connected to the top of the digester. An aftercooler ahead of the aqueous-phase overflow weir cools the sol to about 60°C before it enters the second stage. Effective volume of the digester is 2.8 liters.

Although an evaporator is not shown on the general flowsheet, such a device is usually necessary to concentrate the sol to about 1 M before microspheres are formed. A canned-rotor pump circulates the sol from a flash chamber through the heater to a cyclone vapor-liquid separator. The feed enters through the packed stripping section, where any entrained solvent is removed. The concentrate flows out through a simple jackleg, which maintains a constant liquid level in the body of the evaporator.

The density, which is measured by a gas bubbler system, controls the feed rate. The evaporation rate is set by manual control of the steam pressure on the heater. The single-pass heater has three tubes, each of which is 0.5 in. in diameter × 30 ft long. The sol is circulated at about 15 gpm to obtain a high liquid velocity and hence a low temperature differential in the heater. Back pressure from the cyclone separator prevents boiling in the tubes. These features minimize local drying of the sol. The evaporator can also operate under vacuum to allow evaporation of UO_2 sols at low temperature and prevent oxidation of the uranium.

Preparation of ThO_2-UO_3 Sol

The flowsheet used in most of our tests is Fig. 3.2. The aqueous feed is a nitrate solution containing about 0.3 mole of metal (Th + U) per liter; the thorium-to-uranium atom ratio is 3. The organic solvent is 0.75 M Amberlite LA-2 (a secondary amine[5]) in a normal paraffin[6] having

[5]Product of Rohm and Haas Company, Philadelphia.

[6]Product of South Hampton Company, Houston.

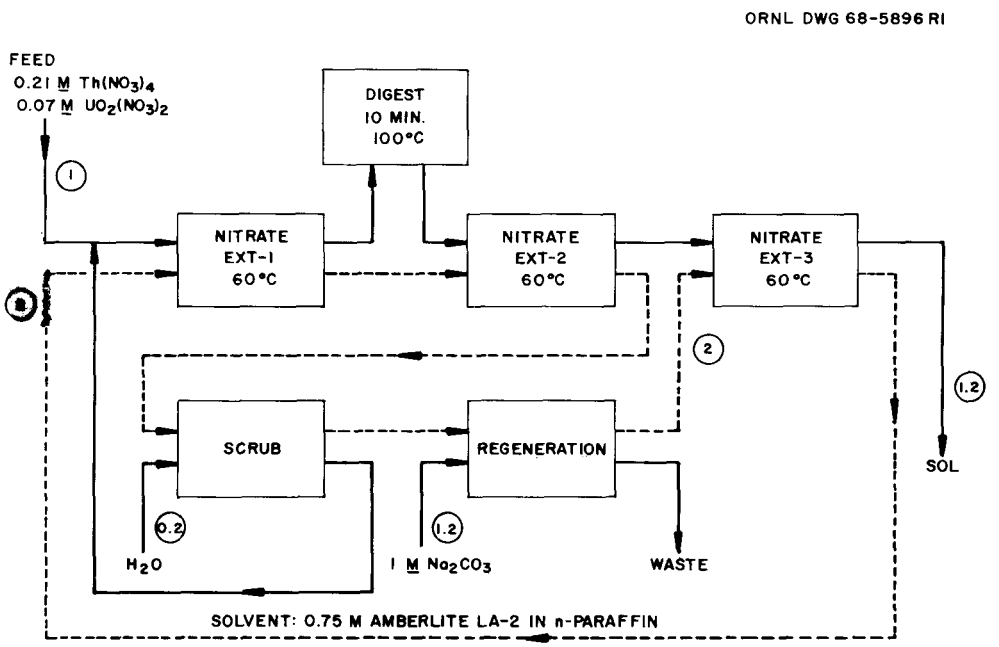

Fig. 3.2. Flowsheet for Preparation of ThO_2-UO_3 Sol by Amine Extraction.

an average of 12 carbon atoms per molecule. Aqueous feed and partially spent amine from stage 3 flow cocurrently through the first extraction stage. The feed is contacted with about 30% excess amine (over the stoichiometric amount required for complete denitration); about 80% of the nitrate is extracted. The concentration of Th + U must be less than 0.5 M to prevent precipitation in this stage. Maintaining about 60°C improves phase separation. The aqueous phase is then digested at least 8 min at gentle reflux. As the sol forms, the color changes from yellow to red-orange.

The additional nitrate released during digestion is extracted in two stages. Amine leaving the first stage is used as the extractant in the second stage so that the small amount of uranium that is extracted in the first stage can be stripped back into the aqueous phase in stage 2, where the low nitrate concentration favors distribution of uranium into the aqueous phase. Extracting with freshly regenerated amine in the third stage facilitates the final removal of nitrate from the sol. The nitrate-laden solvent is scrubbed with water to remove entrained sol and is then regenerated with 1 M Na_2CO_3.

Seven runs, each with 150 liters of feed, have been completed. The equipment operated smoothly, interface control was satisfactory, and only a small amount of emulsion was formed. Good-quality sols were produced at rates up to 1 kg/hr of oxide in all of the runs. Representative samples have been evaporated to greater than 1.0 M and formed into microspheres. All of the sols from runs 3, 4, and 5 were evaporated to about 1.5 M in the full-scale continuous evaporator and formed into spheres in the CPDL column, which is the prototype for TURF.

The first two runs were made with only two extraction stages and an intervening step in which the aqueous phase was digested. (The solvent was regenerated with 1 M Na_2CO_3 without prior scrubbing.) Although the nitrate-to-metal mole ratio in the sol was in the range predicted by the laboratory batch data, the equilibrium ratio obtained by shake-out of the solvent and aqueous phases from the second stage was lower than the laboratory ratio. Because the lower ratio was more desirable, particularly for avoiding cracking during calcination of the microspheres, the sol from run 2 was processed through two additional stages of extraction

(run 3). This demonstrated that more nitrate could be extracted by additional stages. Subsequent runs were made, using the flowsheet shown in Fig. 3.2, in which three extraction stages were used. Detailed results and analyses have been published.[7]

The efficiencies of the mixer-settlers were calculated by comparing the change in nitrate concentration in the aqueous stream across one stage with that obtained by equilibration of the phases at a volume ratio equal to the flow ratio. The efficiency exceeded 90% as the agitator speed increased from 300 to 500 rpm. The few data points at 600 rpm show greater than 95% efficiency. Increasing the flow rate to 150% of design had no effect on the efficiency. The effect of temperature over the range of 45 to 70°C was relatively small.

Preparation of UO_2 Sol

The preparation of UO_2 sols by solvent extraction has been successfully scaled up and operated continuously in engineering experiments. We have made 40 runs, each producing about 2 kg of UO_2 as a dilute (about 0.2 M) sol. Laboratory studies to characterize the sol and aid in the engineering studies are still in progress. We have studied three operating parameters that affect sol properties: nitrate-to-uranium mole ratio during digestion, digestion temperature, and method for preparing the initial U(IV) solution.

The basic method for preparing UO_2 sol by solvent extraction (see the reference flowsheet in Fig. 3.3) was developed from laboratory batch studies. Nitrate is extracted from aqueous U(IV) nitrate-formate with a long-chain amine (e.g., Amberlite LA-2) dissolved in a paraffin. Digestion of the resulting nitrate-deficient solution produces the UO_2 sol. Final nitrate adjustment is obtained in subsequent extractions. The amine is regenerated with sodium carbonate and recycled.

Most recent runs have used U(IV) feed that had been prepared in a slurry reductor, in which finely divided PtO_2 catalyst is suspended in a well-mixed uranium nitrate solution sparged with hydrogen. Since the

---

[7]M. E. Whatley et al., Unit Operations Section Quarterly Progress Report July–September, 1967, ORNL-4234.

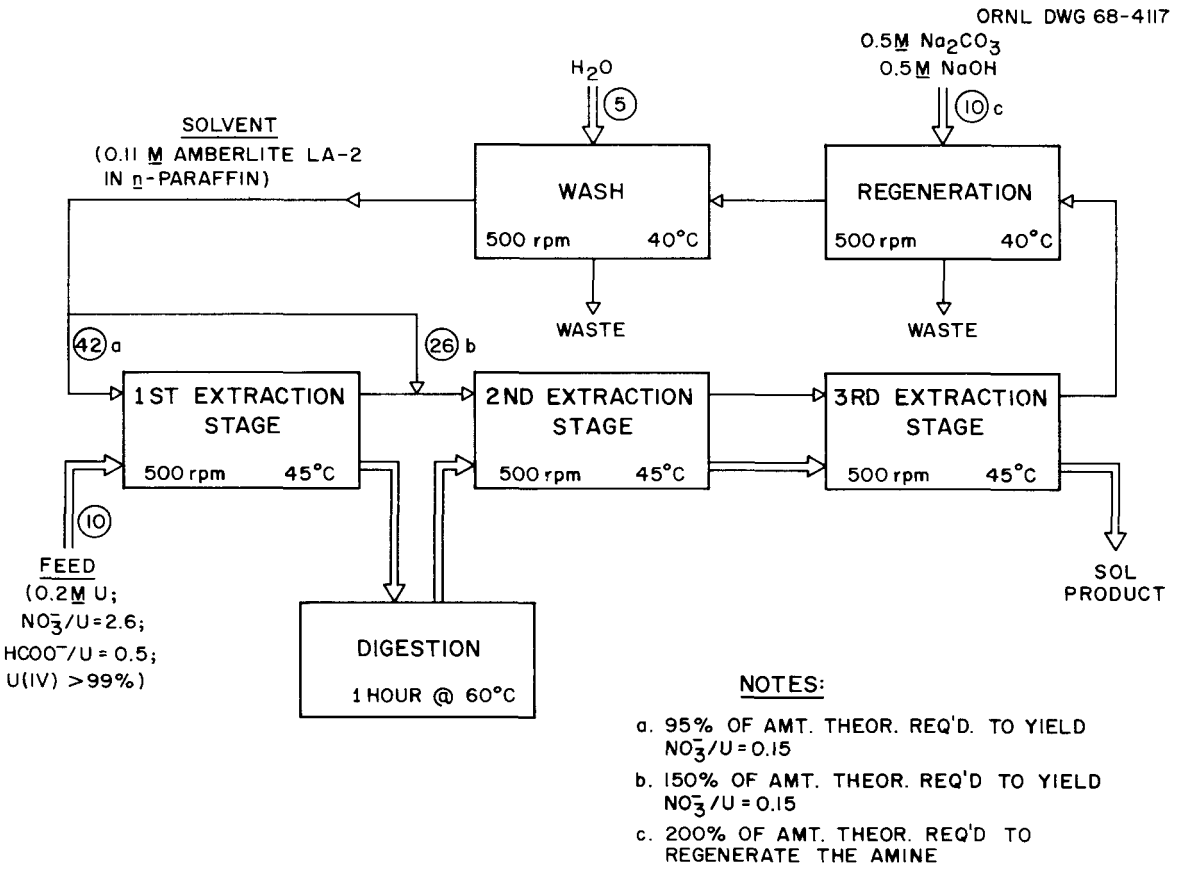

Fig. 3.3. Preparation of UO_2 Sol by Solvent Extraction.

catalyst is reduced to metal and flocculates in the presence of excess hydrogen, it settles very rapidly and is readily retained on a filter when reduction of the uranium is nearly complete. The filter consists of a flat disk of porous stainless steel (10-μ pores) that forms the bottom of the reductor. The reduction is monitored by measuring the redox potential of the solution with a platinum electrode against a reference glass electrode system. (Other reference electrodes such as silver-silver chloride or calomel can also be used but are not as rugged and trouble-free.) The end point is readily detected as a sharp break in emf, which occurs when reduction has progressed to between 96 and 100% U(IV). The feed composition was fixed at 0.6 M $UO_2(NO_3)_2$–0.4 M HNO_3–0.3 M HCOOH, so that the NO_3^-/U mole ratio was 2.6 and the HCOOH/U mole ratio was 0.5.

Both a 1.6-liter laboratory slurry reductor and a 14-liter unit have been evaluated for supplying feed for the engineering tests of the solvent extraction sol process. About 10 kg of uranium was reduced in

the small reductor, demonstrating the feasibility of the slurry catalyst. The large reductor was designed and built, based on the laboratory data. The results of 20 runs, producing a total of 40 kg of U(IV), show excellent performance. The platinum catalyst has shown no sign of loss in activity or of decrease in filtration efficiency (14 liters filtered by gravity in 12 min). Greater than 99.5% of the uranium was easily reduced, very little ammonia was formed (NH_3/U mole ratio ≤ 0.002), and less than 10% of the formic acid was lost. (Some reduction techniques lead to a substantial formic acid loss.) The rate of uranium reduction with 30 g of PtO_2 ranged from 2 moles/hr with only a small excess of hydrogen (96% utilization) to 3.3 moles/hr at 77% utilization.

The solvent extraction equipment operated very satisfactorily — in 20 runs, about 1000 liters of 0.2 M UO_2 sol was produced. No emulsion or entrainment difficulties have been encountered. The entrainment of solvent in the sol product has been consistently less than 0.01 vol %. A small amount of entrained sol in the used solvent is scrubbed with water to prevent loss of uranium to the waste. Although three extraction stages have been used in most of the runs, only two are needed because the nitrate content of the sol changes only slightly in the third stage. The stage efficiency has been consistently greater than 90% at a mixer speed of 500 rpm.

Variation of the uranium concentration from 0.15 to 0.3 M (the reference concentration is 0.2 M) caused no difficulty, and good-quality sols were produced; however, in two attempts a sol having 0.6 M U became thick in the second extraction stage.

The digestion temperature was an important variable. At 50°C the sol contains a significant amount of amorphous UO_2 (as determined by x-ray diffraction). It gels at about 0.5 M U if it is evaporated immediately after preparation; however, after aging overnight it can be concentrated to greater than 1.0 M and will remain fluid for more than 30 days. When the digestion temperature is increased to 60°C, the sol contains more UO_2 crystallites, and the fresh sol can be concentrated without gelling. To minimize oxidation of the uranium at the higher digestion temperature, the laboratory flowsheet was modified to include the use of excess amine in the first stage. This amine extracts sufficient nitrate

to give a nitrate-to-uranium mole ratio less than 0.5. At a digester temperature of 70°C, the sol has a shorter shelf life after concentration, perhaps because extensive oxidation of uranium occurs even at the low nitrate-to-uranium ratio. The digester temperature also affects the nitrate-to-uranium ratio in the sol product; the ratio averages 0.24, 0.10, and 0.07 in sol digested at 50, 60, and 70°C, respectively. From 20 to 70% excess amine has very little effect on the nitrate content of the sol. The average size of the UO_2 crystallites in the sol product is 35 to 40 A and does not seem to depend on either the digester temperature or the period of aging.

A digestion period of about 1 hr and a temperature of about 60°C appear optimum after the first extraction stage. Further digestion after subsequent extraction may also be beneficial.

Dilute sol (~ 0.2 M) must be concentrated to about 1 M U to facilitate the formation of microspheres. Vacuum evaporation below about 35°C avoids overheating the sol. Because the sol is quite sensitive to oxidation, exposure to air thickens or, in extreme cases, flocculates the sol. Seven batches (each containing 2 kg of uranium) of dilute sol have been successfully concentrated in the forced-circulation vertical-tube evaporator at the design boilup rate of 15 liters/hr and an absolute pressure of 30 torr. No foaming or scaling has been observed. Shelf lives of the large batches of concentrated sol were shorter than that of the product from the small laboratory evaporator. We believe that the reason is inleakage of air and the resultant oxidation of uranium in the large evaporator. In several runs in which large leaks were discovered the sol thickened overnight; in other runs the sols were still fluid after 30 days.

Preparation of Urania Sols by Precipitation-Peptization

A. R. Irvine P. A. Haas

For the preparation of UO_2 sols at the Oak Ridge National Laboratory, the first successful flowsheets were for batch precipitation-washing-peptization processes. These processes were used to prepare a large

number of enriched, natural, and depleted uranium sols.[8,9] The sol-gel products for irradiation tests or other uses were all prepared by batch precipitation procedures. Because of the criticality problems and the number of operating steps inherent in the batch flowsheets, continuous equipment would be preferred for large-scale remote operation. The engineering development of continuous equipment for preparation of UO_2 sols by precipitation-washing-peptization was terminated and reported.[10] All the flowsheets for preparation of UO_2 sols by precipitation require the same principal operations:

1. reduction of uranyl nitrate to uranous nitrate by hydrogen in the presence of a catalyst,
2. precipitation of uranous hydroxide by ammonia,
3. washing to remove NH_4NO_3, NH_4OH, and other solutes,
4. dispersion with NO_3^-.

Continuous Equipment for Preparation of Precipitation UO_2 Sols

Since these studies were terminated and reported, only the conclusions and recommendations from this report[10] will be given here.

> Continuous equipment can be used to prepare UO_2 sols by precipitation-washing-peptization flowsheets. When mechanical operation is good, the continuous systems give sols of the desired chemical compositions and good visual appearance. However, these sols (particularly those from the continuous vacuum evaporator) are not identical to those from batch equipment. The characteristics of the sols and the conditions to form them into UO_2 microspheres require further study.
>
> The major problems were with respect to mechanical operability and dependability with transfer of precipitate as the major source of operating difficulty. By increasing the pipe sizes to 1/2 inch diam minimum and limiting the slurry concentrations to 50 gU/ℓ or less, the acid-egg type pumps between

---

[8] W. D. Bond, A. B. Meservey, and A. T. Kleinstuber, Status and Progress Report for Thorium Fuel Cycle Development Dec. 31, 1965, ORNL-4001, pp. 41–46.

[9] P. A. Haas and J. P. McBride, Status and Progress Report for Thorium Fuel Cycle Development Dec. 31, 1966, ORNL-4275, pp. 15–27.

[10] P. A. Haas, Engineering Development of Continuous Sol-Gel Equipment for Preparing UO_2 Sols by Precipitation-Peptization Processes, ORNL-TM-2227 (July 1968).

washer stages were improved to marginal acceptability. When the requirements for remote operation are considered, there are minor mechanical operating problems without obvious solutions. These would probably always be sources of difficulty, but could be tolerated if no alternatives were available. The preparation of UO_2 sol by solvent extraction as reported elsewhere has very few mechanical problems.

The principal conclusions with respect to individual operations were:

(1) The continuous, high-pressure reduction system adequately met the chemical flowsheet requirements. The low-pressure reduction procedures recently developed are now preferred and the high-pressure reduction flowsheets are obsolete.

(2) The continuous precipitators, as revised, operate without difficulty other than those from feed metering problems.

(3) The precipitation can be controlled by metered flows, but pH indicators in the slurry are not dependable.

(4) Washing is excellent in the stage washers with stage efficiencies of about 80%, but the transfer of precipitate between stages is still of marginal acceptability.

(5) Washing in a countercurrent column gives HTU values of 2.3 to 3.6 feet. Fifteen to twenty feet of column would be desirable to give good washing although twelve feet gave acceptable washing for most tests.

(6) Settling of the washed precipitate to give uranium concentration of more than 0.5 M in the sol is not practical.

(7) The continuous peptizers give adequate dispersion with no clear chemical advantages or disadvantages if the slurry, HNO_3, and HCOOH flow rates are controlled.

(8) We do not have an adequate pump to meter washed precipitate from the washer into the peptizer system.

(9) The use of a vacuum evaporator for concentrating UO_2 sols has been adequately demonstrated in other sol preparation studies.

(10) The chemical flowsheet conditions have much more effect on the sol characteristics in continuous as compared to batch flowsheets.

(11) The sols from the continuous preparation equipment (particularly those from the continuous vacuum evaporator) are not identical to those from batch equipment. Their characteristics and the conditions required to form them into UO_2 microspheres require further study.

Batch Preparation of Precipitation UO_2 Sols

Most of the natural-urania sols were prepared in a batch apparatus (1 kg UO_2/batch) with precipitation to a pH of 8.1 to 9. Precipitation, washing, and dispersion were all done in a single PFP (precipitation-filtration-peptization) vessel with a 12-in.-diam porous stainless steel plate as the bottom and a slow paddle-type agitator. Supernates (present after precipitation and after each of four washing steps) were removed by filtration. To wash, 10 liters of H_2O was agitated with the 5 liters of slurry or cake remaining on the filter. Peptization was accomplished by agitation and heating after the addition of HNO_3 ahd HCOOH. Precipitation to pH of 7.3 to 7.5 and washing with hydrazine in the wash water (as shown for enriched uranium in Fig. 3.4) gives a more dispersable precipitate and a more stable and less thixotropic sol.

The equipment for preparation of enriched UO_2 sols (300 g ^{235}U per batch) was moved to an alpha laboratory in Building 3019. The reduction apparatus is a laboratory flask slurry reactor modified to use the oxidation-reduction electrodes. The sol preparation vessel is of the PFP type with a 9-in.-diam stainless steel filter. The flowsheet currently in use (Fig. 3.4) incorporates additional washing and less nitric acid addition for peptization to give more fluid and stable sols. Table 3.1 lists recent analyses of PFP sols. After one more demonstration run, the routine preparation of enriched urania sol will be turned over to Pilot Plant personnel.

A slurry reduction reactor of 25-liter capacity was installed for the PFP preparation of natural UO_2 sol. With 20 g of platinum slurry catalyst, 8-liter batches of uranyl nitrate were reduced at rates of 2 to 3 moles U(IV) produced per hour. As compared to the previously used fixed-bed reactor, the slurry reductor has no holdup of uranium and eliminates the anomalous initial batch after long shutdowns of the fixed-bed reductors.

ORNL DWG. 68-10541

BASIS: CONCENTRATIONS OR AMOUNTS OF U(IV), NO_3^-, OR HCOOH ARE IN MOLES / MOLE U, 1.37 MOLES U/BATCH

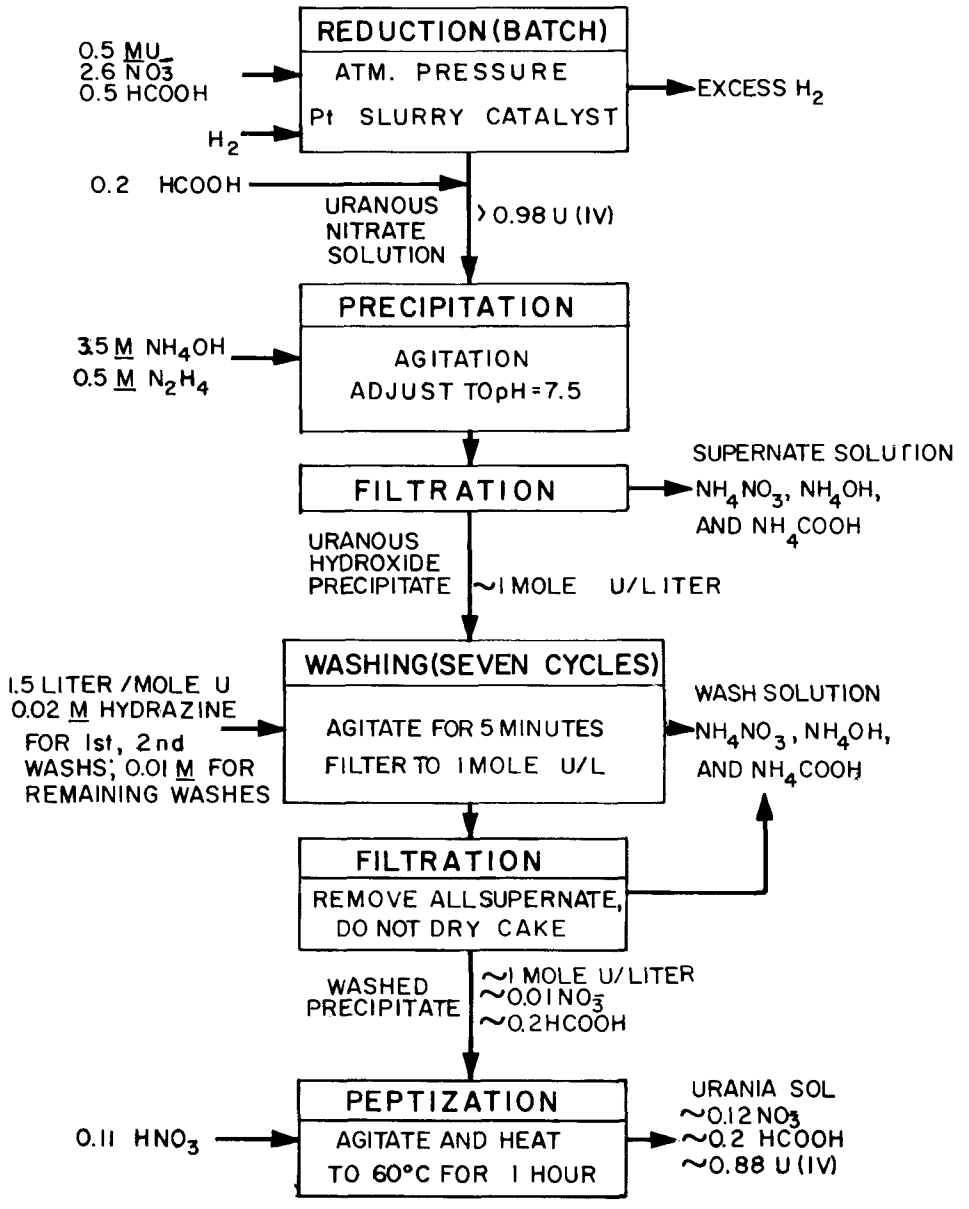

Fig. 3.4. Batch Precipitation-Filtration-Peptization (PFP) Preparation of Enriched Urania Sol.

Table 3.1. Analyses of Precipitation (PFP) UO_2 Sols[a]

Vessel Diameter (in.)	Uranium Enrichment	Sol	Uranium Concentration (M)	Mole Ratios, mole/mole U				Sol Conductivity[b] (mhos)
				U(IV)	NO_3^-	C	$HCOO^-$	
								$\times 10^{-6}$
9	Natural	ET-2	0.90	0.90	0.142		0.34	5050
	93%	S-8	0.90	0.88	0.163		0.24	6600
	93%	S-9	0.83	0.89	0.155		0.29	~ 4800
12	Natural	F-125	0.98	0.89	0.124	0.23	0.22	6700
	Natural	F-126	0.91	0.88	0.132	0.24	0.25	7000
	Natural	F-127	1.04	0.89	0.134	0.25	0.24	8700
	Natural	F-128	1.01	0.90	0.143	0.29	0.30	7000
	Natural	F-129	1.01	0.80	0.145	0.25	0.25	7000

[a]Flowsheets: batch precipitation-filtration-peptization in agitated filters with precipitation at pH of 7.4 to 7.6 as shown in Fig. 3.4.

[b]Meter readings; corrected absolute values are about 1.8 times meter readings.

Microsphere Preparation Process Development

P. A. Haas S. D. Clinton C. C. Haws

The preparation of samples of and the development of equipment and procedures for small spherical particles have continued. In these processes, droplets of sol are gelled by extraction of water into an immiscible organic liquid such as 2-ethyl-1-hexanol (2EH). The following operations are required:

1. disperse the sol into droplets,
2. suspend these droplets in the 2EH to extract water and cause gelation,
3. separate the gel microspheres from the 2EH,
4. recover the 2EH for reuse,
5. dry and calcine the gel microspheres.

Feeding and Dispersion of Sol

No sol disperser is optimum for all the fluidized bed sphere forming operations. The two-fluid nozzles with laminar flow of the 2EH and varicose breakup of the sol stream is the most flexible, useful, and reliable dispersion device. Other devices are simpler for large sol drops. The two-fluid nozzles have capacity limitations that are lower and more restrictive as the sol drop diameter decreases.

To obtain a controllable and uniform dispersion of sol as drops in an alcohol, a controllable and uniform force should be applied to a uniform configuration of undispersed sol. Formation of the new surface requires energy. But dispersion is usually very inefficient, and most of the energy supplied is dissipated as fluid friction. An important practical requirement is capacity, and the number of drops per unit weight increases with the inverse cube of the diameter. The sol viscosity and the sol-alcohol interfacial tension are variable and difficult to control; therefore, control is simpler if these are not significant variables for disperser operation. The uniform and controllable configuration of sol is usually obtained by feeding the sol through 0.004- to 0.040-in.-ID capillaries or orifices. The forces to disperse the sol

may be from gravity, fluid shear or drag, inertia, interfacial tension, electrostatic repulsion, and centrifugal effects. Even when one type of force is controlling, one or more other types are commonly present and complicate the disperser operation.

The apparently preferred dispersion devices depend on the overall requirements (Table 3.2). Two-fluid nozzles are the most flexible and reliable for small-capacity experimental tests. Multiple two-fluid nozzles provide higher capacities but require careful cleanout and assembly. Other devices can give better uniformity and simpler operation for large drops.

Sol drops from capillaries that are mechanically connected to and vibrated by electronic vibrators are more uniform at optimum conditions than those from any other disperser. The natural breakup of a liquid jet is the mechanism for varicose operation of the two-fluid nozzles. The vibrating capillary imposes a controlled frequency on the breakup of the liquid jet. A simple, sinusoidal displacement of the capillary tip appears to be the best wave shape. The sol streams from vibrating capillaries are thickest at the extreme displacements, where the velocity is low or zero, and thinnest at zero displacement, where the velocity is a maximum. This greatly favors the formation of two drops per cycle of vibration. In practice, the jet velocity and amplitude of vibration must be adjusted to optimum conditions.

The vibration sources for most of the studies were Agac Derritron model VP-2 vibrators. These are constructed like loud speaker coils and are supplied with sine-wave potentials of controlled frequency and voltage. The movable coil is not intended to support large weights, and any secondary vibrations will adversely affect the dispersion. The reproducibility and durability of the vibrating capillaries were greatly improved by suspending them at the ends of pivoted arms.

The most serious limitation of the vibrating capillary dispersers is that they must be observed visually and "tuned" with respect to amplitude and frequency each time they are used. The sol stream may be displaced to an amplitude greater than the displacement of the capillary tip. If the sol stream amplitude is too small, the oscillations will damp out and the sol will break up by its natural varicose mechanism

Table 3.2. Preferred Sol Dispersion Devices for Several Types of Operation

Device	Mechanism and Force	Product Mean Diameter (μ)	Capacity (cm^3/min)	Sol Properties Allowable
Orifices in plastic bucket	Free fall drop, gravity	> 400	Any	Must be fluid and uniform
Multiple nozzle with electrical potential	Electrostatic plus gravity	> 250	Any	Must be fluid
Vibrating capillary	Interfacial tension and inertia	> 200	< 25	Must be fluid
Two-fluid nozzle	Varicose, interfacial tension	100 to 300	< 5	Variable
Two-fluid nozzle	Modified free fall, gravity and drag	200 to 600	< 10	Variable
Multiple two-fluid nozzle	Either varicose or modified free fall	200 to 600	< 50	Must be fluid
Two-fluid nozzle	Turbulent, fluid shear and drag	< 100	Any	Variable

instead of at the vibration nodes. If the amplitude is too large, the stream will spray out to give many nonuniform drops per cycle. The optimum conditions depend on a large number of variables including the sol viscosity, the sol density, the velocity from the capillary, the vibration frequency, the capillary diameter, the presence of secondary vibration frequencies (even of small amplitude), and the arrangement of the pivot arm, the vibration source, and connecting lines.

The ranges of conditions that give the best operation are limited. The average sol velocity in the capillaries should usually be 60 to 100 cm/sec. The sol properties are fixed by the sol feed available, and dilution to decrease the viscosity is usually the only independent sol variable. The sol drop size is easily calculated from the sol flow rate and the number of drops per unit time. The relationship for two drops per cycle is

$$D_I = 2500(F/f)^{1/3} , \qquad (1)$$

where F is sol flow in cm^3/min, f is vibration frequency in cps, and D_I is the drop diameter in μ. For sol jet velocities from 60 to 100 cm/sec good dispersion is usually possible for some amplitude at any frequency between 30 and 120 cps and usually up to 160 cps. The best amplitudes are usually in ranges of 1 to 4 mm for less than 60 cps and 0.2 to 2 mm above 60 cps. Stable operation was possible at some frequencies up to 800 cps but for 200 to 800 cps was for limited ranges of conditions, which depended on resonance effects.

Operating conditions for the vibrating capillary dispersers are generally selected as follows. The sol drop size is calculated for a known product size and the sol concentration. An f/F value in $cps/(cm^3/min)$ is determined from Eq. (1) or a graph (Fig. 3.5). The sol flow rate, F, and capillary size are matched to be within the preferred 60 to 100 cm/sec range and selected to keep f below 160 cps if possible. The amplitude of vibration is adjusted to locate the best dispersion conditions for the selected sol flow rate, capillary size, and frequency. If the dispersion is not good at any amplitude, the sol flow and frequency are changed together to keep the f/F ratio required to give the desired

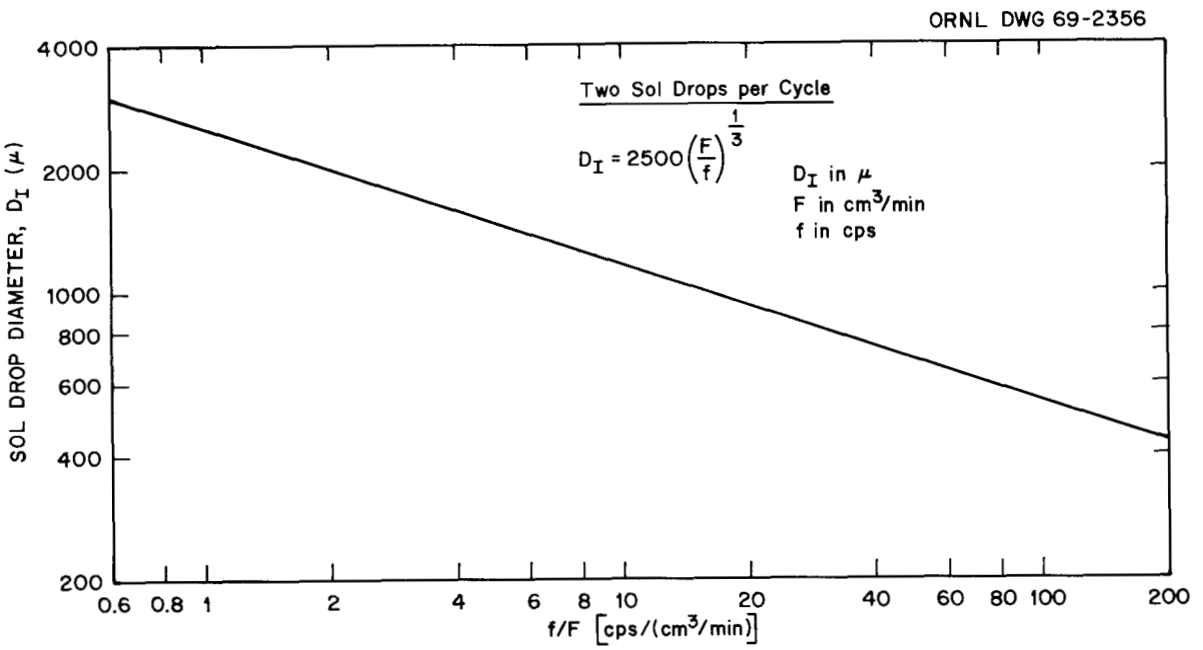

Fig. 3.5. Diameters of Sol Drops Produced by Vibrating Capillary Dispersers as a Function of f/F.

sol drop size. Since D_I is proportional to $(F/f)^{1/3}$, the F/f ratio can be varied small amounts with only one-third as much percentage change in D_I. Experience with "tuning" the disperser is important and leads to more effective operation than any instructions without experience.

Fluidization

A tangential flow to produce a swirl at the bottom of the fluidized bed may greatly improve the fluidization for laminar flow. The tangential inlet is below the bottom of the bed. The swirl extends with decreasing intensity on both sides of the tangential inlet, and its effect becomes negligible at 0.5 to 3 ft up the bed.

The amount of swirl can be varied along with the superficial fluid velocity to control the fluidization behavior. Thus, for a given column and fluid, there are optimum amounts (or perhaps ranges) of swirl and superficial fluid velocity; these amounts depend on the diameter and density of the particle to be fluidized. The energy required to give a specified amount of swirl would depend on the configuration of the column, the fluid viscosity, and other parameters.

Two fluidization flow inlets, a tangential inlet to produce swirl and a nontangential or "upflow" inlet, provide a simple, independent control of the amount of swirl and the superficial velocity. The two flows together give the superficial flow. For a constant total flow, the amount of swirl is increased by increasing the fraction that enters through the tangential inlet. A smaller tangential inlet area results in a higher velocity and thus more swirl from the same tangential inlet flow. In theory, the tangential inlet size could be optimized for one specified combination of conditions without use of the second flow. In practice, changing the inlet size is difficult but controlling two flows is simple.

Operating Procedure. — The optimum swirl and upflow are selected by visual observation of the fluidized bed in the glass columns. The holdup time is selected from consideration of the sol drop diameter and measurement of gelation times. After the first sol drops have been in the column this selected time, the flows are adjusted to allow gel spheres to drop through the column's minimum cross section. The split between upflow and swirl flow can be adjusted to the minimum total flow by observing where the spheres fall out of the fluidized bed. If the spheres fall out near the wall, increasing the swirl and decreasing the upflow will give a better flow split. If the spheres fall out in the center three-quarters of the column, a better flow split comes from increasing the upflow and decreasing the swirl. The minimum total flow and optimum fluidization are generally with some of the spheres dropping out through the center and most of them dropping out near the wall. The rate of discharge of spheres will be cyclic or fluctuating. The fluidization is not as smooth at the beginning as it is after the bed approaches a steady state.

Examples. — The use of the tangential inlet will be illustrated for fluidization in columns with minimum inside diameter from 1.5 to 2.0 in. The swirl to improve fluidization has been used in sol-gel sphere-forming columns from 0.25 to 3 in. minimum inside diameter and for gel spheres 80 μ in diameter to sol drops 1800 μ in diameter. The product spheres smaller than 150 μ in diameter settle slowly and gel rapidly, so good fluidization is not required. Fluidization is less troublesome in the

columns smaller than 0.5 in. in diameter. Therefore the most significant results are for the larger columns and larger sphere diameters.

The conditions for discharge of product spheres from the bottom of the fluidized bed are viscosity of 2EH about 7 centipoises and solid-liquid density difference about 3.0 g/cm^3; density of 2EH is 0.83 g/cm^3. Thus we have laminar flow settling ($Re < 3$) for spheres up to 480 μ, and Stokes' law is adequately accurate for spheres no greater than 600 μ.

The fluidization results are correlated by a ratio of the superficial fluid velocity at the minimum column inside diameter to the Stokes' settling velocity for the fluidized spheres. In theory, a uniform flow would keep the spheres in the fluidized bed when this ratio is at least 1. For all upflow and no swirl, ratios of 2 or 3 still allow loss of spheres at the wall and give undesirable axial mixing throughout the bed. With the optimum swirl, the fluidization is good for continuous discharge of product spheres at ratios of 1.4 to 1.2 for 350- to 600-μ gel spheres (Fig. 3.6). Larger spheres can be fluidized at lower ratios (about 0.8) because of the centrifuging effect previously mentioned. The ratio is calculated on the basis of d_{80}; 80 wt % of the gel spheres are smaller than this diameter. The d_{80} is used instead of d_{50} because the conditions must be selected to fluidize the larger spheres present.

The preferential discharge of spheres with the highest settling velocity was shown for gel spheres varying in size. The fluidizing flow into a fluidized bed of ThO_2 gel spheres was reduced until about half of the bed was discharged through the 1.5 in. minimum diameter. The spheres discharged and those remaining in the column were collected, dried, and sieved separately. The ratios of the weights discharged to the weights retained decreased by about factors of 10 for each U.S. Sieve Series size range (Table 3.3). The common cylindrical fluidized bed would give mixing throughout the bed and would not give any significant size separation for this range of sizes.

Mass Transfer During Gelation

The rate of water extraction from thoria sols was investigated by fluidizing single thoria sol droplets in 2EH and measuring the drop

ORNL DWG. 68-12234

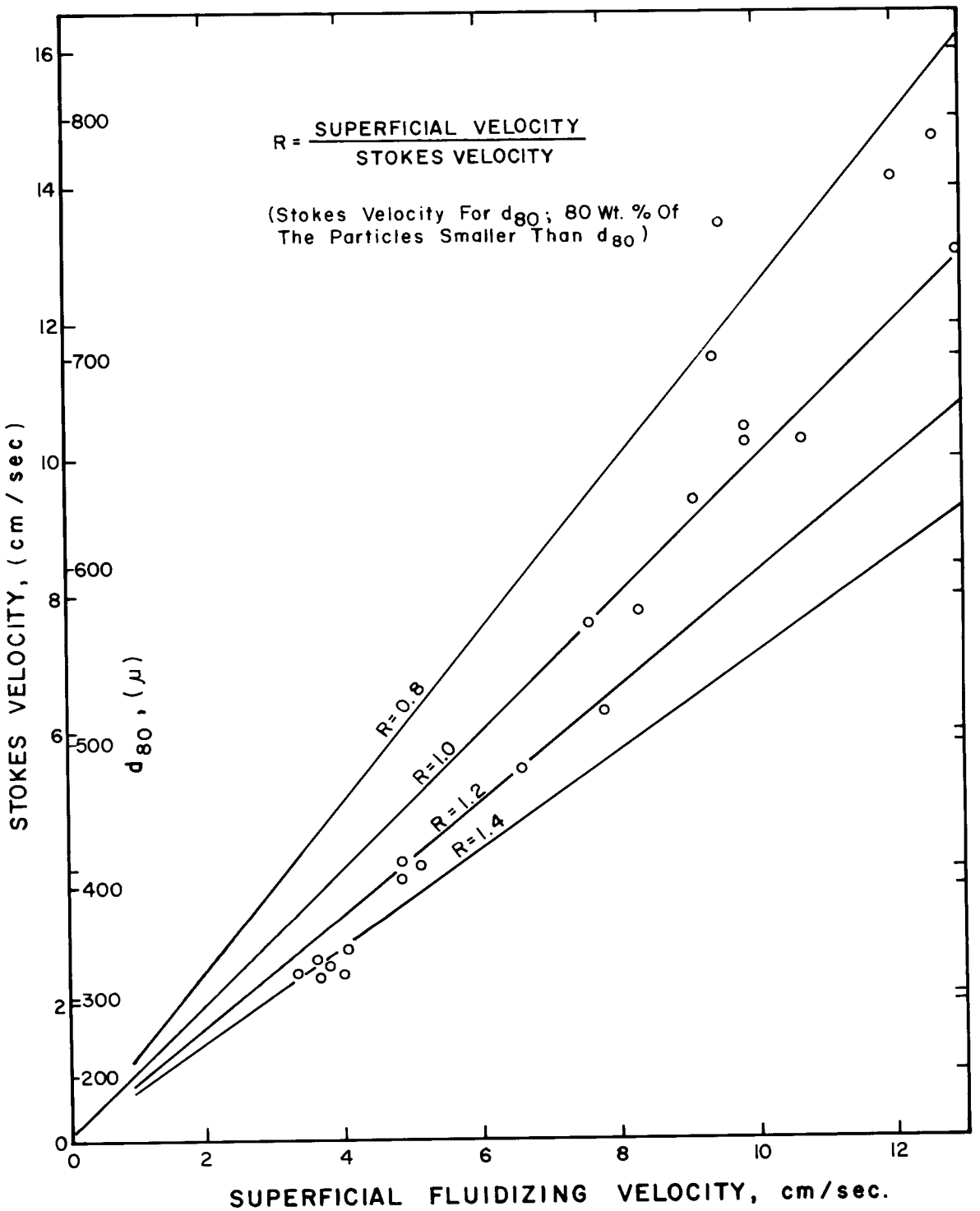

Fig. 3.6. Stokes' Settling Velocities for Gel Spheres Plotted Against Experimental Fluidization Velocities.

Table 3.3. Size Separation in a Fluidized Bed With Laminar Flow Using a Tangential Inlet[a]

Sphere Size		Amount Discharged (g)	Amount Retained in Bed (g)	$\left(\frac{\text{Discharged}}{\text{Retained}}\right)$ Ratio
U.S. Sieve (mesh)	Diameter (μ)			
−30 +35	500–590	19.0	0.2	95.0
−35 +40	420–500	88.0	8.0	11.0
−40 +45	350–420	80.8	100.1	0.80
−45 +50	297–350	10.0	113.0	0.088

[a]Conditions: ThO_2 gel spheres; fluidizing alcohol density 0.83 g/cm^3 and viscosity about 7.0 centipoises; sphere-liquid density difference of about 3.0 g/cm^3.

diameter with time until shrinkage no longer occurred. Diameter data from both water and sol drops were obtained at 25°C. The experimental variables were drop diameter (0.10 to 0.20 cm), sol molarity (0 to 2.5 M), and water concentration in the bulk solvent (2 to 12 mg/cm^3). The complete results and procedures were reported.[11]

The Sherwood number for the water and sol droplet data was a linear function of the product of Reynolds number to the 1/2 power and Schmidt number to the 1/3 power. The common correlation for the fluidized water and sol drops verified a proposed mass transfer model based on an organic phase film surrounding the drop as the rate-controlling resistance. The drop Reynolds number was based on an average organic fluidizing velocity and varied from 0.2 to 7. The Schmidt number for the system was fixed at 35,700.

During the extraction of water, the mass transfer coefficients for fluidized sol drops depended only on the increasing thoria concentration. By correlating the mass transfer coefficients with the density difference between the sol and 2EH, we derived an expression to predict the gelation time required for any initial sol molarity and drop diameter.

[11]S. D. Clinton, Mass Transfer of Water from Single Thoria Sol Droplets Fluidized in 2-Ethyl-1-Hexanol, ORNL-TM-2163 (June 1968).

Control of Alcohol Compositions

For a specified sol feed, the composition of the organic fluidizing medium is the principal operating variable for minimizing problems. Variations in surfactants, H_2O content, alcohol composition, and pH can all change the amounts of sticking, clustering, coalescence, cracking, or distortion. Variations in these problems normally do not require variations in the column configuration or the fluidizing flows; good configurations and good fluidizing conditions are relatively independent of the sol characteristics and operating problems. The sol characteristics are the most important quantities, but these cannot be varied after the sol is specified. The usual procedure with a new sol is to start with a commonly used alcohol composition and then vary it to obtain satisfactory operation.

Demonstration Run Criteria. — Successful continuous operation of a sphere-forming column depends on controlling the alcohol composition within satisfactory ranges. This is still largely a complex and difficult empirical art. There are several significant time criteria for the column conditions. If the initial conditions are not satisfactory, this will become apparent by the time the first particles are completely gelled. The sphere-forming behavior after 1 hr may change slowly as surfactants are depleted or degraded. Normally these changes are tolerable for at least 10 hr and sometimes as long as 100 hr. We are convinced that satisfactory long-term operation requires additions of surfactants to the 2EH. While continuous additions should be ideal, additions every 6 to 12 hr of operation appear completely adequate. The periodic additions must be the right amounts to give satisfactory column operation after a long-term equilibrium is reached. Thus, demonstration of satisfactory column operating conditions requires several steps as follows.

1. Demonstrate satisfactory initial operation. This will be for more than 1 hr with a sol feed volume greater than 5% of the fluidized bed volume.

2. Demonstrate a surfactant addition schedule that prevents unsatisfactory depletion of surfactant. This will require more than 50 hr cumulative operation and a volume ratio (sol feed/2EH inventory) > 0.5.

3. Demonstrate satisfactory long-term operation without excessive accumulation of surfactants or degradation products. We consider more than 200 hr and (sol feed/2EH inventory) > 2 significant.

The first step demonstrates an acceptable initial composition. Distortion and cracking can be determined with just a few particles. But sticking, clustering, and coalescence depend on the inventory of sol drops and partially gelled spheres and on the loading of the fluidized bed. For this reason, the 1-hr time and 5% volume criteria are necessary to fully demonstrate satisfactory initial conditions.

Our limited surfactant depletion data mostly show apparent surfactant half-lives of one to two days. This depends on the sol and on the still temperature. The surfactant addition schedules we have used agree with this rate of depletion. If we do not add enough surfactants to maintain the initial concentration the long-term equilibrium amount may be too low. This will show up from the step 2 demonstration criterion.

The third step is to check on the effects of long-term accumulations of surfactants or degradation products. The only certain test is to actually operate for the full time of interest. However, we feel that 200 hr without visible effects is significant. Much longer times are then probably possible, as effects of long-term accumulations are unlikely to show up and become intolerable in a short time. Also, the 2EH could be completely reprocessed or replaced after more than 200 hr if absolutely necessary.

Effects of Column Operating Variables. — Any selection of column operating conditions represents a compromise of conflicting requirements. Any change to lessen one problem usually increases another. Since the significance of the different problems for a new sol can be determined only by testing that sol, the best operating conditions for a particular sol can be determined only experimentally. Once the operating problems have been so identified, previous experiences show which changes are most likely to provide solutions.

Our principal experiences with column operating problems are generalized in three tabulations. Table 3.4 lists the operating problems and the changes in variables that significantly lessen the problems for ThO_2 or UO_2 sols. The experiences with ThO_2-UO_2, ThO_2-UO_3, PuO_2, and

Table 3.4. Microsphere Preparation Column — Generalized Results and Variables for Operating Problems with ThO_2 and UO_2 Sols

Column Operating Problem	Surfactant Concentration Changes to Minimize Problem		Drop Diameter Change to Minimize Problem	Remarks
	Change	Order of Effect[a]		
Coalescence of drops (while fluidized)	Increase	S-80, A-0, E/15[a]	Not certain	Not a controlling problem
Sticking to column wall (usually near top)	Increase	S-80, A-0, E/15[a]	Increase	Much more likely for poor sols and nonuniform drops
Clustering of partially dried drops	Increase	S-80	Increase	Much more likely for poor sols
Distortions of dimple type. Extreme is shell (perhaps due to premature surface gelation)	Decrease amine Increase Span	E/15, A-0 S-80	Decrease	Not a problem for pure ThO_2 sol
Other distortions. Extreme is raisin shape (perhaps due to low interfacial tension)	Decrease Span Increase amine[b] Decrease amine[b]	S-80 E/15, A-0 A-0, E/15	Decrease	More likely for good sols
Cracking of spheres (perhaps due to excessive concentration gradients in gel)	Decrease	E/15, A-0, S-80	Decrease	Sol is most important variable, but cracking also depends on H_2O in 2EH and drying-firing conditions

[a]Listed in order of effectiveness; S-80 for Span 80, A-0 for Amine-0, and E/15 for Ethomeen S/15.

[b]Amines can compete with and decrease effect of Span 80; amines can also cause distortions.

UO_2-PuO_2 sols are similar. Table 3.5 gives the same type of information organized to emphasize the conflict in requirements and which effects may be controlling (principal) and which are usually not controlling (secondary). Table 3.6 shows which characteristics of the sols seem to contribute to operating problems.

Most operating problems are solved by varying the Span 80, Ethomeen S/15, and H_2O contents in 2EH as the fluidizing alcohol. If these variations do not allow satisfactory operation, then we consider improving the sol. In only a few cases, mostly borderline situations, other variables have provided the solutions to operating problems. The most important was operating the column at 40 to 50°C to reduce clustering for sols containing carbon black. The normal temperature of 2EH in the column is about 30°C. The ThO_2 and UO_2 sols cluster much worse if the temperature is increased, but the same sols with carbon added for carbide preparation cluster less if the temperature is increased.

We tested a number of variables without finding any conditions generally superior to those already described. A common result was a small advantage with one sol but poorer results for most sols. Amine O is a useful surfactant similar in effect to Ethomeen S/15, but it has not given us any result superior to Span 80 and Ethomeen S/15 together. Gel spheres may be formed in other alcohols, such as octanol-2, methylpentanol, isoamyl alcohol, or alcohol mixtures. For the fluidized bed columns, the solubilities of H_2O in 2EH and 2EH in H_2O appear to be a better combination than those for any other alcohol.

Still Operation and Water Content. — The water content of the 2EH in the column is controlled by controlling the flow of 2EH through and the temperature in a single-stage distillation. The water content for steady-state operation is easily calculated from material balances. From 75 to 90% of the water in the sol is extracted into the 2EH. At steady state, the water content in the column is constant and the water input from the sol equals the still 2EH flow rates times the difference in H_2O content for the 2EH flows to and from the still. The water content in the 2EH returning to the column from the still is determined by the still temperature. Values we use for our usual still temperatures are:

Table 3.5. Effects of Column Conditions on Formation of ThO_2-UO_3 Gel Spheres

Change	Favorable Effects		Unfavorable Effects	
	Principal	Secondary	Principal	Secondary
Increase span	Less sticking (clustering)	Less dimple distortion	Raisin distortion	More cracking
Increase Ethomeen[a]	Less raisin distortion	Less sticking[a]	More cracking	Dimple distortion
Increase H_2O in 2EH	None	Less cracking	None	More clustering, longer gelation time
Add HNO_3 to 2EH	None	Less dimple distortion[b] Less cracking	More clustering[b]	
Increase sphere diameter	Less sticking	Less clustering	More cracking More distortion	Longer gelation time
Digestion of sol	Less cracking		More clustering	
Higher NO_3^- in sol	More fluid		More cracking	More clustering

[a]Ethomeen appears to "compete" with Span and decrease both the principal favorable and principal unfavorable effects of Span when both are present. It "buffers" the effects of Span.

[b]Additions of HNO_3 have temporary effects; we have no experience with continued pH control of the 2EH.

Table 3.6. Effects of Sol Characteristics on the Formation of Gel Spheres

Sol Deficiency	Deleterious Effects on Gel Sphere Formation	
	Principal	Secondary
A. High nitrate/metal mole ratio	Cracking, clustering, sticking	Dimple distortion; prohibits use of 2EH with other sols
B. Finely divided suspension instead of true sol	Clustering; raisin distortion; rough surface; low strength	Shedding of fines into 2EH; coagulation of suspension to give sphere of solids in drop of H_2O
C. Large fraction of amorphous (noncrystalline) material	Cracking	Dimple distortion
D. Thick; thixotropic (thick UO_2 sols are thixotropic)		Sol difficult to feed and disperse; clustering; sticking
E. Thick; high viscosity (thick ThO_2-UO_3 sols are relatively nonthixotropic)		Difficult to feed and disperse; distorted particles
F. Low-metal concentration[a]		Clustering; dimple distortion; raisin distortion
G. Low U(IV)/U ratio in UO_2 sol	Precipitation; clustering; raisin distortion	Same as for (B) above
H. High HCOOH concentration in UO_2 sol	Raisin distortion; clustering	Prohibits use of 2EH with other sols

[a]Less than one-half the concentration required for gelation.

2EH temperature, °C	140	150	160
Water content, vol %	0.7	0.5	0.35

The 2EH loses some surfactant from still operation, and the loss increases as the still temperature is increased. Thus the amounts of surfactants needed and the accumulation of degradation products depend on the still temperature. We feel that 2EH temperatures above 155°C are definitely undesirable. If temperatures below 140°C are used the still 2EH flow must be greatly increased. The desirability of an upper temperature limit requires that the still be designed and operated to avoid localized overheating. Steam heat accomplishes this very effectively.

The water content of 2EH can be measured by an in-line determination of boiling point. This was demonstrated by an apparatus in which a small, metered stream of 2EH was heated electrically with sufficient power to heat dry 2EH to its boiling point (183°C). The vapors are completely condensed and returned to the heated pot by an oversize, close-coupled condenser. The pot temperatures remained at approximately the inlet 2EH boiling point independent of moderate changes in heat input or 2EH flow rates. The relatively large, regular change of boiling point from 183°C for dry 2EH to 99°C saturated with water can thus be easily measured and calibrated to show the water content.

Example of Operating Conditions. — Most column operating problems are solved by varying the Span 80, Ethomeen S/15, and H_2O contents in the 2EH. The sol characteristics and still temperature are important variables; thus, the operating conditions may change considerably for what appear to be small changes in the sol or the still.

The initial surfactant compositions and surfactant addition schedules for the most important sols are listed in Table 3.7. The significance of the addition schedules depends on the demonstrated operation listed for that schedule. The schedule for ThO_2 has been demonstrated for more than 200 hr, but some others are proposed schedules with no long-term demonstrations. Low water contents in the 2EH sometimes cause more cracking, whereas high water contents result in slower gelation and sometimes more clustering. These effects are usually noticed only for such extreme water contents as less than 0.7 and 2 vol %. Changes in

Table 3.7. Initial Surfactant Concentrations and Addition Schedules for 2EH in Fluidized Bed Columns[a]

Type of Sol	Method of Preparation	Initial Concentrations (vol %)		Additions per 6–8 hr: Based on 2EH Volume (vol %)		Additions per 6–8 hr: Based on Sol Fed (cm^3/liter)		Demonstrated for	
		Span 80	Ethomeen S/15	Span 80	Ethomeen S/15	Span 80	Ethomeen S/15	Step	Period (hr)
ThO_2	Hydrothermal denitration	0.05	0.2	0.01	0.05	2	10	3	> 200
UO_2	Precipitation at pH 9	0.8	0.1	0.1	0.02	20	5	2	50
UO_2	Precipitation at pH 7.5	0.4	0.05	0.02	0.01	5	2	2	50
ThO_2-UO_3	Solvent extraction; Th/U = 3	0.2	0.05	0.02	0.01	5	2	2	50
ThO_2-UO_3	Solvent extraction; Th/U = 4.25	0.2	0.05	0.05	0.01	10	1	2	50
UO_2	Solvent extraction; ~ 0.2 M U feed	0.2	0.05	0.02	0.01	5	2	2	30
UO_2	Solvent extraction; > 1 M U feed (CUSP)	0.4	0.05	0.03	0.01	8	2	1	1

[a]Other conditions: about 1.2 vol % H_2O in 2EH; temperature of 2EH in still, 155°C.

water content in the normal 1.0 to 1.5 vol % range are rarely a controlling variable and most demonstration runs were in this range.

Preparation of Small (< 100-μ-diam) Spheres

The relative importance of operating problems for forming microspheres is much different for small (5- to 300-μ mean diameter) than for large (300- to 2000-μ mean diameter) sol drops. Products from the smaller diameters are important for some uranium fuel cycle applications; therefore, we tested procedures and equipment to prepare the smaller sizes more efficiently.

Several dispersers were tested for preparing uniform drops with mean diameter controlled in the range 50 to 300 μ. None of the disperser mechanisms that gave uniform drops in the 300- to 2000-μ range were practical for 50 to 300 μ. The capacity of a two-fluid nozzle with streamline flow was too small. The other mechanisms were completely ineffective. Three dispersers were used to prepare samples with mean drop diameters in the 50- to 300-μ range. A paddle agitator in a baffled vessel gave mean sol drop diameters up to 200 μ depending on the speed, but the uniformity was poor. A vibrating nozzle-plate agitator at 60 cps gave uniform drops within a 20- to 60-μ mean diameter range, depending on the amplitude, but it was not effective for larger drops. Either agitator could be controlled to give larger drops if an organic liquid denser than 2EH was used.

We presently use two-fluid nozzles with turbulent flow of the alcohol drive fluid to give 20- to 150-μ mean sol drop diameters and much higher sol flow rates than for varicose breakup with streamline flow. The uniformity is poor compared to the varicose breakup for streamline flow but is good when compared to other dispersers for the same small drop size. In the turbulent two-fluid nozzle, turbulence of the continuous (alcohol) phase flowing through a tube provides uniform and controllable forces for dispersion of a sol stream introduced into the channel. The degree of turbulence is easily and reproducibly varied by varying the alcohol flow rate. The transition from viscous or laminar flow to turbulent flow is commonly recognized to depend on the Reynolds number. The localized forces that cause dispersion and the sizes of the turbulences in the

turbulent two-fluid nozzle depend on the channel dimensions and continuous fluid properties in addition to the Reynolds number.

The important function of this disperser is to use controlled turbulence as the primary force to disperse the sol into a flowing alcohol stream. The promotion of turbulence by the sol inlet configuration and the addition of shearing forces to the turbulent forces are unavoidable accessory effects, which supplement the basic function. The sol stream from a capillary inlet gives a uniform configuration. The force causing dispersion is easily controlled and is more uniform than the somewhat similar forces for dispersion by agitation or by fluid-driven atomizing nozzles. According to literature on dispersion by agitation, the sol viscosity is probably not a controlling variable if it is of the same magnitude as or less than the alcohol viscosity.

The results from turbulent two-fluid nozzle operation have been correlated by dimensional analyses. The dimensionless relationship developed is

$$D_{sol}/ID = 1630(G/F)^{0.1}\ Re^{-1.5}\ ,$$

where D_{sol} is the sol drop diameter, ID is the alcohol flow channel diameter, G is the alcohol flow rate, F is the sol flow rate, and Re is the alcohol Reynolds number. For our two-fluid nozzle configuration with the sol inlet capillary perpendicular to the axis of the alcohol channel, this expression was valid for $Re > 600$, perhaps due to promoted turbulence for $600 < Re < 2000$. Terms for ratios of the viscosities and densities of the alcohol and sol were omitted from the equation because we do not have data to determine their components. Table 3.8 lists data to illustrate the range of variables. The relationship in our common units becomes

$$D_{sol} = 7.0 \times 10^6\ ID^{2.5}\mu^{1.5}/G^{1.4}F^{0.1}\ ,$$

where D_{sol} is in μ, ID in cm, G in cm^3/min, F in cm^3/min, and μ is the alcohol viscosity in centipoises.

Table 3.8. Equation Fit for Turbulent Two-Fluid Nozzle Dispersers[a]

Nozzle ID (cm)	Alcohol Flow, G (cm^3/min)	Alcohol Viscosity, μ (centipoises)	Sol Flow, F (cm^3/min)	Alcohol Reynolds Number	Mean Sol Diameter, D_{sol} (μ)	Calculated Value of k
0.15	520	2.5	7.6	2440	25	1340
0.195	330	5.0	4.9	595	230	1120
	520	5.7	4.9	825	185	1420
	560	2.2	9.6	2240	40	1450
	620	5.1	4.9	1100	165	1910
	860	2.0	9.6	3790	20	1490
0.200	210	2.3	9.6	785	170	1370
	240	3.5	9.8	605	300	1630
	368	4.8	9.8	675	300	1820
	385	2.2	9.6	1500	80	1600
	405	2.3	9.6	1510	75	1530
	430	2.8	9.6	1320	95	1570
0.265	535	2.65	9.8	1310	145	1740
	550	2.7	9.8	1320	145	1770
	650	2.7	3.7	1565	127	1770
0.28	500	2.7	9.6	1140	180	1650
0.38	710	3.0	10.0	1070	280	1710
	740	2.9	7.6	1150	265	1710

[a]Equation: $D_{sol}/ID = k(G/F)^{0.1}\ Re^{-1.5}$.

The most important advantage of the turbulent nozzle operation is that much less product is produced as spheres much smaller than the mean diameter. Other dispersers that give controllable diameters and practical capacities give much higher yields of small spheres. Table 3.9 gives data for products of two mean sizes for a paddle agitator[12] and the turbulent nozzle. For visual observations, the differences are even greater at 0.2 d_{50}, but we do not have numerical measurements at the small diameters.

Suspension of the sol droplets during gelation is easier for smaller droplets. The higher surface-to-volume ratio results in faster gelation and, along with lower settling velocities, eliminates the need for fluidization. Small drops are less likely than large drops to crack or give hollow particles if the rate of mass transfer of water is increased by using drier 2EH or an alcohol with a higher solubility of water. Smaller drops show more clustering and sticking to the vessel walls for otherwise equal conditions. However, we can gel the small drops without fluidization and we can use more or more effective surfactants without cracking or distortion. Therefore, clustering and sticking do not seriously restrict the preparation of smaller spheres.

---

[12]M. E. Whatley et al., Unit Operations Section Quarterly Progress Report July–September 1965, ORNL-3916, p. 44–50.

Table 3.9. Comparison of Products from Paddle Agitators and Turbulent Nozzles

	Paddle Agitator	Turbulent Nozzle	Paddle Agitator	Turbulent Nozzle
Mean diameter, d_{50}, μ	92	90	78	76
Wt % smaller than				
0.8 d_{50}	42	30	38	28
0.6 d_{50}	30	13	26	11
0.5 d_{50}	24	7	~ 19	~ 4
0.4 d_{50}	~ 18	~ 3	~ 14	< 2

The separation of the gel microspheres from an organic liquid becomes increasingly troublesome as the sphere diameter decreases. The equipment is limited to critically safe geometries for fissionable materials. Since the solubility of water in 2EH requires a 2EH-to-sol volume ratio of about 100, alternate methods of gelation were tested to simplify the gel sphere separation problem. From tests of chemical gelation with ammonia or organic amines, it appears that the gel spheres smaller than 100 μ in diameter must be partially dehydrated before they are collected in settled beds. The "wet" gel (without dehydration) of this size shows excessive caking or coalescence when collected in multilayer beds. Also the chemical gelations can be so rapid that they interfere with formation of the spherical sol drops. We now prefer to extract water with isoamyl alcohol to form small gel spheres. The lower viscosity and the lower alcohol-to-sol volume allowable for the water solubility (9% compared to 2.5% for 2EH) simplify the separation of the gel spheres, but the more important advantages of the original process with 2EH are retained.

Optimization of Process Equipment

Any production use of the ORNL fluidized bed process for making spheres should be designed for a specific product or a relatively narrow range of similar products. Even when two or three different products are for one end use (as for spheres of different sizes for Sphere-Pac fuel elements), they are best produced in different lines optimized for the different products. This is because the problems will be different for the different products and the compromises to solve them will differ greatly. Differences in sol composition mean that different 2EH compositions are needed. Large spheres require conditions to minimize cracking or distortion, while small spheres require conditions to minimize sticking and clustering. Production of low-enrichment materials may be in large quantities, while high-enrichment materials will be in smaller quantities and will have to be in smaller equipment to provide critically safe geometries. No sol disperser is optimum for all sizes of drops. Therefore, optimum design and evaluation of a fluidized bed sphere forming system are possible only after a product size and composition are specified.

Once this is done, the selection of a sol disperser, the sizing of the column, etc. are greatly simplified.

Maximum Product Diameters. — The maximum practical diameter of product spheres is limited by one of three factors.

1. Cracking and distortions become much worse as the product diameters increase. These problems depend on the sol characteristics and alcohol composition, and the maximum practical diameter may be from less than 100 μ on up until other effects are controlling.

2. The initial sol drop size is limited because drops above a certain diameter will spontaneously break into two. This size limit depends on the interfacial tension and sol density and is commonly 1800 to 2000 μ (0.18 to 0.20 cm) for dilute sols in 2EH. For good sols, this would limit the product size to about 500 μ for 0.7 M UO_2.

3. Elongated gel particles are formed if the interfacial tension does not keep the drop spherical during gelation. This limit depends on the interfacial tension and the density at gelation. This limits the maximum product size for concentrated sols; for ThO_2 the maximum product sphere diameter is about 700 μ.

Avoiding limit (1) is discussed above, while limits (2) and (3) are inherent in the process flowsheet. If product diameters above 600 μ are of great importance, limits (2) and (3) might be increased with a high density fluidizing liquid, such as a mixture of tetracholorethylene with isoamyl alcohol. This would require a restudy of surfactant requirements. Also the optimum column configuration would be much different because the ratio of velocities of the gel sphere and the sol drop would be much larger. The initial sol must be denser than the organic or the sol drops will float at the organic surface.

Minimum Product Diameters. — The process has no inherent lower limit of product diameters, but there are good reasons to avoid fluidization if the sol drops can be gelled without fluidization. Eliminating fluidizing flows would simplify the process. The surfactants required to control sticking or clustering during fluidization may contribute to cracking, distortion, and carbon in the fired product or may be otherwise undesirable. The continuous operation of a fluidized bed requires uniform sol

drops; disperser operation is simplified if less uniform drops are acceptable.

Small spheres can be prepared without fluidization if the gelation is complete before the drops fall to the bottom of the vessel. This type of operation has been studied and was reported above. Both the settling velocity and the gelation time increase with the sol drop diameter, so the distance a particle will settle increases very rapidly with diameter — approximately proportional to the cube. An alcohol with a higher solubility for water would give proportionately shorter gelation times, but the settling velocity would be greater if the alcohol is also less viscous. The faster gelation usually increases distortion and cracking.

The sphere size that can be prepared without fluidization depends on the column height or head room allowable. For the usual range of sol molarities, the column height required for gelation varies mainly with the initial drop diameter and varies little with the initial sol molarity. The drop of less concentrated sol has a longer gelation time, but the average settling velocity is smaller. As a first approximation, the maximum drop size of 1.2 to 2.5 M sols that will gel in 2EH of 0.5 to 1 vol % water without fluidization is:

Column height, ft	2	8	16	32
Maximum initial drop size for gelation, μ	230	360	450	600

The same sol drops can be gelled in one-half to one-third of these heights in isoamyl alcohol, but distortions and cracking are very probable for initial sol drop diameters larger than 300 μ.

Chemistry of Microsphere Forming Column

W. D. Bond A. B. Meservey K. J. Notz

Our principal purpose has been to study the chemical variables associated with the operation of 2EH UO_2-microsphere-forming columns using Span 80 and Ethomeen S/15 as surfactants at room temperature. Fundamental knowledge of the mode of operation of these two surfactants, for example, may allow operating the columns more predictably. This study

area involves the interactions of two complex colloidal systems — UO_2 and other sols, and surfactants. Complexity is increased by the use of two liquid phases (aqueous and organic) and the use of two surfactants whose combined effects differ from their separate effects. In summary, the chief findings are as follows.

1. The pH of the 2EH containing Ethomeen S/15 profoundly affects bead clustering and coalescence. For example, in 2EH containing 1.5% Span 80, 0.5% Ethomeen S/15 and 1.2% H_2O, microspheres formed from a UO_2 sol were perfect at pH 3.5, but as NH_4OH was added clustering began at pH 4.0 and became severe at pH 6.5. In ThO_2—25 mole % UO_3 sols formed in 2 EH containing 0.05% Ethomeen S/15 without Span, clustering took place at pH 6 to 7 but disappeared at pH 2. This explains some of the column startup difficulties experienced with fresh batches of 2EH before it had become acidified by long contact with the acidic sol. The remedy, of course, is slight initial acidification of the 2EH before column startup. Measurement of the pH of the 2EH by direct immersion of electrodes is possible but somewhat erratic and unreliable because of the extremely low electrical conductivity (for example, 0.03 μmho/cm for 0.001 M HNO_3 and 1.5 vol % H_2O). A more reliable and stable value results from measuring the pH of an equal volume water extract of the 2EH, whose conductivity is much higher (300 μmho/cm for the above example). These are the pH values quoted above. In a production microsphere column at equilibrium, this aqueous pH was 0.5 to 0.8 units lower than that measured directly on the organic phase.

2. When the 2EH contains 0.1% Span 80 without Ethomeen S/15, UO_2 sol droplets do not cluster up to a pH of at least 4.8. Bead defects resembling blowholes occurred in a precipitation-type sol at a pH of 2.2 (after extraction), but no defects were found in beads from a solvent-extraction sol. In 0.05% Ethomeen without Span UO_2 clustering continued even down to pH 2.1.

3. Gel beads were susceptible to severe oxidation and subsequent breakage in air in a few hours when formed in 2EH columns at pH 2.2 to 2.4 (aqueous extract). The oxidation behavior differed between the two types of UO_2 sols and between the two surfactants. The gel beads resisted air oxidation for many days when formed at pH 3.5 to 4.8.

4. The pH of the 2EH also affects the organic-to-aqueous distribution coefficients (O/A DC) of the two surfactants and alters the fate of the nitrate ion, as follows: (a) Ethomeen S/15 reacts with HNO_3 (at acidic pH) to form a compound with a high O/A DC (not yet measured). Nitrate is thus extracted from the sol and carried over into the 2EH distillation column, where it causes oxidation reactions. The nitrate removal problem is thus related to Ethomeen content and to pH. (b) Span 80 does not extract nitrate from the sol. The Span has a high O/A DC only when the 2EH is basic, which would be foreign to the mode of operation with acidic sols. When acidic, the Span 80, under pH conditions not yet defined, can have a low O/A DC, which could cause Span depletion by loss to the sol.

5. Interfacial film studies were made to find conditions for minimizing the water solubility of this film between the sol (aqueous phase) and 2EH (organic phase). Film insolubility in water promotes the stability of water-in-oil emulsions, and by analogy in our sol-2EH system should minimize bead coalescence and clustering. Minimum film solubility occurred with Ethomeen and Ethomeen-Span mixtures when acidified to about 0.005 M HNO_3 in 2EH, and maximum film solubility (hence, maximum bead coalescence) occurred when the pH was slightly basic. Span 80, by these film studies, was a poor emulsifier when compared to Ethomeen S/15.

6. Microsphere pitting studies, still in progress, have shown several causes of the uneven shell hardening that results in pits. With UO_2 sols, for example, wrinkle pits appear from drying with 2EH–0.05% Span 80 when the UO_2 sol has been oxidized above 12% U(VI). With solvent-extracted ThO_2-UO_3 sols, Span 80 is a pit-promoter, and Ethomeen S/15 is the antidote under some conditions. Even steam-denitrated thoria sol, normally pit-resistant, is pitted slightly by 0.5% Span 80–0.05% Ethomeen S/15 in 2EH containing little water (0.5%). Pitting occurred also for ThO_2-UO_3 sols with Ethomeen only as functions of water, acid, and Ethomeen concentrations, and it also depended on sol properties.

7. Cracking in mass-produced solvent-extracted ThO_2–25 mole % UO_3 microspheres led to studies on the optimization of column chemistry conditions for these sols. The main finding was that these sols are exceptionally prone to crack and pit in the 2EH column unless produced

with a sol digestion step to enhance crystallinity. Column conditions that produced the best microspheres from the most sols tended toward using about 0.05% (0.001 M) Ethomeen S/15, about 1 to 1.5% H_2O, and nitric acid adjusted to 0.001 M in the 2EH. The inclusion of Span 80 in the 2EH again caused pitting, partly remedied by increased Ethomeen concentrations. Sols of the composition ThO_2–19 mole % UO_3, produced by countercurrent solvent extraction and digested for increased crystallinity, produced good microspheres over wider operating levels.

A report[13] on microsphere forming conditions for ThO_2-UO_3 sols was issued. An abstract is given below.

> The effects of three variables in the sphere forming column solvent (2EH) on the properties of microspheres produced from ThO_2-UO_3 sols were examined by a 2^3 factorial experiment. The three variables tested were: water content (at 0.4 and 1.6%), acidity (at 0.001 and 0.01 N), and Ethomeen S/15 content (at 0.05 and 0.5%). Over this range of variables a very wide range of microsphere qualities was obtained, and a pictorial evaluation is included. The low Ethomeen level gave the least cracking and deformation, and also two cross effects are prominent, namely, acid × Ethomeen, and water × Ethomeen. The nature of these cross effects is such that improved product yield is obtained when acidity and Ethomeen are in balance (either both high or both low), and when water and Ethomeen are out of balance. All of these conditions are satisfied when acidity and Ethomeen content are low and water content is high. Other less general effects were also noted. Five oxide sols were tested; of the four cocurrent produced sols, those that had been digested either during or after the concentrating step gave the best microspheres. The one countercurrent produced sol, with a low nitrate-to-metal ratio, performed well. The factorial design was replicated with three of the sols; in general, replication was good, but a number of prominent differences occurred. The significance of these differences is discussed.

Sol-Gel Process and Equipment Demonstration

P. A. Haas C. C. Haws

The objective of these studies is to demonstrate processes and equipment for remote operation for the recycle of thorium and ^{233}U to

---

[13] K. J. Notz and A. B. Meservey, Microsphere Forming Conditions for ThO_2-UO_3 Sols: A Factorial Experiment, ORNL-TM-2516 (April 1969).

heterogeneous reactors. We have emphasized the development of procedures and prototype equipment for preparing oxide microspheres in the Thorium-Uranium Recycle Facility. These studies seek: (1) to improve and to simplify existing equipment and operations, (2) to obtain data on the reliability and behavior of both the equipment and the process over extended operating periods, (3) to adapt the equipment to the exacting requirements of remote operations, and (4) to provide 100-kg lots of ThO_2 microspheres for use in large-scale pyrolytic carbon coating experiments.

Pilot plant operation covers two periods, one in which the equipment originally built for large-scale (1 kg ThO_2/hr) microsphere preparation was operated and another in which a new and greatly simplified pilot plant of the same scale was tested. Thoria sols were used almost exclusively in this work because of our overriding interest in equipment and the availability of large quantities of high-quality thoria sol. Equipment development is now sufficiently advanced to allow UO_2 feeds to be processed when operation resumes. The pilot plant was shut down in October 1967 to await development of ThO_2-UO_3 and UO_2 sol preparation in sufficient quantity to make pilot-scale operations practical.

Extended, stable operation of the column has been demonstrated with ThO_2. During the early period, the entire system was emptied and filled twice with 2EH. Each charge (about 45 gal) was used for about 300 hr of operation in the column-distillation system. Operation was satisfactory with both charges.

Samples of 2EH were analyzed for nitrate ion, amine, total nitrogen, and thorium periodically throughout each of the two periods. The results of these analysis over the last four months of the second charge (Table 3.10) show no trend with time for the three suspected degradation products. Only thorium (ThO_2) concentration built up steadily throughout the period, causing turbidity of the solvent. This buildup was primarily the result of occasional equipment malfunction. Turbidity hindered visual observations of microspheres through the column wall and was the prime reason for discarding both 2EH loadings; however, the alcohol could have been used longer if we had so desired. The thoria causing the turbidity was present as extremely fine particles (300 A), which settled out upon long standing (15 days), leaving clear 2EH.

Table 3.10. Concentration of Impurities in the 2EH Related to Length of Time of Column Operation with ThO_2

Impurity	Concentration (M)	Trend with Time
	$\times 10^{-4}$	
Nitrate ion	1.5 to 4	None
Total nitrogen	2.0 to 5	None
Amine	6.0 to 10	None
Thorium	2.0 to 7	Increasing

Operating the original pilot plant, 250 kg of 210- to 250-μ-diam and 150 kg of 250- to 590-μ-diam ThO_2 were prepared. An uninterrupted period of sustained operation was undertaken to demonstrate the reliability of the equipment and the process. A full month of operation was scheduled on a two-shift-per-day basis three days per week and carried out without event. During this test 140 kg of 210- to 250-μ microspheres were produced. Note that product yields ranged from 60 to 70%; thus the quantities of thoria fed to the column were correspondingly larger.

Surfactants must be added to the 2EH to prevent coalescence of droplets, sticking of droplets on column walls, and clustering of partially dried drops. Adequate control of surfactant concentration was simple. Surfactants were added to each charge of fresh 2EH. For thoria sols these were 0.3 vol % Ethomeen S/15 and 0.07 vol % Span 80. At the start of each shift, surfactants were added in amounts proportional to the volume of sol fed during the previous shift. These additions were 10 ml of Ethomeen S/15 and 2.5 ml of Span 80 per liter of ThO_2 sol. When we operated with mixed sols (ThO_2–25% UO_2) the concentration of each surfactant was adjusted to 0.5 vol %. Subsequent adjustments at the beginning of each shift were 10 ml of each surfactant per liter of sol fed during the previous shift. This empirical method was adequate under all operating conditions.

For producing uniform sol drops, two-fluid nozzles were the most flexible of the dispersers tested. Single two-fluid nozzles gave an 85% yield of microspheres in either the 210- to 250-μ or 500- to 590-μ size

range. Using 6- to 11-nozzle parallel arrangements of the basic two-fluid nozzles, we obtained yields ranging from only 70 to 55% of the 210- to 250-μ-diam product. Even so, the bulk of the beads was not in the desired size range (210 to 250 μ) but fell within the 250- to 297-μ range. The combined yield of these two size fractions usually exceeded 90%. Thus if our specification for this narrow size range could be increased to 210 to 297 μ a much larger quantity of product would be available. A plastic cup with a perforated bottom gave excellent yields if only larger sizes were needed. This cup (with thirty-three 0.010-in.-diam orifices in its bottom) gave yields of 90% in the 350 to 500 μ range. Its simplicity is a great advantage.

Because the original pilot plant was complex to operate, and our work suggested some design changes, we dismantled the old equipment and essentially replaced it by a new installation, whose flowsheet is shown in Fig. 3.7. These changes and their effectiveness are described below.

1. Settler Installation. — Filters placed in process lines in the old equipment effectively removed dry gel microspheres. However, any faulty operation of the column allowed wet particles to enter one of the five recirculating pumps before they could reach a filter. Passing through a pump effectively dispersed the wet particles, causing the build-up of thoria turbidity in the 2EH. Settlers were designed and placed in the circuit at the overflow of the forming column and on the inlet side of the dryer to remove any wet particles occurring at these column exit points (see Fig. 3.7). Four months of operating with a single charge of 2EH has resulted in only a slight browning of the 2EH (from surfactant degradation products). The thoria sludge encountered in earlier work is absent, and the alcohol is water-clear.

2. Simplification of the Process Flowsheet. — The new pilot plant was rebuilt around one pump (rather than five in original equipment). Of the original equipment, only the distillation train and the glass sphere-forming column were retained. Elevations were selected for each equipment piece to allow unimpeded gravity-flow return of the 2EH to a single surge tank. All level controls and control valves were thereby eliminated along with the possibility of overflowing any piece of process equipment.

ORNL DWG 67-3687R2

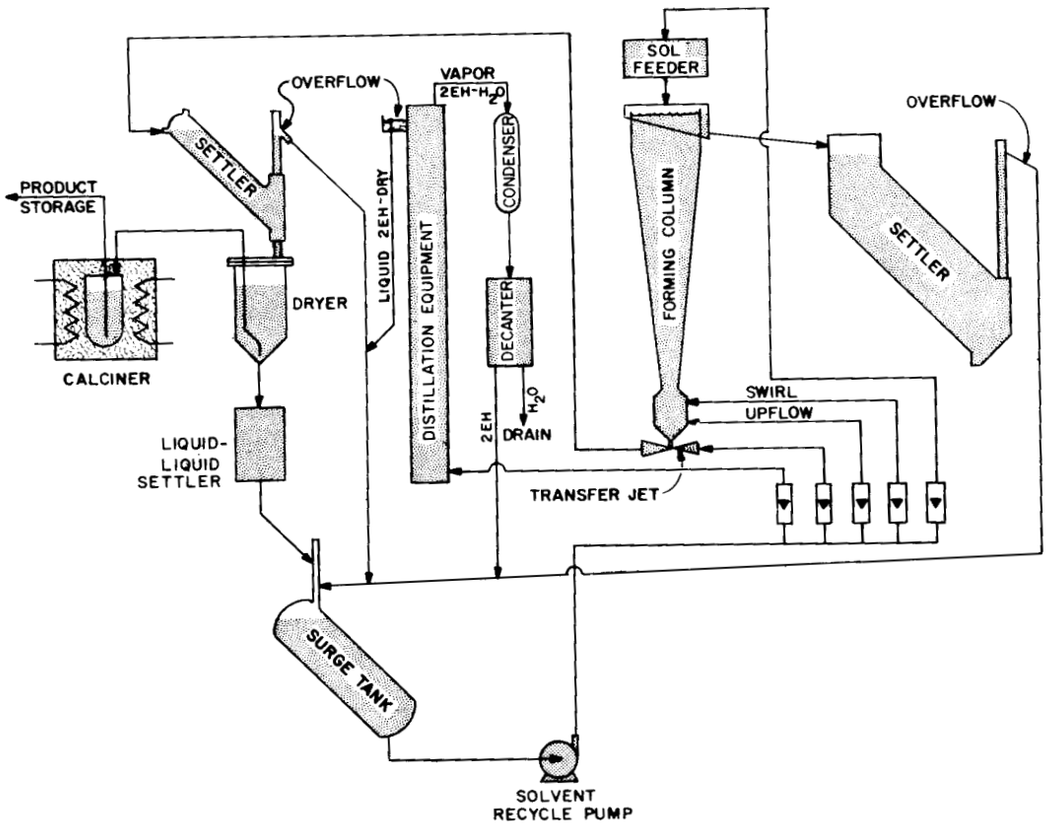

Fig. 3.7. Improved and Simplified Equipment Flowsheet. A one-pump solvent recycle system.

3. Material Transfers. – In the new equipment, all material transfers are accomplished either pneumatically, hydraulically, or by gravity. No manual or mechanical transfers are required. This system has been tested and performs well. Microspheres falling from the bottom of the forming column are continuously transferred by hydraulic jet to the settler-dryer. Batches of dried microspheres are pneumatically transferred from the dryer to a storage hopper above the calciner. The calciner is loaded by gravity and discharged pneumatically to a storage hopper.

4. Dryer and Calciner. – The features of a prototype dryer design are shown schematically (Fig. 3.7). The ThO_2 microspheres enter the settler with the 2EH transfer fluid. Part of the 2EH flows down through the

stainless steel wire cloth in the dryer bottom, while the rest overflows the settler. Both streams combine and return to the column circuit. The microspheres remain on the screen. The settler was installed to allow the transfer jet to operate at constant pressure, since otherwise the pressure drop across the bed of microspheres increases as the dryer is filled. When the dryer is filled with microspheres, excess 2EH is blown down through the screen with nitrogen, the steam is turned on, and the bed is allowed to dry (150 to 250°C). After drying, the batch is transferred pneumatically to the calciner station.

In the conceptual design of the remotely operated calciner the charge is contained in a crucible fixed in the furnace. The charge will be loaded by gravity and discharged pneumatically. The present calciner is actually a muffle furnace with crucibles loaded by hand.

Performance of the new equipment was outstanding. Over a four-month period of operation no equipment breakdowns or process upsets were experienced. Column operation and the equipment in the forming column part of the circuit appear adequate for remote operation. The settlers in the column circuit effectively dry and remove fines; turbidity of the 2EH (due to suspended ThO_2 fines) is no longer a problem. Additional particulate removal and flexibility in operation of the microsphere transfer jet are obtained by the settler in the dryer circuit.

An in-line, hydraulic transfer sampling device for taking microspheres from the bottom of the column was built and successfully operated. The microspheres may be examined optically in the sampler for shape and surface characteristics and then returned to the system. The optical requirements necessary for this examination and for the observation of droplet formation were defined.

Additional work will be required to improve the dryer and the calciner for remote operation. Loose sintering of ThO_2 microspheres and apparent devitrification of the crucibles (99% Al_2O_3) were observed in firing. The sinters of ThO_2 microspheres are easily broken but may prove troublesome in the proposed deep-bed calciner operation. Devitrification can be eliminated by prefiring the microspheres to 500°C, a possible extension of dryer operation.

Material Preparation

P. A. Haas

Materials supplied as samples to other parts of this program or to related programs furnish the most reliable illustration of typical properties for sol-gel products. Large samples of microspheres from ThO_2 or ThO_2-UO_3 sol were supplied from operation of the CPDL microsphere preparation system (Table 3.11). Smaller samples of special compositions or sizes were prepared from operation of smaller process development equipment (Table 3.12).

Table 3.11. Thoria Microspheres Supplied from Operation of the CPDL Microsphere Preparation Pilot Plant[a]

Particle Size Range (μ)	Amount Delivered (kg)	Disposition
88–125	10	M and C Division, to be coated with pyrolytic carbon
210–250	95	M and C Division, pyrolytic carbon coating development studies
250–297	10	M and C Division, pyrolytic carbon coating development studies
297–420	42	M and C Division, pyrolytic carbon coating development studies
350–500	40	M and C Division, pyrolytic carbon coating development studies
350–500	20	For HTGR fuel sticks – processing studies
420–500	2	For power reactor fuel reprocessing studies
350–500[b]	7[b]	For firing development studies
420–400	1	Babcock and Wilcox Company
420–590	5	M and C Division, for thermal conductivity measurements

[a]Supplied from January 1967 through February 1968; the column did not operate after October 1, 1967.

[b]$(Th,U)O_2$ from ThO_2-UO_3 solvent extraction sol preparation.

Table 3.12. Typical Properties of Fired UO_2 Microspheres[a]

Composition or Sol	Transferred		Size (μ)	Amount (g)	Density (g/cm³)[b]	Surface Area (m²/g)	Analyses	
	Date	To					Carbon (ppm)	O/U Ratio
47-8-97	6-27-67	M and C Division	210–250	125	10.54		180	< 2.002
47-8-97	6-27-67	M and C Division	210–250	97	10.18		150	< 2.002
20% ^{235}U	9-11-67	M and C Division	350–420	549	10.62	0.006	140	2.0022
F-56	9-27-67	M and C Division	150–250	617	10.01	0.011	400	2.000
P^2C^2D-6C			350–500	510	10.60	0.008	30	2.002
F-83			150–500	380	10.91		< 20	2.007
EV-7			~ 400	190	10.59	0.017	50	2.007

[a]From UO_2 sols prepared by precipitation, except EV-7, which was prepared by solvent extraction.

[b]By mercury porsimetry at 100 or 200 psi.

4. FUELED-GRAPHITE FABRICATION DEVELOPMENT

F. J. Furman J. D. Sease

We are developing methods to fabricate recycle fuel particles, fuel sticks, and fuel elements. The necessary quality control inspection procedures also must be developed. Since the fuel will contain significant quantities of ^{232}U, all processes will have to be remotely operable and the equipment remotely maintained. Central to the fabrication operation is the particle coating. Considerable progress has been made in developing large-scale equipment for this operation. Inspection procedures for assuring quality of product have been developed. For transferring particles between various operations and eliminating unacceptable particles, various handling techniques have been developed. Work has been done on blending and bonding of particles into fuel sticks. These aspects of fueled-graphite fabrication development are discussed further in the following paragraphs.

Particle Handling

S. E. Bolt J. T. Meador F. J. Furman

The fabrication of HTGR particulate fuels requires the transfer and classification of kilogram amounts of 150- to 850-μ-diam ^{233}U-bearing particles. Equipment has been developed to do these tasks remotely. Transfer equipment includes pneumatic lines between storage hoppers and processing equipment and various connections to feed multiple lines into a single line or divert one line to another.

The transfer equipment moves particles through 1/4-in.-diam stainless steel lines pressurized by air or argon. The particles fall by gravity into the line through which the transfer gas is flowing. The particles are then carried by the gas and are injected into a cylindrical receiving hopper. A transfer line 50 ft long with a 15-ft rise in elevation has been used to repeatedly cycle particles over an extended period. All components were reliable, and only minor particle abrasion occurred.

Classification equipment consists of vibratory screens to remove over- and undersized particles and shape separators to remove irregularly shaped particles. The vibratory screens are in stacks of two or more so that over- and undersized particles are removed in one operation. The shape separator is a flat plate on which the particles are slowly fed. The plate is vibrated in one direction and tilted in another. The irregular particles move in the direction of the vibration, while the spherical particles roll with the tilt; thus a separation is achieved.

Although this equipment has been used only on a laboratory scale, only minor modifications are needed to redesign and scale the equipment for a remotely operated production process.

Particle Coating

R. B. Pratt C. F. Sanders W. H. Pechin

Deposition of pyrolytic carbon coatings on nuclear fuels is probably one of the more difficult and expensive steps in the fabrication of HTGR fuel elements. Analysis has shown that increasing the production scale of coated fuels can reduce the cost of this step. Therefore, we are developing a pilot-scale process for depositing pyrolytic carbon coatings on sol-gel particles in quantities to 10 kg/day. Not only do we have the normal problems of increasing the scale of a process, but we are also concerned with ensuring that the process is suitable for remote fabrication of ^{233}U-bearing recycle fuels in the Thorium-Uranium Recycle Facility (TURF).

We have been establishing cold-processing equipment, delineating coating parameters, and designing and fabricating a prototype remotely operated fluidized-bed coating system. We have made significant progress in each of these areas.

The 5-in.-ID coating furnace system has become existing technology and is operated routinely. Enough coating parameters have been defined that most coatings can be reproducibly controlled over a wide range of specifications. We are continuing to investigate deposition of low-density

coatings from acetylene along with our main effort to characterize high-density coatings produced from propane and propylene.

Major progress was made on a prototype of an in-cell, remotely operated coater, for which installation is 95% complete.

The 5-in.-ID Coater

Coating development has been done in a furnace consisting of a cold-wall, three-phase, carbon-element resistance unit capable of 2500°C at steady-state nonflow conditions. Pyrolytic carbon coatings are deposited on fuel particles by pyrolyzing hydrocarbon gases in a 5-in.-ID graphite reaction cone located within the heating zone of the furnace. Particles are fluidized in the reaction cone by gas introduced at the bottom of the cone through a water-cooled nozzle, as shown in Fig. 4.1. The furnace is mounted on a motor-driven frame, which separates the components for maintenance and evaluation.

The overall coating system also includes components for loading, unloading, and effluent disposal. Figure 4.2 schematically illustrates the relationship of the coating furnace to the process gas and effluent disposal systems.

The flow control system for gases consists of routes for hydrocarbon, diluent, and inert carrier gases. It establishes a carrier gas flow, which fluidizes the particles while the furnace temperature is stabilized. Frequently process control requires mixing an inert diluent such as helium with the hydrocarbon gas. The hydrocarbon gas or mixture is routed to a three-way valve, which substitutes the hydrocarbon gas for carrier gas for a predetermined time period during which the hydrocarbon is pyrolyzed. At the end of the coating period, carrier gas replaces the coating gas, and the furnace is cooled and unloaded. The gas control panel used in these experiments was originally designed for use with a dual-flow nozzle system but has since been modified to increase its total flow capacity for use with the single-flow, water-cooled nozzle. A schematic diagram of the gas control panel is shown in Fig. 4.3.

ORNL-DWG 67-5480

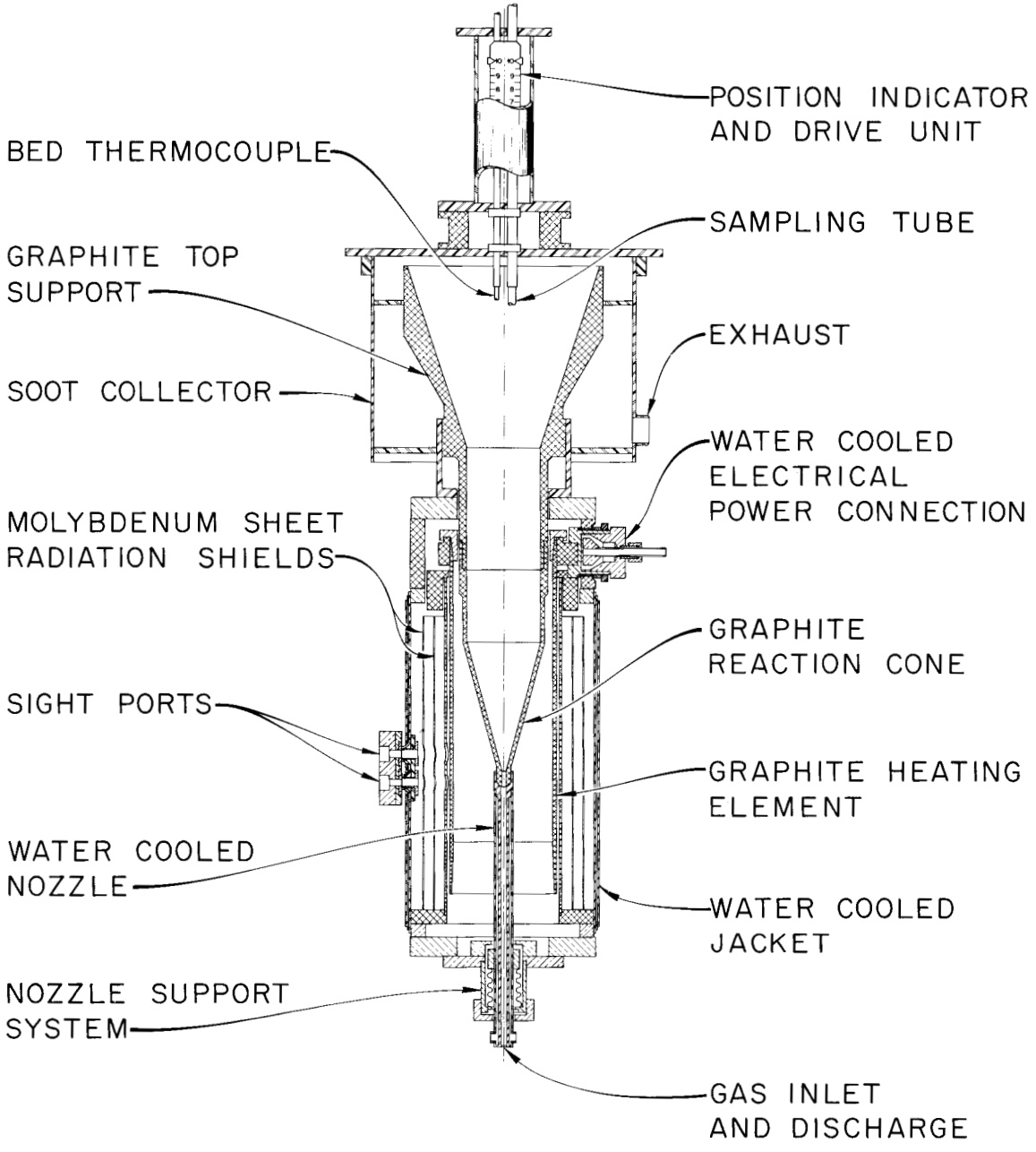

Fig. 4.1. Sectional View of the 5-in.-diam Coating Furnace.

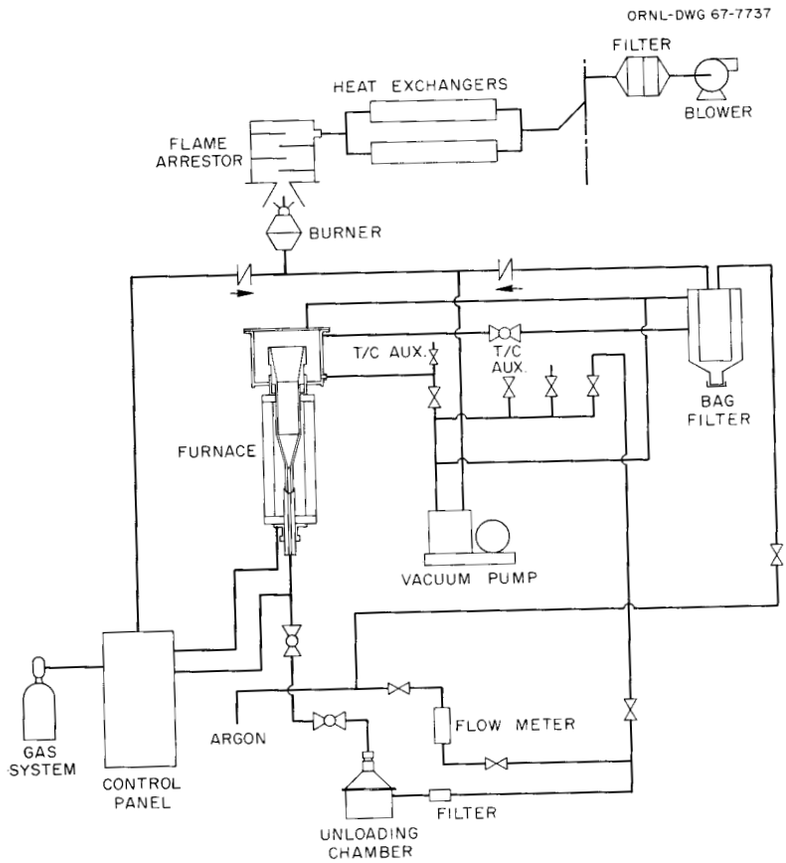

Fig. 4.2. Schematic Diagram of the Process Piping for the 5-in.-diam Coating Furnace.

The effluent system is concerned with products of the pyrolyzing reactions, namely hydrogen, uncracked hydrocarbon gases, and soot. Soot particles are removed by a bag filter, while hydrogen and uncracked hydrocarbon gases pass through the filter and are ignited and burned in a center-diffusion burner. The combustion products are cooled and discharged to the building exhaust system, where they pass through high-efficiency filters before being released to the atmosphere.

Development of this equipment has enabled us to extend particle coating technology from laboratory-size systems to an engineering-scale system capable of quality and quantity production of coated nuclear fuels.

ORNL-DWG 67-7736

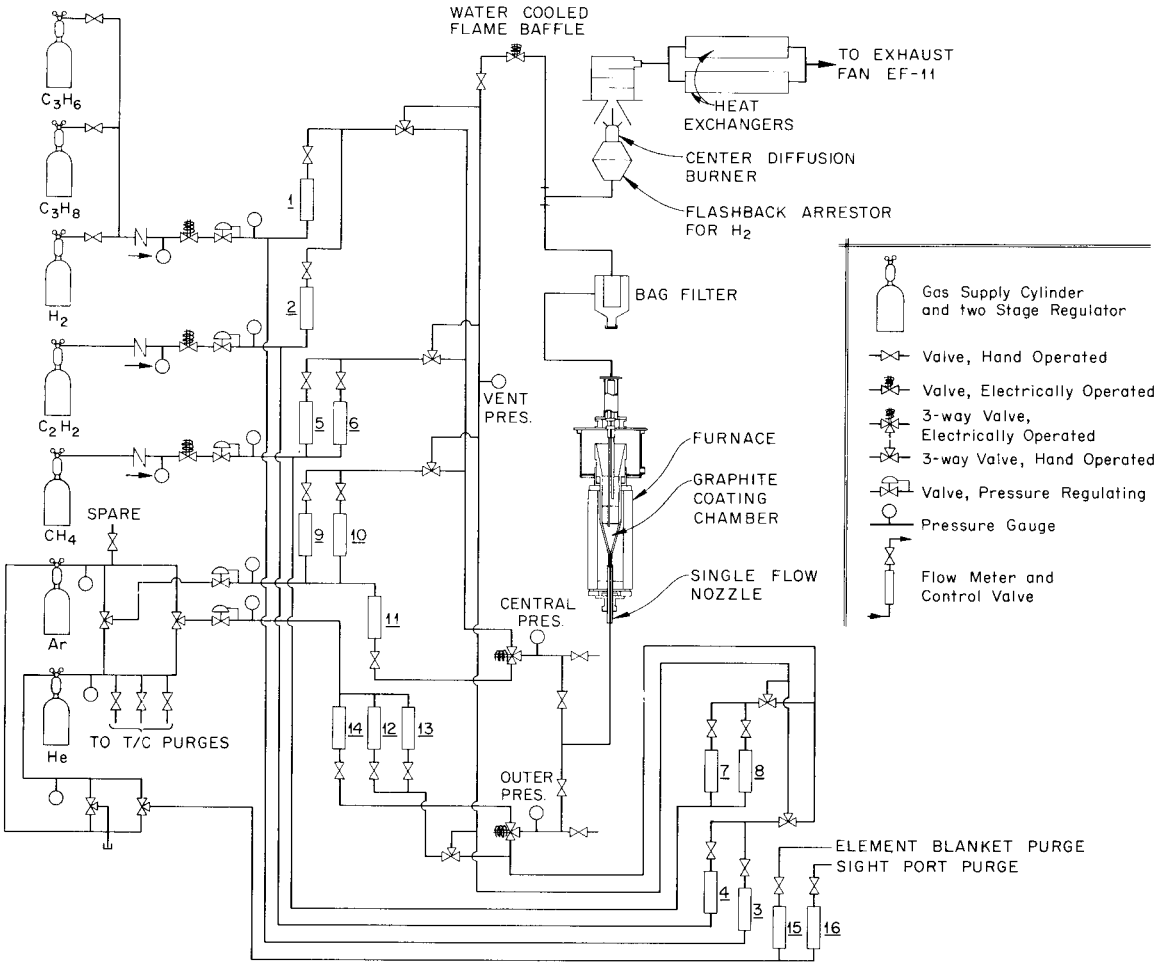

Fig. 4.3. Gas Control Panel Schematic Diagram.

Coating Process Development

The principal requirements for HTGR-type coatings are that the particles should have triplex pyrolytic carbon and silicon carbide coatings. The interior coating is pyrolytic carbon having a density less than 1.0 g/cm^3, the middle silicon carbide with a density near 3.2 g/cm^3, and the outer layer is isotropic pyrolytic carbon having a density near 2.0 g/cm^3. Our developmental work is directed toward describing the best combinations of processing conditions, gases, and equipment for coating fuel particles to these specifications. These coatings were deposited by a batch-type fluidized-bed coating process.

Low-Density Coatings. — Low-density coatings were deposited by pyrolysis of acetylene. Our development of the low-density coating process was based on laboratory-scale work performed by Beutler *et al.*[1] Material logistics required that most experiments be done on 500-g charges, although charges as large as 2 kg were coated. For our system, effluent disposal capability limited batch sizes to 2 kg. All of our process development was done using sol-gel microspheres having a mean diameter of 230 μ.

The low-density coating properties of interest include density, mean thickness, and thickness variations, both within a batch and from batch to batch. The principal conditions that affect coating density are bed temperature, the amount of diluent in the hydrocarbon gas, and gas flux, which is the ratio of the total gas flow rate to the initial charge surface area. The effects of bed temperature, gas flux, and helium dilution on coating density have been reported.[2] Manipulating temperature, dilution, and gas flux has yielded densities ranging from 0.35 to 1.4 g/cm^3.

In general, the coating rate and deposition efficiency (the ratio of carbon deposited to carbon supplied) increased with rising temperature. Coating rates were rapid, ranging from 10 to 40 μ/min. For 50-μ-thick coatings, coating thickness standard deviation within a batch ranged from 5 to 10 μ. Larger batch sizes did not significantly shift any of the coating properties except that coating thickness variation within a batch apparently improved. In production runs, the batch-to-batch density variation could be controlled to within the experimental error of the density determination. Coating thickness was more difficult to control from batch to batch. The observed thickness standard deviation was 3.5 μ.

Silicon Carbide Coatings. — The silicon carbide coatings were applied over the low-density inner coating after a thin sealer layer of

---

[1]H. Beutler, R. L. Beatty, and J. H. Coobs, "Low-Density Pyrolytic-Carbon Coatings for Nuclear Fuel Particles," Electrochem. Technol. 5(5–6), 189–194 (May–June 1967).

[2]R. B. Pratt and S. E. Bolt, Status and Progress Report for Thorium Fuel Cycle Development Dec. 31, 1966, ORNL-4275, pp. 61–78.

high-density pyrocarbon had been deposited over it to prevent leaching of the oxide kernel by hydrogen chloride during coating. Methyltrichlorosilane (CH_3SiCl_3) was the source of silicon and carbon. For coating in a 3-in. laboratory-scale coater, we used fluxes of 0.125 to 0.310 cm^3 min^{-1} cm^{-2} CH_3SiCl_3 diluted with 8 to 11 times as much hydrogen to provide the necessary reactants with sufficient gas to fluidize the bed of particles. Deposition temperatures used were 1500 to 1600°C. The particles were (400 ± 100)-μ-diam thoria coated with 75 μ of pyrocarbon inner layer in batch sizes of 500 to 1000 g.

High-Density Isotropic Outer Coatings. — The high-density isotropic coatings were applied over the buffer coating or silicon carbide at low temperatures, with propane and propylene as the hydrocarbon sources. This work was based on laboratory-scale work done by Scott and Beatty.[3] Properties of interest for applying high-density coatings include those of interest for low-density coatings plus the additional requirement that the deposits be nearly isotropic.

In Fig. 4.4 properties of coatings deposited from propane on buffer-coated ThO_2 particles at gas fluxes of 1.0 and 2.0 cm^3 min^{-1} cm^{-2} are compared as functions of temperature. The best compromise between coating density, deposition efficiency, coating rate, and anisotropy factor appears to be a bed temperature between 1250 and 1300°C and a gas flux of 1.0 cm^3 min^{-1} cm^{-2}. In this region, coating density ranged from 1.98 to 2.02 g/cm^3, efficiency from 15 to 25%, coating rate from 0.9 to 1.1 μ/min, and anisotropy factor from 1.07 to 1.2.

Differences between propane and propylene were minimal; propane produced the densest coating, and anisotropy of coatings produced from propylene was less temperature-sensitive. For both gases, the coating efficiency and rate are strong functions of temperature. For coatings of interest, efficiencies ranged from 20 to 50% and coating rates ranged from 2 to 6 μ/min.

---

[3] J. L. Scott and R. L. Beatty, "Pyrolytic-Carbon Coatings Formed at High Deposition Rates," (Summary) Trans. Am. Nucl. Soc. 10(1), 96 (1967).

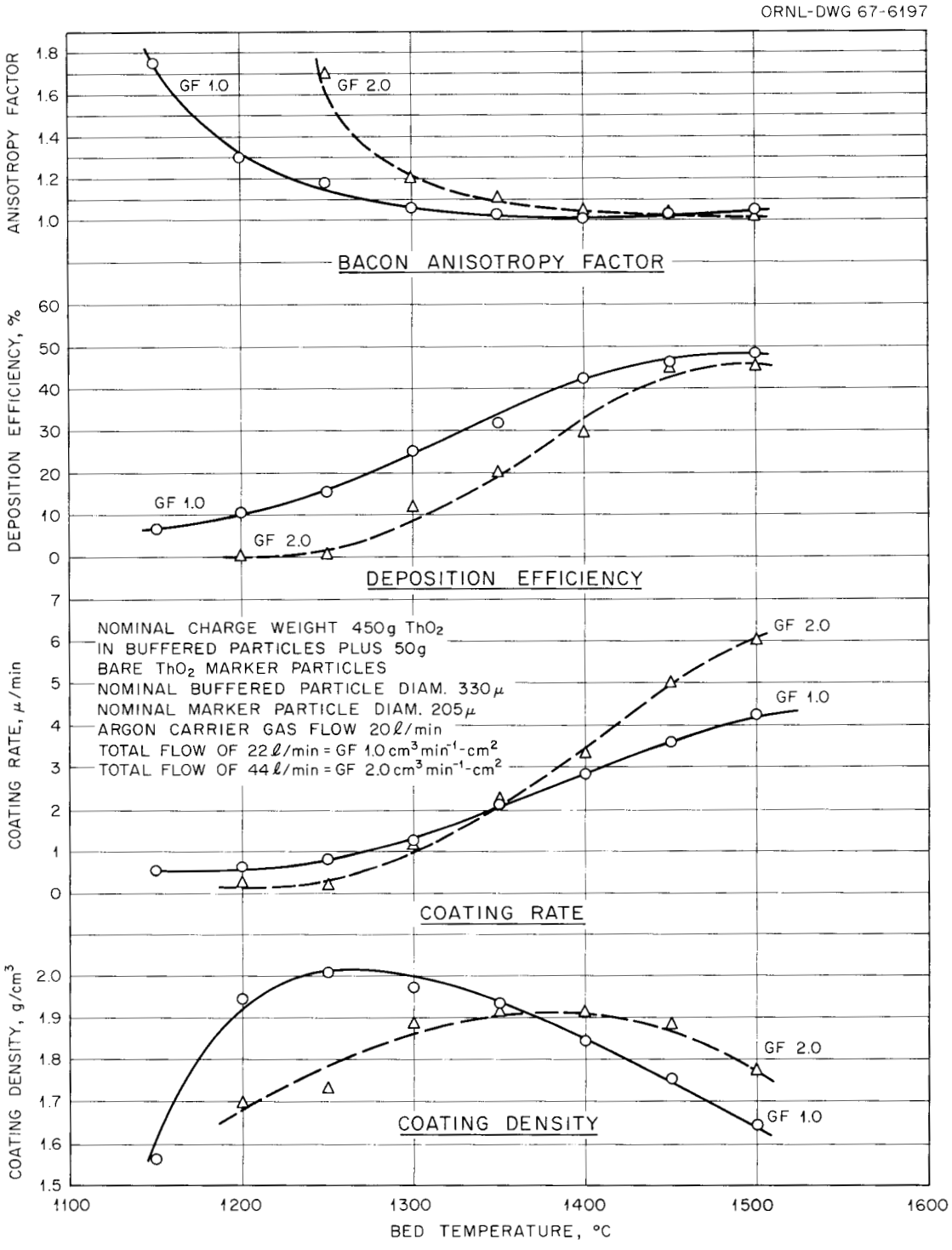

Fig. 4.4. Properties of Propane-Derived Coatings Deposited on Buffer-Coated ThO_2 Particles at Gas Fluxes of 1.0 and 2.0 cm^3 min^{-1} cm^{-2} as Functions of Temperature.

Remote Coater

The design of a prototype remotely operated coating system has been described.[4] At present, construction is approximately 95% complete.

The remote prototype coater also serves as a vehicle for demonstrating instrumentation philosophies proposed for TURF processing equipment. Means for preprogrammed or manual operational modes are provided. Critical system parameters are automatically monitored and provided with appropriate safety interlocks and are compatible with the data logging and computer control system ultimately proposed for the fueled graphite fabrication process.

Particle Inspection

W. H. Pechin S. E. Bolt F. J. Furman

The quality of all fuel produced in a fabrication operation must be determined to assure reliable reactor operation and prevent costly reactor shutdowns or early refueling. The required particle specifications are determined before large-scale fabrication by irradiation experiments as described in Chapter 5 of this report. The particle specifications include coating anisotropy, density, and thickness. Inspection for these properties must be made quickly and accurately to ensure process control. The present status of development of these inspection operations is described in the following paragraphs.

Measurement of Coating Anisotropy

The anisotropy of the carbon coating has a pronounced effect on the coating performance. A coating as nearly isotropic as possible is desirable. The anisotropy is described in terms of the Bacon Anisotropy Factor[5] (BAF), which is determined from an x-ray diffraction analysis of

---

[4] R. B. Pratt and S. E. Bolt, Status and Progress Report for Thorium Fuel Cycle Development Dec. 31, 1966, ORNL-4275, pp. 61–78.

[5] G. E. Bacon, "A Method for Determining the Degree of Orientation of Graphite," J. Appl. Chem. (London) 6, 477–481 (1956).

the coating deposited on a flat disk charged to the furnace along with the particles. The high-density coating should have a BAF as near 1.0 as possible and certainly less than 1.1.

We have adopted the method of judging the acceptability of the coating anisotropy from the appearance of the "Maltese Cross" when metallographic samples are viewed under polarized light.[6] This appears to be an acceptable semiquantitative method when used for coatings of similar structure and BAF less than 1.3.

Measurement of Coating Density

Coating density is determined by measuring the density of the coated particles with a mercury porosimeter and measuring the weight of carbon per unit weight of kernel by burning off the carbon coating. This information together with the known kernel density allows one to calculate the density of the coating. The mercury porosimeter measurements are made at a pressure of 80 psig to ensure that the space between particles is filled with mercury. For particles with duplex coatings, when the volume and weight of the first coating were subtracted from the mercury porosimeter and burnoff results to allow calculation of the outer coating density, the density was found to be higher than the theoretical density of graphite. This was attributed to the deposition of carbon inside the pore structure of the low-density coating, increasing the weight of carbon with no increase in volume.

This infiltration effect has been investigated by including undersized bare particles with each batch charged to the furnace for overcoating. These undersize particles are sifted out after the run and used to determine the density of the overcoat. With this information the fraction of the open porosity in the buffer coat that is filled during the overcoating can be calculated. This fraction can be as high as 55% with propylene and 70% with propane.

---

[6] R. J. Gray and J. V. Cathcart, "Polarized Light Microscopy of Pyrolytic Carbon Deposits," J. Nucl. Mater. 19, 81–89 (1966).

Particle Counting and Size Analysis

In a typical high-temperature gas-cooled reactor, the fuel loading tolerances are ±1% for the complete core or ±5% for an individual fuel element. To obtain the tolerances required, the size and density of the fuel particles before and after coating must be accurately known. In a large-scale production facility, these determinations must be made swiftly to keep the process under control. The conventional means of determining particle size by microradiography and the density by sink-float or combustion are too slow. For the rapid determination of these properties we favor a particle-size analyzer that will determine precisely the diameter of a large number of particles and at the same time count the number of particles in a given weight of material.

Considerable progress in particle-size analysis has been made in the past two years. A particle-size analyzer has been obtained and, after development, should fulfill these needs. The principle of operation is shown in Fig. 4.5. The sample, which may be in air or a clear fluid, passes in front of a light beam. The passage of a particle interrupts the light beam, and the magnitude of the interruption is proportional to the size of the particle. The decrease in light produces a dip in the photodetection output current. This current dip, again

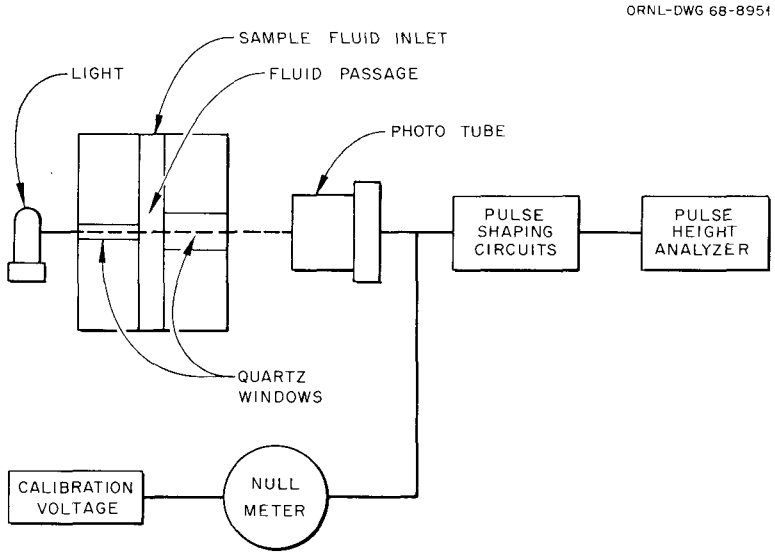

Fig. 4.5. Particle-Size Analyzer.

proportional to the particle size, is electronically shaped so that it can be accepted by a pulse-height analyzer. The pulse-height analyzer presently used consists of ten channels, each calibrated to count particles within a 10-μ range of diameters, giving a 100-μ range for the instrument at any one calibration. The counter can be calibrated for particles from 150 to 850 μ in diameter. Analysis of the particle counts in each of the channels gives the mean diameter, size distribution, and, with a weight measurement, density.

Various feed devices can be used with the particle-size analyzer. For most of the development work a vibratory V-block feeder has been used. This device consists of a V milled into a metal block down which particles are vibrated. With proper setting of the slope and vibratory amplitude, the particles move in single file. As the particles reach the end of the V-block, they are pulled by a vacuum into a tube that leads to the particle-size-analyzer window. Another method that has been successfully used for feeding particles to the particle-size analyzer is fluid suspension. A fluid stream, generally water, is allowed to continuously flow through the particle-size-analyzer window. The particles are then dropped into the flowing stream.

With either of the feeding methods, approximately 1000 particles can be analyzed in 3 min; hence, the analyzer easily achieves the speeds required for particle analysis in large production facilities.

Electronics of the instrument presents some problems in stability and accuracy. With the voltage supply presently used, the instrument must be recalibrated approximately every hour. However, considerable improvement may be obtained with a constant voltage source. Extremely careful adjustments must be made during this calibration. However, a skilled technician can perform the adjustment in 10 min. Present calibration procedures give an accuracy of approximately 1% in the measurement of mean particle diameter. To obtain 1% accuracy in the analysis of the mean size plus reliable information on the particle-size distribution, statistical techniques must be used. Calculation of standard deviation can be somewhat misleading, since the maximum and minimum sizes have generally been eliminated by screening or some other sizing technique. The size distribution can be determined more accurately

graphically, using either probability paper or log probability paper. The probability paper is useful when the particles follow a normal distribution. Frequently, the particle distribution is not normal but skewed, so log probability plots produce the better fit to a straight line. From these plots, confidence levels can be found.

Repeated analyses of particle batches have been made using the particle-size analyzer, and the results were found to be as accurate and reproducible as those found by manually reading the sizes of 50 individual particles with a split-image microscope.

Bonding of Coated Fuel Particles in Fuel Elements

J. M. Robbins R. L. Hamner H. Beutler[6]

We are developing processes to be used in the Thorium-Uranium Recycle Facility (TURF) for the remote fabrication of fuel elements for advanced high-temperature gas-cooled reactors. The reference fuel element for the study in TURF is essentially a mockup of that proposed for the Fort St. Vrain Reactor of the Public Service of Colorado (PSC). The mockup (Fig. 4.6) is a hexagonal graphite block 30 in. long × 3 1/2 in. across flats, with 12 holes approximately 0.45 in. in diameter that are to be filled with pyrolytic-carbon-coated fuel particles.

We are developing techniques for loading the fuel holes according to a tentative plan for experimental elements to be irradiated in the Peach Bottom Reactor. The fuel loading specifications at present require that the coated fertile and fissile fuel particles be of two different sizes, approximately 600 and 400 μ in diameter. These are homogeneously blended and loaded into the holes to a packing density of 60 to 64 vol %, bonded together in the fuel holes, and provided with as much carbon as possible in the bonding material for cesium absorption.

---

[6]Present address, Sulzer Bros., Winterthur, Switzerland.

Photo 89049

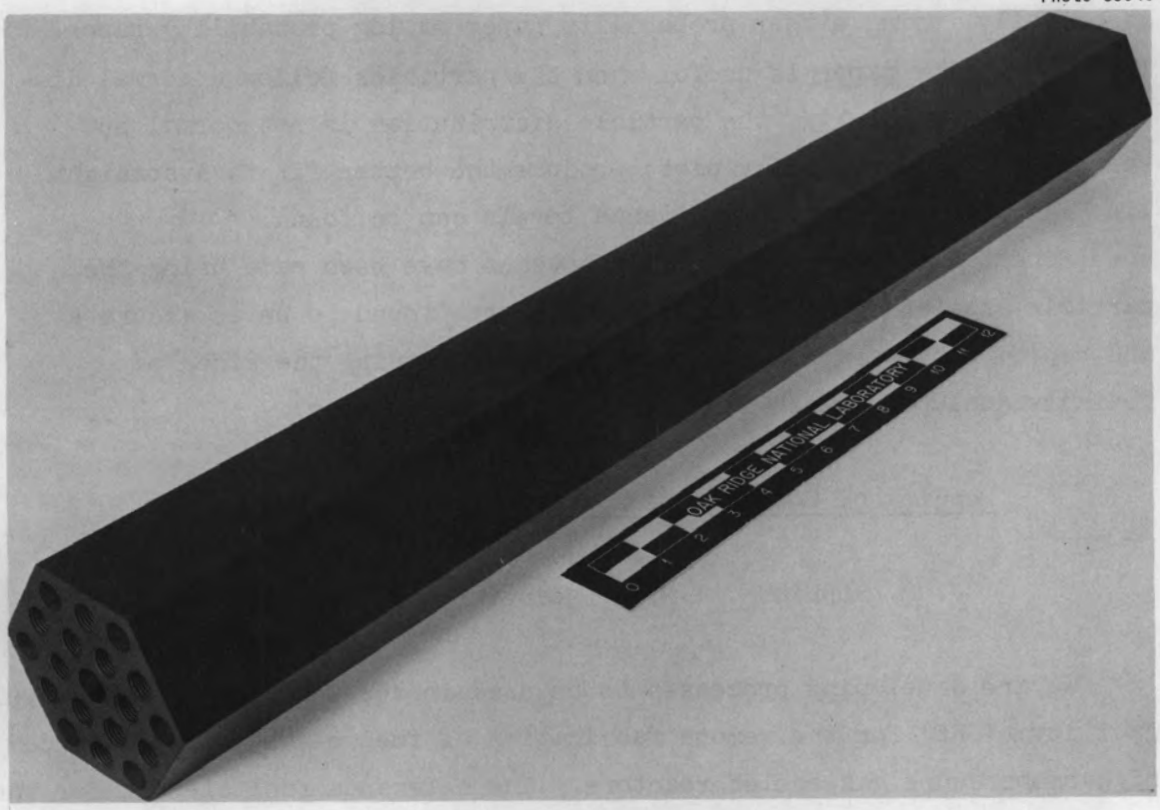

Fig. 4.6. Mockup of the PSC Fuel Element Block for Studies in TURF.

Blending

We are blending the two sizes of particles by allowing them to flow into a fuel hole simultaneously from hoppers with rectangular orifices that can be adjusted with micrometers, as shown in Fig. 4.7. Satisfactory blending depends on uniform flow rates and coincident times of feed of given weights of the components. In evaluating this blending technique, we fed the particles into a graphite tube, extracted samples at 1-in. intervals, and separated them into their original size fractions. The weight ratios of these components were then compared to that for the fuel blend. For a blending ratio of 2.5 the maximum deviation from the ideal blend did not exceed 5% in the samples extracted.

Bonding

In preliminary work, we bonded particles in graphite tubes, which were used to simulate a fuel block. We poured the particles into the

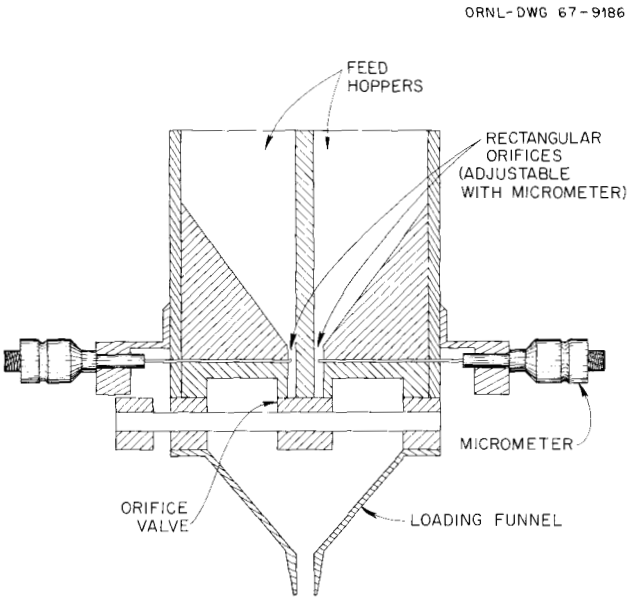

Fig. 4.7. Device for Blending Coated Particles by Feed Control.

tube, injected a mixture of liquid phenolic resin with charcoal or graphite, and then carbonized the resin at 1000°C in helium. However, there are several objections to bonding the particles directly in the fuel block: (1) the fuel holes cannot be inspected for fuel loading and homogeneity, (2) a mistake during loading cannot be readily rectified and the whole element may have to be discarded, (3) the graphite fuel block soaks up resin during injection, (4) the particles will be bonded to the graphite block, which might shrink during the initial stages of irradiation. Our concept of fuel loading is to bond the fuel in the forms of rods called "fuel sticks" and then insert these into the fuel block.

Preparation of Fuel Sticks

We blended and loaded the particles at the same time into a metal mold and then injected the bonding material (phenolic resin plus 15 wt % graphite powder) into the fuel bed, as illustrated in Fig. 4.8. The assembly was then heated at 80°C for 40 hr to polymerize or "cure" the resin to a solid mass. We have made fuel sticks having fuel volume loadings up to 63% in lengths up to 28 in. After curing, the fuel sticks were heated to 1000°C in helium to carbonize the resin. In actual

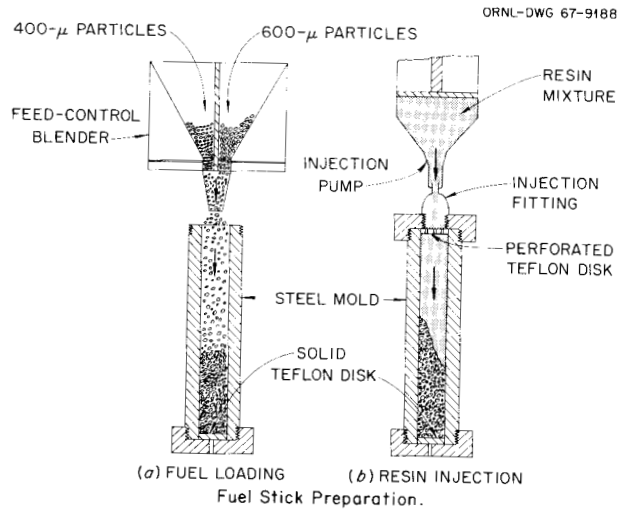

Fig. 4.8. Fuel Stick Preparation.

loading of the fuel blocks, we propose to insert the fuel sticks into the graphite block after curing but before carbonizing because they are somewhat flexible in the cured state and much stronger than carbonized sticks. Also, the fuel sticks warp during carbonization unless they are restrained, and they could probably not be inserted in the fuel block after carbonization.

Resin Curing

To meet production requirements for the TURF (about 420 sticks/day) at a reasonable cost, we had to reduce the resin curing time to no longer than 2 hr. We therefore investigated the use of accelerators to shorten the curing time and found that the addition of 10 wt % maleic anhydride and a curing temperature of 80°C could shorten the curing time to 2 hr. At 90°C the curing time was 1 hr.

Effects of Bonding Matrix on Coatings

Our present coating consists of a porous layer deposited from acetylene at 1100°C, next a silicon carbide layer deposited at 1550°C, followed by a high-density, isotropic layer deposited from propylene at 1250°C. We favor the propylene coating because dense isotropic coatings can be deposited rapidly at relatively low temperatures. Also, such

coatings have stood up well under irradiation.[7] However, they were cracked drastically by the bonding matrix after carbonization, as shown in Fig. 4.9. We attributed this to surface-connected porosity of the outer coatings (about 7%), which should contribute to the strength of the bond between matrix and coating. In comparative experiments, there was little or no bonding between the resin and smooth, dense, anisotropic coatings deposited from propylene. Rather than change our reference coating design, we propose to alter the surface of the isotropic coating by first depositing a thin, nonbonding, anisotropic layer on the reference coating and then depositing a bonding "sacrificial" outer layer, which we would expect to crack without detriment to the isotropic coating. These layers can be applied with the isotropic layer in one coating run

[7] O. Sisman, "Sweep-Capsule Coated-Particle Irradiation Tests," GCR Program Semiann. Progr. Rept. March 31, 1967, ORNL-4133, pp. 36–37.

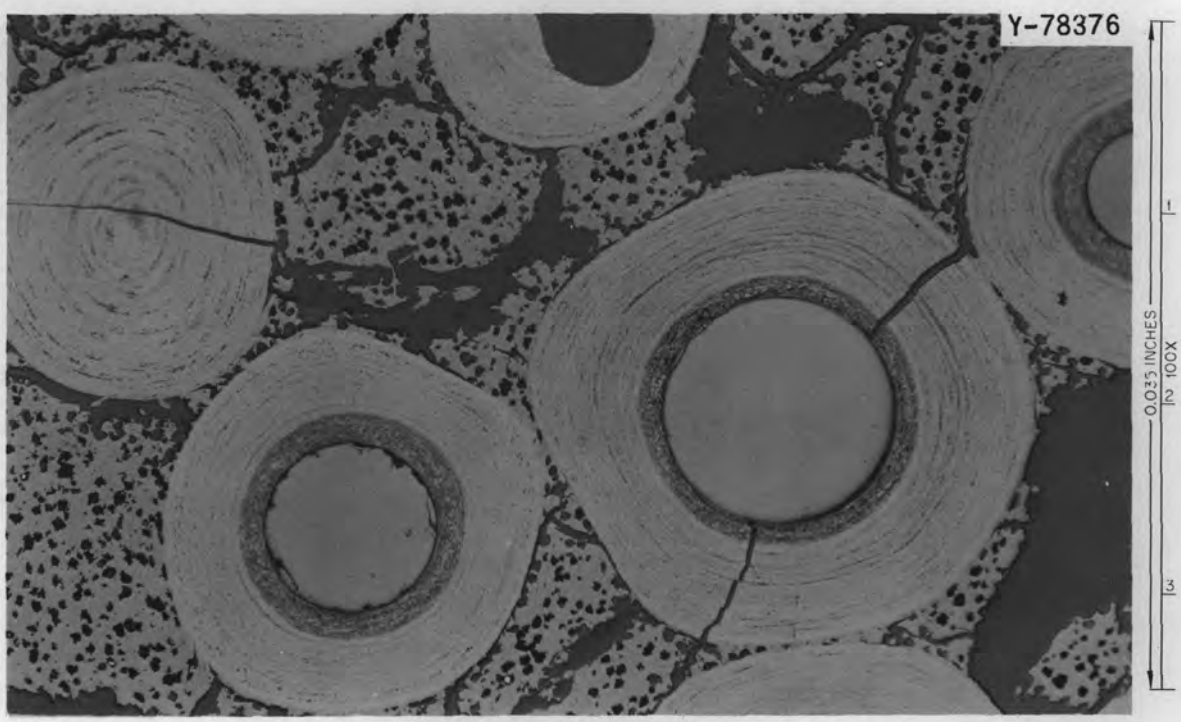

Fig. 4.9. Polished Section of a Carbonized Fuel Stick Containing ThO_2 Particles Coated with Propylene-Deposited Pyrolytic Carbon. In the interstices, the light-gray phase is the bonding matrix, the darker gray phase is metallographic mounting material, and the black areas are voids. As polished.

by reducing the propylene supply rate from 3.1 to 0.1 $cm^3\ min^{-1}\ cm^{-2}$ and the temperature from 1250 to 1100°C to deposit the nonbonding layer and then depositing the sacrificial layer by resuming the initial coating conditions. A microstructure illustrating the functions of the nonbonding and sacrificial layers is shown in Fig. 4.10. The addition of the nonbonding and outer sacrificial layers had no detrimental effects on the integrity or strength of the carbonized fuel sticks, and we have incorporated these features into the coating design for fuel-stick irradiation experiments.

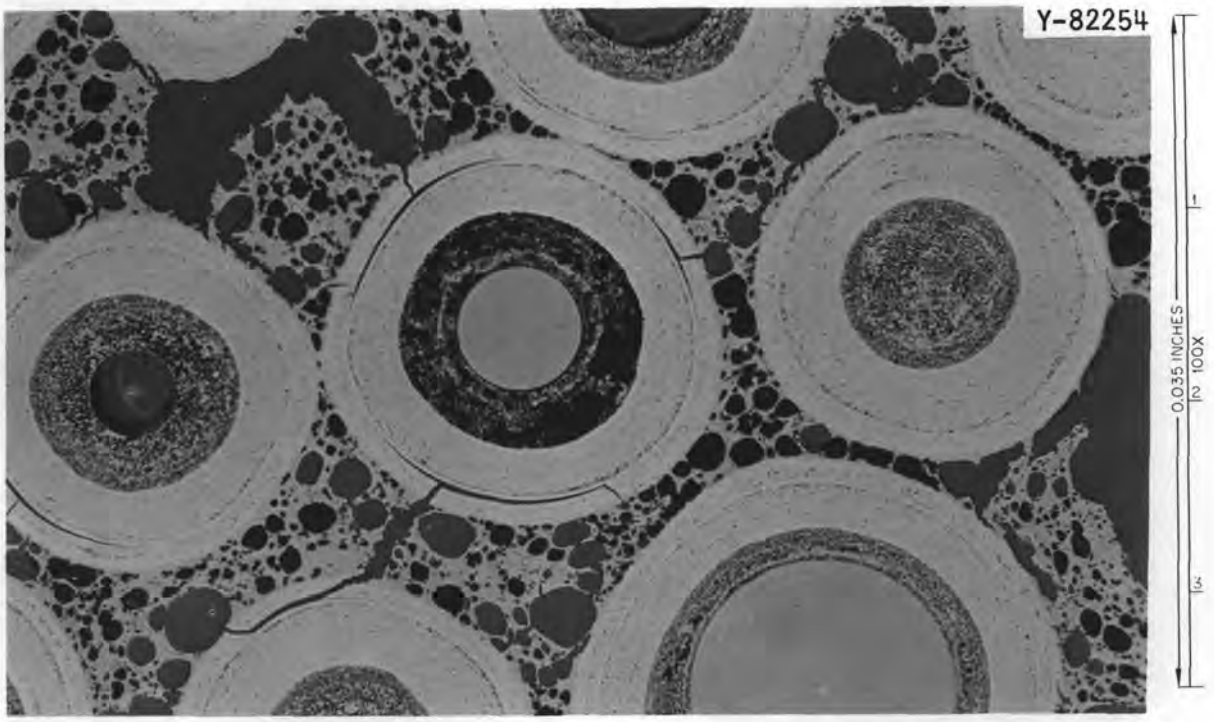

Fig. 4.10. Microstructure of Pyrolytic-Carbon-Coated ThO_2 Particles Bonded with a Mixture of Phenolic Resin, Graphite, and Maleic Anhydride and Carbonized at 1000°C. The cracked outer coating layer is the "sacrificial" layer superimposed on a nonbonding layer that has been applied to the base coat. As polished.

Characterization of the Carbonization Process

To obtain a better understanding of the carbonization process, we investigated the physical changes that occurred in bonding materials

during and after carbonization. In most of these studies we used as the bonding material P514 resin with additions of 10% maleic anhydride and 15% graphite.

In preliminary differential thermal analysis (DTA), endothermic reactions occurred at approximately 120, 250, and 410°C; these we attributed to the release of volatiles. We then prepared fueled resin sticks with and without maleic anhydride and heated them to 1000°C according to the following schedule:

Temperature Interval (°C)	Average Heating Rate (°C/hr)
Room temperature to 500	24
400 to 600	39
600 to 1000	127

We retracted specimens at temperatures of 185, 400, 600, and 1000°C for visual examination, weighing, and measurements of dimensional changes and compressive strengths.

The matrix of the fueled specimens had uniformly distributed pore structure and maintained good contact with the fuel up to 400°C; at this temperature large cracks appeared in the matrix and huge voids in the interstitial areas, but the resin adhered to the fuel. The propylene-deposited coatings cracked at some temperature between 185 and 400°C.

Figure 4.11 shows the weight and dimensional changes of fueled and unfueled resin sticks during and after carbonization. Most of the changes in the resin take place by the time 600°C is reached, and the greatest changes occur between 185 and 400°C. The carbonized resin was essentially amorphous, having a crystallite size of less than 20 A, as measured by x-ray diffraction. Figure 4.12 compares the compressive strengths of fueled and unfueled sticks, during and after carbonization. The fueled stick is comparable in strength to the unfueled resin at 185°C but becomes consistently weaker as it carbonizes, and finally it is only one-eighth as strong as the carbonized unfueled resin.

A more comprehensive treatment of the mechanical properties of fuel sticks is given below.

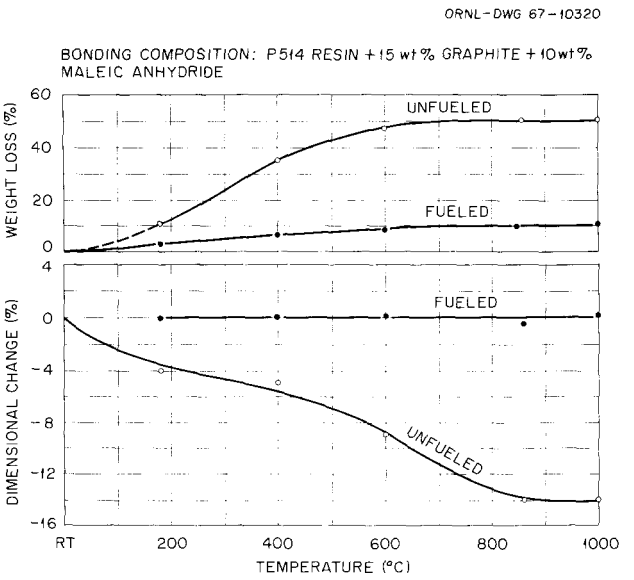

Fig. 4.11. Weight Loss and Dimensional Changes in Fueled and Unfueled Resin Sticks During and After Carbonization at 1000°C.

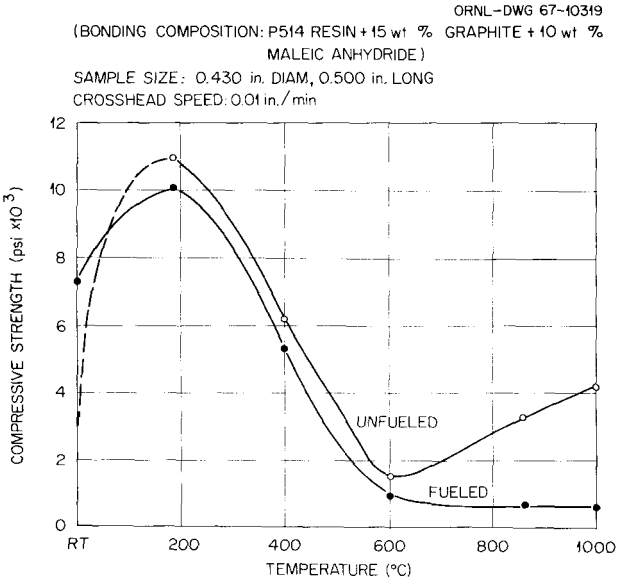

Fig. 4.12. Comparison of Compressive Strengths of Fueled and Unfueled Sticks.

Evaluation of Fuel Sticks and Bonding Matrices

We evaluated fuel sticks and bonding matrices according to their mechanical properties, the effects of curing time and heat treatment, and the interaction between fuel sticks and graphite holders.

Mechanical Properties. – If we are to load cured sticks into fuel blocks according to our present plan, we must know the strength of the sticks for the design of remote transfer and loading mechanisms for use in TURF. We must also know the strength and integrity of carbonized fuel sticks to predict their behavior in fuel element failure. We are, therefore, measuring the mechanical properties of fueled and unfueled resin sticks by bend, compression, and tension tests.

We used a three-point bend-testing jig consisting of two fixed rollers that carried the specimen and a third roller attached to the cross beam of an Instron testing machine. We used a beam span of 4 in. and a constant crosshead speed of 0.01 in./min. Load deflections were recorded as a function of time. We calculated the modulus of rupture with simple beam formula without correcting for the changes in lever-arm length of the beam due to bending or for frictional forces.

We carried out compression tests on the Instron machine by applying the load parallel to the axis of the stick. The specimens used for these tests were cut to a length of 1 in. from a section of the same composite used for bend-test measurements. Compressive cracking was followed by a breakout of isolated particles and chunks of particles and bonding matrix. After each compression test, we ran a screen analysis on the remains. About 1% of the fragments were smaller than the fuel particles (400 to 600 μ), about 15% were just larger than the fuel particles, and about 70% were chunks about 1/8 in. or larger.

To determine the tensile strengths of resin composites, we cemented carbonized fuel-stick specimens approximately 1 in. long into metal holders, attached wires to each holder, and pulled the specimens apart with the Instron machine at a rate of 0.05 in./min. Our preliminary results on mechanical testing are summarized in Table 4.1. These data, in particular, reflect the superior strength of the polymerized or "cured" sticks over the carbonized sticks. The range in the compressive

Table 4.1. Mechanical Properties of Fueled Resin Composites[a]

Condition	Strength, psi		
	Compressive	Flexural	Tensile
Polymerized at 80°C	7320–8200	3110–4530	Not measured
Carbonized at 1000°C	500–2720	190–367	66–302

[a]Coated ThO_2 particles, 400 to 600 μ in diameter, bonded with phenolic resin, 15 wt % graphite, 10 wt % maleic anhydride.

strengths of carbonized specimens was wide, but the low values were obtained on fuel sticks that had been cured for only 1 hr, whereas the higher values were obtained on sticks cured from 16 to 24 hr. Obviously, some compromise must be made between the curing time required in the TURF and the strength of the carbonized sticks.

Effects of Heat Treatment. – We heated fuel sticks at 1900°C for 8 hr and at 2000°C for 1 hr and observed no detrimental effects by mechanical strength measurements or metallographic examination. Changes in dimensions were negligible. The x-ray crystallite size of the carbonized matrix was not significantly affected.

Interaction Between Fuel Sticks and Holders. – As shown in Fig. 4.13, we simulated a fuel element failure by simple fracture of a fuel stick, which had been carbonized in a graphite holder. We observed a few fragments at the break, but the fuel sticks remained intact in the holders.

Fuel Stick Fabrication

Approximately 600 fuel sticks were made for particle debonding experiments. The mold used is shown in Fig. 4.14. It produced a 0.43-in.-diam × 12-in.-long fuel stick, although 28-in. fuel sticks were made by the same process. The end cap B (a cylindrical brass plug) is inserted and locked into place with a retainer clip. Any spacers required are inserted into the mold. A screen is placed into the mold to prevent particles from flowing around the spacer. The particles are then loaded and held in place with another screen. Any additional spacers needed are loaded, and the end cap A, with a grease fitting, is locked into place. The resin-accelerator-filler mixture is injected into the mold

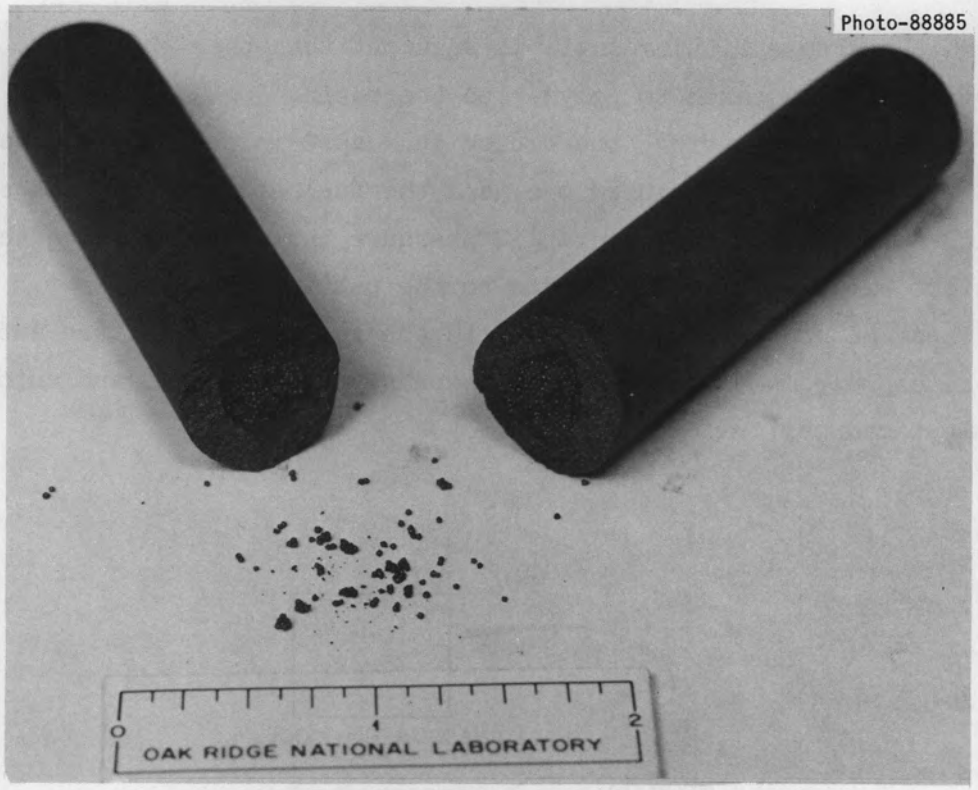

Fig. 4.13. Carbonized Fuel Stick in a Graphite Holder Broken to Simulate a Fuel Element Failure.

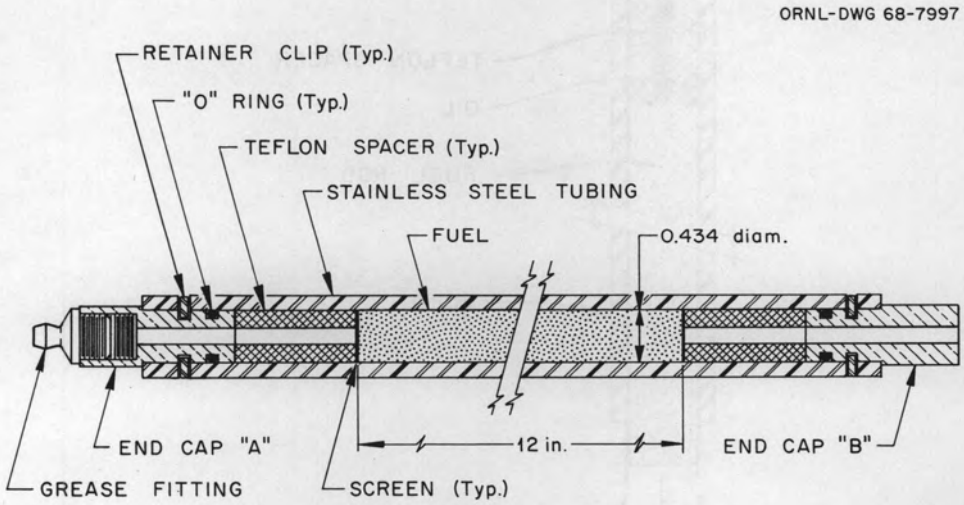

Fig. 4.14. Fuel Rod Mold.

through the grease fitting until it runs out the other end. Then the whole assembly is baked to polymerize the resin.

After polymerization, the bottom end cap B is removed, the top end cap A replaced with an unused one, and the fuel stick ejected as shown in Fig. 4.15. The use of hydraulic pressure instead of pushing the fuel stick out with a rod avoids damage to the particle coatings.

These methods were developed with the intention of future automation. The molds we developed are inexpensive to produce, and automatic equipment can perform each step.

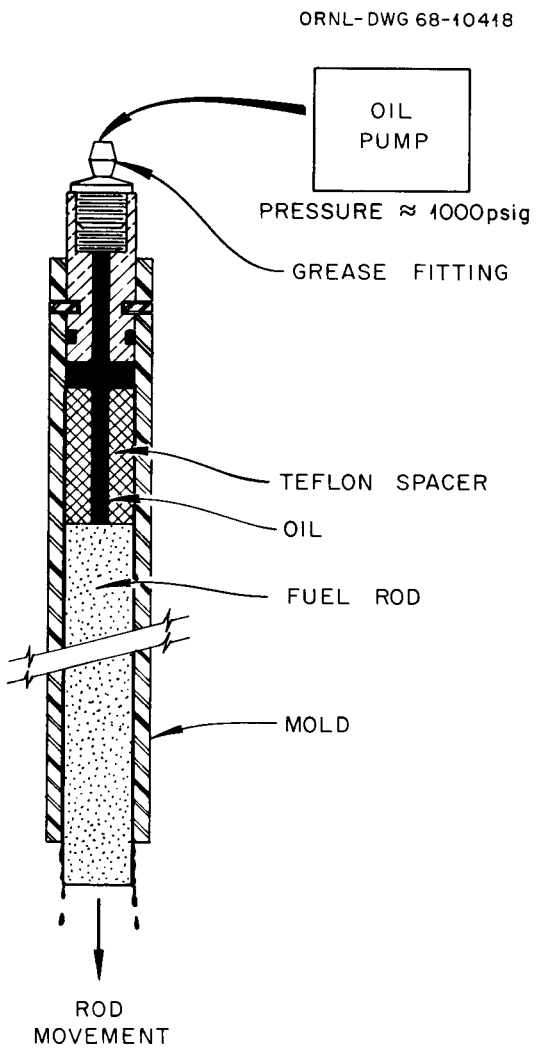

Fig. 4.15. Fuel Rod Ejection.

5. IRRADIATION OF COATED-PARTICLE FUELS

A. R. Olsen J. W. Prados
J. H. Coobs E. L. Long, Jr.

Coated-particle fuels for use in high-temperature gas-cooled reactors have been irradiation tested for a number of years. As part of a cooperative effort with the Advanced Gas-Cooled Reactor Program at ORNL, we have been testing the performance of coated sol-gel-derived UO_2 and $(Th,U)O_2$ microspheres. In these experiments, the results are compared with the performance of similar coated particles having sintered oxide or melted carbide fuel kernels. All tests are compared with predicted performance based on our mathematical model of coated-particle behavior. Some results on the irradiation performance of sol-gel-derived microspheres were reported previously.[1-5] The program has been expanded to investigate fuel kernel variations, such as diameter and composition, to improve our estimates of model parameters.

---

[1]A. R. Olsen, J. H. Coobs, and J. W. Prados, Status and Progress Report for Thorium Fuel Cycle Development Dec. 31, 1966, ORNL-4275, pp. 88–98.

[2]A. R. Olsen, J. H. Coobs, and J. W. Ullman, "Current Status of Irradiation Testing of Thorium Fuels at Oak Ridge National Laboratory," pp. 475–494 in Thorium Fuel Cycle (Proceedings of Second International Thorium Fuel Cycle Symposium May 3–6, 1966) R. G. Wymer, Coordinator, U.S. Atomic Energy Commission/Division of Technical Information, Oak Ridge, Tennessee, February 1968.

[3]J. W. Prados, R. L. Beatty, H. Beutler, J. H. Coobs, A. R. Olsen, and J. L. Scott, "Development of Coated-Particle Fuels for Advanced Gas-Cooled Reactors," pp. 273–292 in Thorium Fuel Cycle (Proceedings of Second International Thorium Fuel Cycle Symposium May 3–6, 1966) R. G. Wymer, Coordinator, U.S. Atomic Energy Commission/Division of Technical Information, Oak Ridge, Tennessee, February 1968.

[4]J. H. Coobs, R. L. Beatty, A. R. Olsen, H. L. Krautwedel, J. W. Prados, and J. L. Scott, "Testing of a Design Analysis for Coated-Particle Fuels," Trans. Am. Nucl. Soc. 9(2), 421–422 (1966).

[5]A. R. Olsen, J. H. Coobs, D. M. Hewette, II, H. L. Krautwedel, A. W. Longest, E. L. Long, Jr., J. W. Prados, and J. L. Scott, "Performance of Pyrolytic-Carbon-Coated Sol-Gel UO_2 Microspheres in High-Burnup Irradiation Tests," Trans. Am. Nucl. Soc. 10(1), 96–97 (June 1967).

To supplement the static and swept instrumented capsules used primarily in the Advanced Gas-Cooled Reactor Program tests, we are conducting a series of irradiation tests using static uninstrumented capsules. These have been designated as "X-basket" tests. The basic design of the first two capsules in this series was reported previously.[1] The design illustrated in Fig. 5.1 for X-basket 4 is typical of that used for X-baskets 3, 4, and 5. The basic change was to remove one low-temperature sleeve and extend the high-temperature sleeve to accommodate more fuel samples. The desired operating fuel temperatures of 400 and 1400°C are obtained by varying the dimensions of a helium-filled gap between the graphite sleeves and the metal tube. We include a series of melt wires to estimate the temperatures achieved. A stainless steel tape, which extends the full length of the capsule, monitors the neutron flux.

Comparison of Test Results with Model Predictions

The first two capsules in the X-basket series, X-baskets 1 (ORNL 43-89) and 2 (43-97), have been completely examined, and comparisons of test results with earlier model calculations are presented elsewhere.[5]

We recently developed improved techniques for calculating the influence of fast-neutron-induced dimensional changes and creep on coated-particle irradiation performance[6,7] and applied them to revise our predictions of the burnups at failure for coated particles irradiated in ETR X-basket experiments 1 and 2. The properties and assumptions employed in our revised calculations were those used in the previous comparisons, with the following exceptions: (1) the coating rupture criterion was taken as an "effective creep stress" of 60,000 psi rather than a tangential tensile stress of 30,000 psi, (2) the release of fission gas from the kernels of particles irradiated at the low temperatures (nominally 400°C) was taken as 10% rather than 100%, (3) the irradiation creep

---

[6] J. W. Prados and T. G. Godfrey, STRETCH, A Computer Program for Predicting Coated-Particle Irradiation Behavior; Modification IV, December 1967, ORNL-TM-2127 (April 1968).

[7] J. W. Prados and T. G. Godfrey, "Improved Method for Calculating Creep of Spherical, Anisotropic Pyrolytic-Carbon Coatings," GCR Program Semiann. Progr. Rept. March 31, 1968, ORNL-4266, pp. 71-76.

ORNL-DWG 69-3329

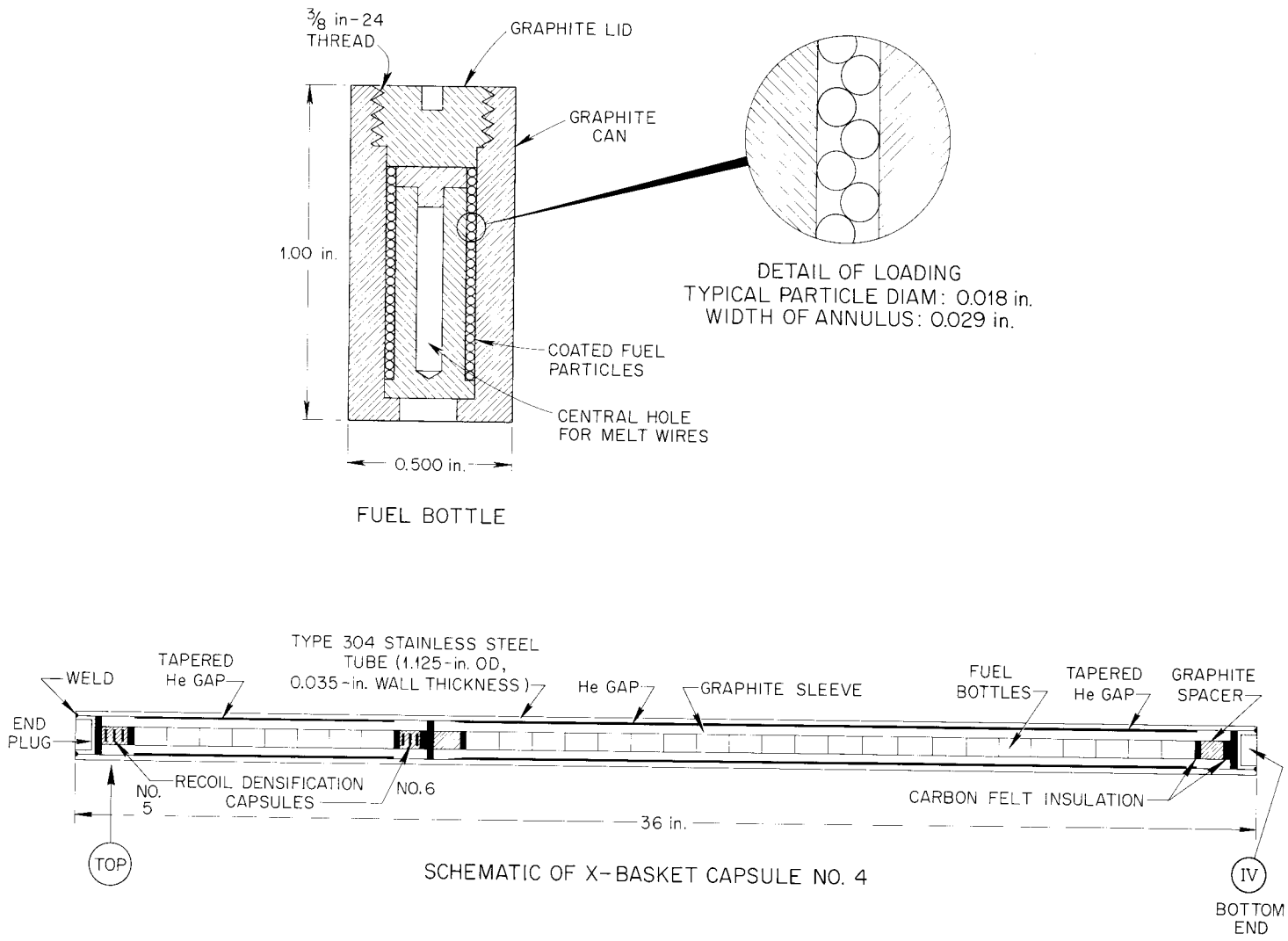

Fig. 5.1. Schematic of X-Basket Capsule 4.

coefficient was decreased from 1.5×10^{-27} to 1.0×10^{-27} psi^{-1} (neutrons/cm^2)$^{-1}$ (> 0.18 Mev), and (4) densification of outer coatings in accordance with the Bokros-Schwartz model[8] was incorporated into the calculations. The revised predictions are compared with experimental results in Table 5.1 and Fig. 5.2. In general,

[8] J. C. Bokros and A. S. Schwartz, "A Model to Describe Neutron-Induced Dimensional Changes in Pyrolytic Carbon," Carbon 5, 481–492 (1967).

Table 5.1. Performance Comparison of X-Basket 1 and 2 Coated Particles[a]

X-Basket 1						X-Basket 2					
Lot	Type of Coating,[b] Inner/Outer	Nominal Temperature[c] (°C)	Burnup Attained (%)	Predicted Burnup at Failure (%)	Particle Failures (%)	Lot	Type of Coating,[b] Inner/Outer	Nominal Temperature[c] (°C)	Burnup Attained (%)	Predicted Burnup at Failure (%)	Particle Failures (%)
		Sintered Oxide						**Sol-Gel Oxide**			
OR-339	L/G	400	10.8	18.1	0	YZ-60	L/G	400	18.5	17.4	0
		1000	23.3	14.8	87			1400	25.3	13.0	1
OR-341	L/G	400	17.5	28.6	0						
		1000	23.3	22.5	5						
		400	14.6	28.6	1						
OR-342	L/I	400	18.5	28.0	0	YZ-47	L/I	400	21.3	28.3	0
		1000	23.1	22.2	39			1400	25.4	22.5	0
		400	12.9	28.0	0						
OR-343	I/I	400	14.4	26.7	0	YZ-56	I/I	400	16.8	26.1	0
		1000	22.5	21.0	17			1400	24.5	19.9	4
		400	18.5	26.7	0			400	22.0	26.1	0
OR-344	I/G	400	13.2	27.8	0	YZ-57	I/G	400	18.3	26.6	0
		1000	22.1	21.9	0			1400	24.8	19.6	0
		400	19.6	27.8	0			400	21.1	26.6	0
OR-348	P/L	400	15.5	39.5	0	YZP-29	P/L	400	20.4	>60	0
		1000	22.9	31.4	0			1400	25.3	46.7	0
		400	17.4	39.5	0			400	16.6	>60	0
OR-349	L/I	400	12.0	15.7	0	YZ-66	L/I	400	20.0	15.0	<1
		1000	23.6	13.0	100			1400	25.1	13.0	70
OR-354	P/I	400	16.6	43.8	0	YZP-28	P/I	400	19.3	>60	0
		1000	23.2	34.8	0			1400	25.4	45.8	0
		400	15.9	43.8	0						
						YZ-54[d]	L/G	400	21.8	16.7	0
								1400	25.4	12.7	1
								400	14.0	16.7	0
		Carbide Particles						**Control Samples of Sintered Oxide**			
OR-352	P/I	400	20.6	13.9[e]	2	OR-343	I/I	1400	23.7	19.9	1
		1000	21.5	11.9[e]	42	OR-348	P/L	1400	24.2	29.3	0
OR-357	P/G	400	21.3	12.9[e]	30						
		1000	20.9	10.9[e]	30			**Additional Samples of Sol-Gel Oxide**			
						YZ-58	L/I	400	15.5	14.2	0
								1400	24.9	10.7	66
								400	22.8	14.2	25
						YZ-45	L/I	400	13.9	14.6	0
								1400	25.1	10.5	100
								400	23.5	14.6	3

[a] For easy comparison, samples in the two experiments with similar coating type and particle size are listed in the same line.
[b] Coating designation: L – laminar; G – granular; I – isotropic; P – porous.
[c] Actual irradiation temperatures are estimated to have ranged from 300 to 500°C in the low-temperature compartments and from 1000 to 1400°C in the high-temperature compartments. Nominal values reported are estimates of average temperatures prevailing over the major portion of the irradiation.
[d] Corresponds to OR-339.
[e] Calculated value based on minimum measured inner-layer thickness.

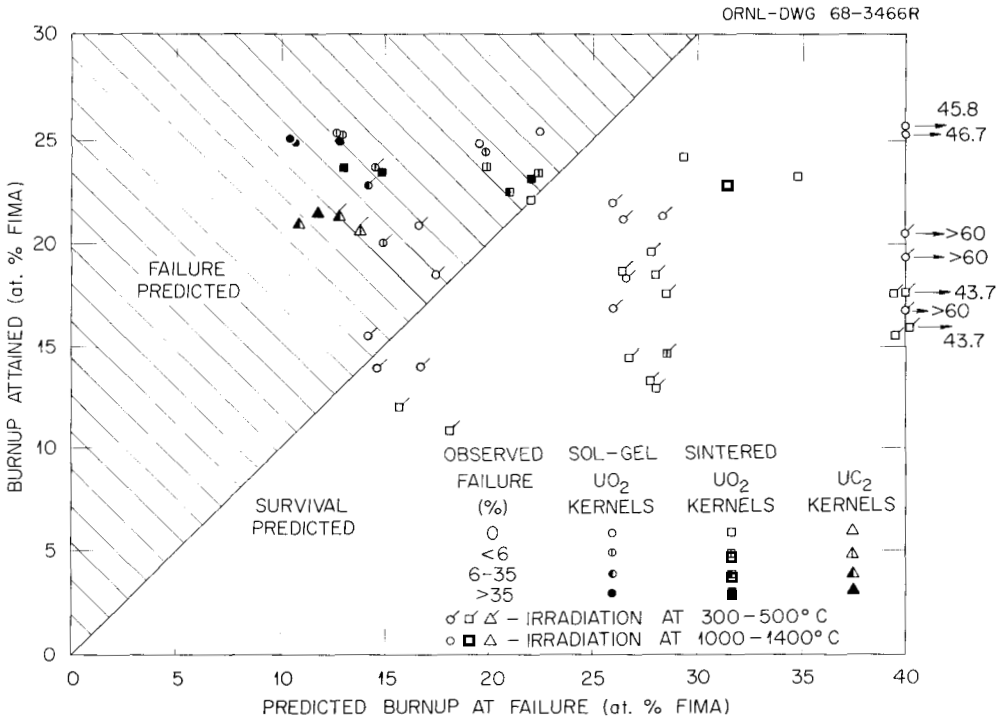

Fig. 5.2. Comparison of Observed and Predicted Performance of Pyrolytic-Carbon-Coated Particles Irradiated in ETR X-Basket Experiments 1 and 2.

the agreement between observed and predicted failures has been significantly improved, although several batches that survived the irradiation were still predicted to fail. Particles with granular outer coatings most frequently exhibited this anomaly; apparently the properties we have assumed for the granular coatings are conservative.

The comparisons of experimental results with predictions should help to resolve some of the remaining uncertainties on parameters used in the existing calculational code. We are modifying our mathematical model to include the analysis of the effects of an intermediate silicon carbide layer in the coating. This modification is similar to that proposed in a similar model.[9]

---

[9] J. L. Kaae, A Mathematical Model for Calculating Stresses in a Four-Layer Carbon and Silicon-Carbide-Coated Fuel Particle, GA-9031 (October 1968).

Comparison of Sol Gel with Sintered Spheroids

The coated particle fuels in X-basket 2 were principally 220-μ-diam sol-gel-derived UO_2 microspheres with a variety of pyrolytic-carbon coatings applied in a fluidized-bed coater with acetylene and methane as the carbon source gases. The test was primarily designed to compare the sol-gel-derived UO_2 microspheres with the sintered UO_2 spheroids tested in X-basket 1. Consequently, the coating parameters were essentially duplicates of those in X-basket 1. The microstructures of the unirradiated coated sol-gel particles are shown in Fig. 5.3. These

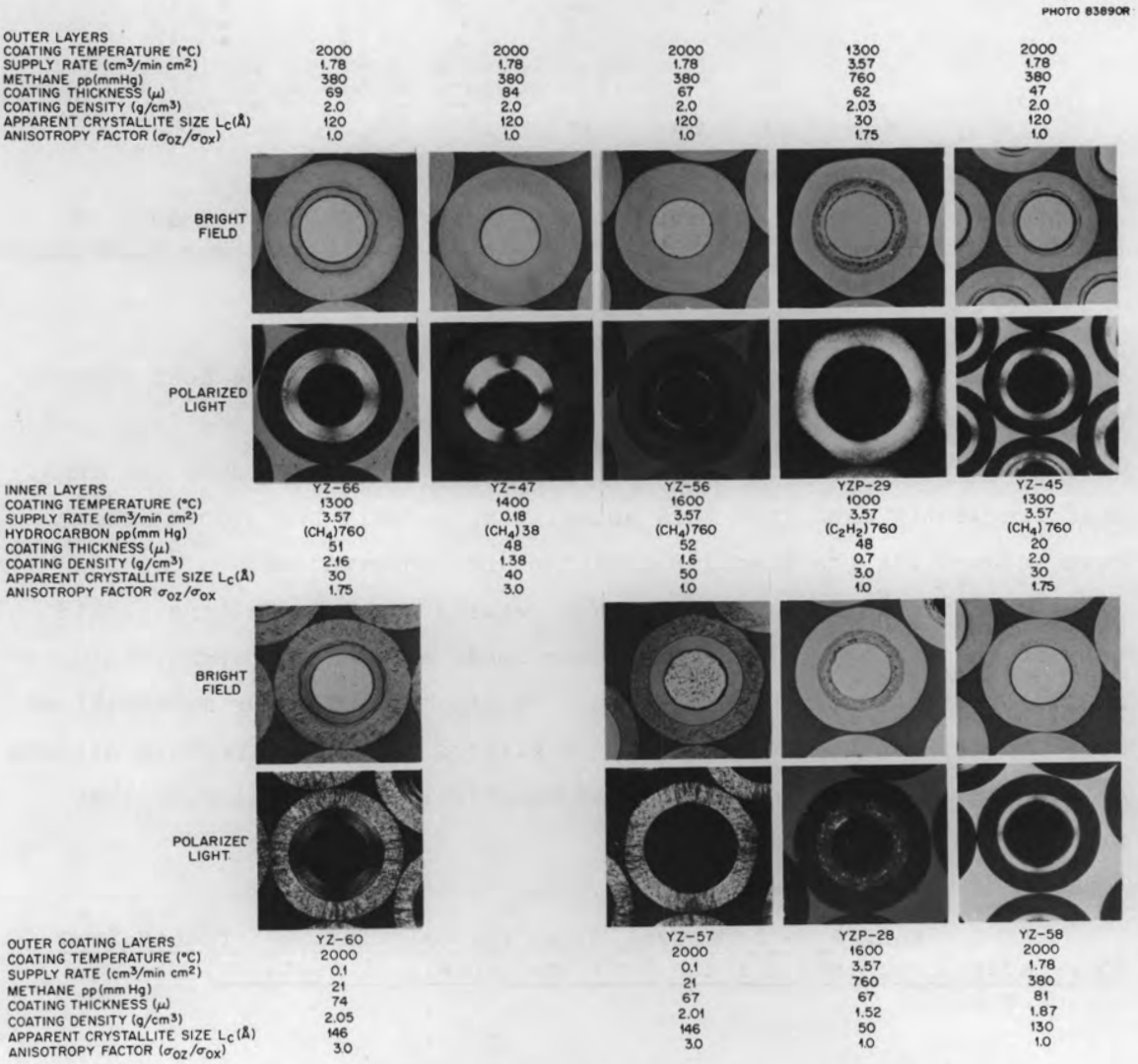

Fig. 5.3. Microspheres of Unirradiated Coated Sol-Gel Particles Typical of Those Irradiated in X-Basket 2.

coated particles, together with two types of coated particles tested in X-basket 1, were incorporated in the test. Table 5.1 compares the performance.

The principal difference in the two experiments is that the high-temperature samples in X-basket 1 apparently operated at about 1000°C instead of the intended 1400°C, while those in X-basket 2 achieved the intended temperature. This difference in temperature probably had a greater effect on particle performance than the change in fuel kernel production processes. This is shown in Figs. 5.4 and 5.5. Two sintered-kernel particle batches that were included in both experiments, together with the comparable sol-gel kernel particles, are shown in these figures. The coated particles of OR-348 were predicted by the model to survive the irradiation, while OR-343 was predicted to fail. The better coated particles survived both tests, but there is a significant difference in the failure percentages for the two temperatures with the OR-343 particles. These results indicate a need for further refinement in our model to account for temperature dependence in the irradiation damage or irradiation-induced creep properties of the pyrolytic carbon coatings. This is further substantiated by the difference in performance between two similarly coated particles shown in Fig. 5.6. The predicted survival of both the sintered particles (OR-342) and the sol-gel particles (YZ-47) was borderline; yet 39% of the sintered particles failed at 20% burnup at 1000°C, while none of the sol-gel particles failed at 25% burnup at 1300°C. A more dramatic difference is shown in Fig. 5.7, in which the outer coating layer was granular on both particles. In addition to the marked temperature effect, the low failure rate for the sol-gel (YZ-60) particles indicates the failure stress or creep properties of the granular coatings must be considerably different from those we are currently using in the model calculations. This difference is also shown by the comparison of performance predictions and test results shown in Table 5.1 for particles YZ-54 and YZ-67 in X-basket 2.

The results of these two tests show conclusively that coated particles with sol-gel-derived UO_2 microsphere fuel kernels perform as well as similar particles with sintered fuel kernels. This conclusion has been verified in other experiments conducted under the Advanced Gas-Cooled

R-37762

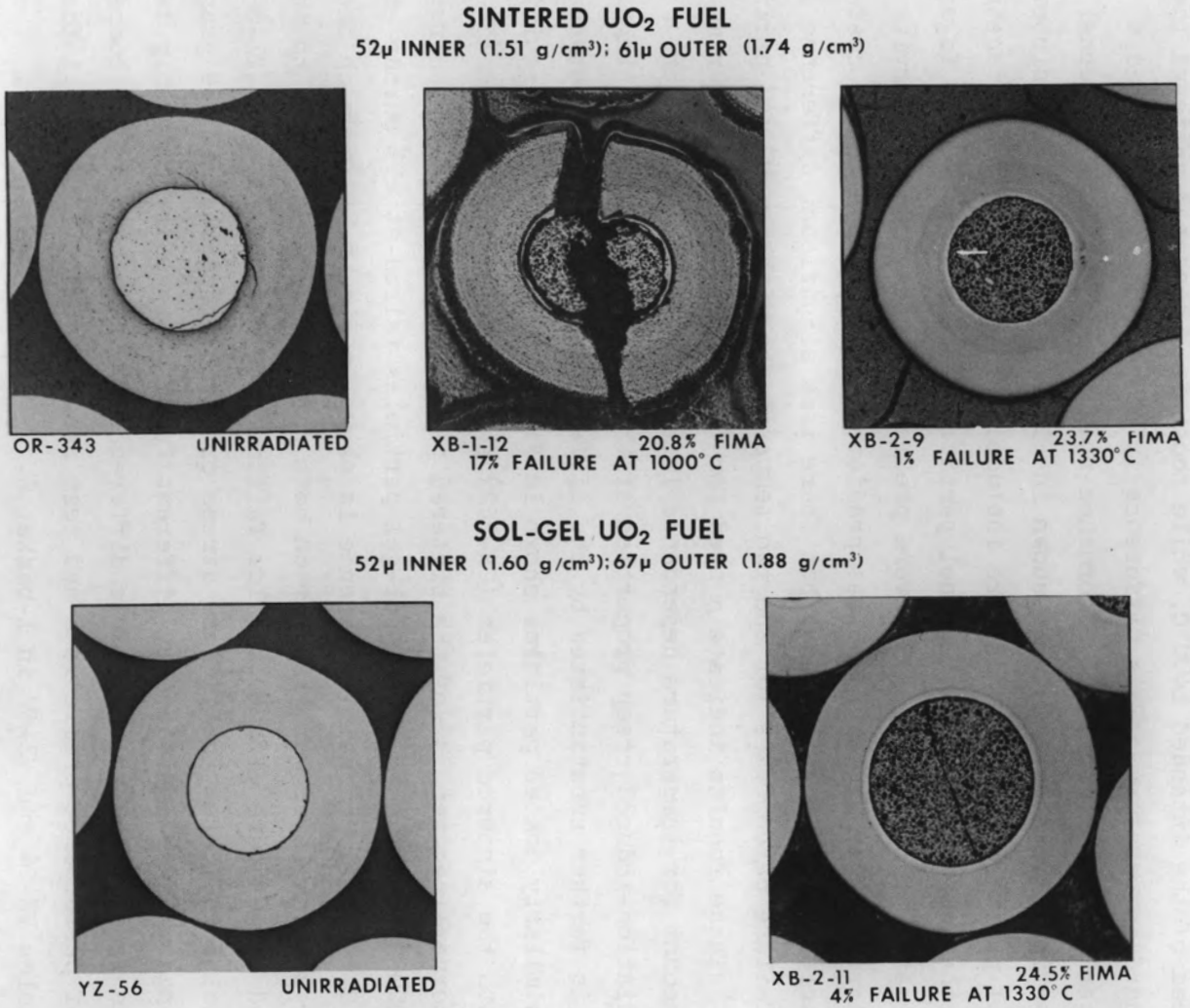

Fig. 5.4. Comparison of Irradiated Particles with Low-Density Isotropic Inner Coatings and Isotropic Outer Coatings.

R-37761

SINTERED UO_2 FUEL

35μ INNER (0.8 g/cm³); 86μ OUTER (2.01 g/cm³)

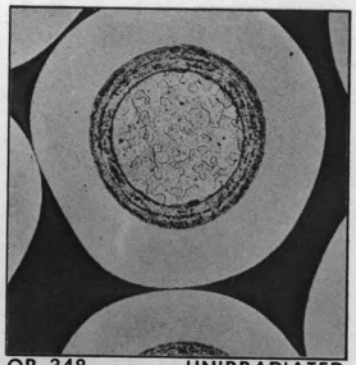

OR-348 UNIRRADIATED

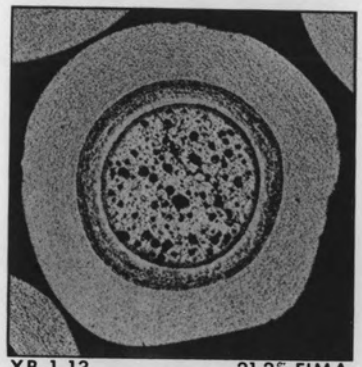

XB-1-13 21.2% FIMA
0% FAILURE AT 950°C

XB-2-10 24.2% FIMA
0% FAILURE AT 1340°C

SOL-GEL UO_2 FUEL

48μ INNER (1.0 g/cm³); 62μ OUTER (2.03 g/cm³)

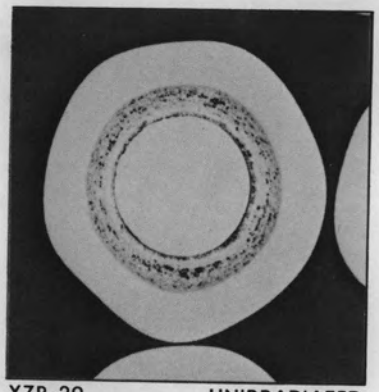

YZP-29 UNIRRADIATED

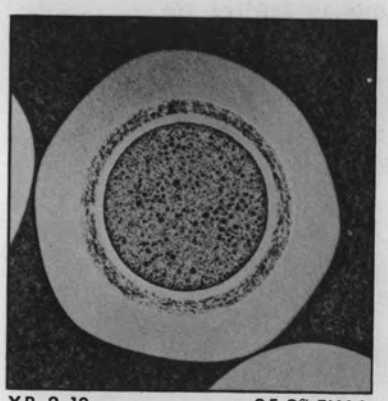

XB-2-18 25.3% FIMA
0% FAILURE AT 1330°C

Fig. 5.5. Comparison of Irradiated Particles with Porous Inner Coatings and Laminar Outer Coatings.

R-37757

SINTERED UO_2 FUEL

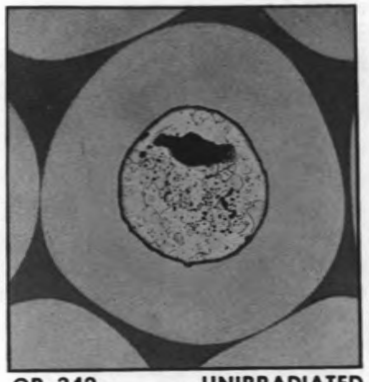

OR-342 UNIRRADIATED

48μ INNER (1.47 g/cm³)
63μ OUTER (1.75 g/cm³)

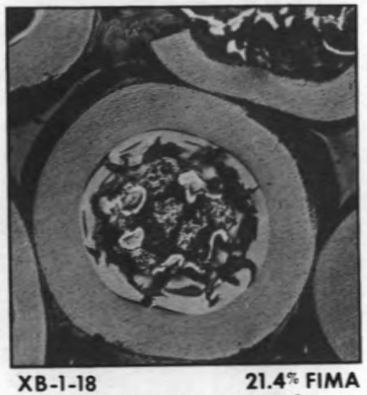

XB-1-18 21.4% FIMA
39% FAILURE AT 1010°C

SOL-GEL UO_2 FUEL

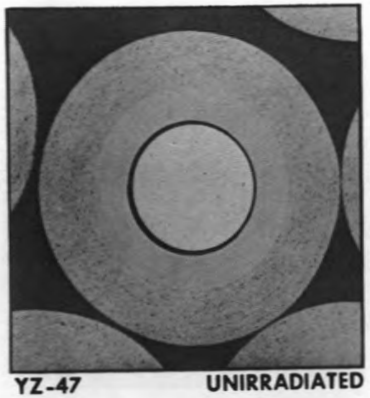

YZ-47 UNIRRADIATED

48μ INNER (1.38 g/cm³)
84μ OUTER (1.86 g/cm³)

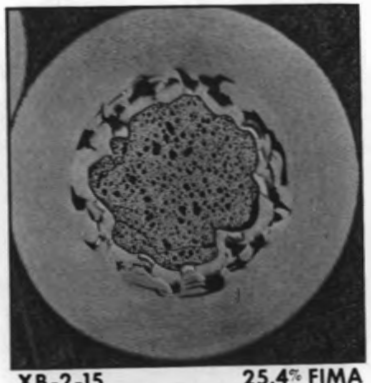

XB-2-15 25.4% FIMA
0% FAILURE AT 1320°C

Fig. 5.6. Comparison of Irradiation Performance of Particles with Low-Density Laminar Inner Coatings and Isotropic Outer Coatings.

R-37758

SINTERED UO_2 FUEL

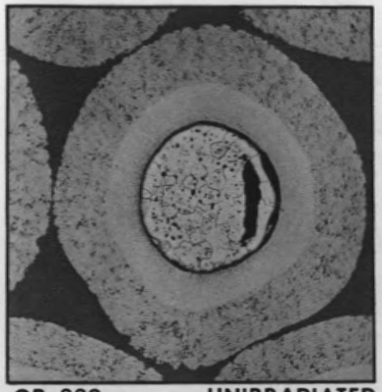

OR-339 UNIRRADIATED

53μ INNER (2.03 g/cm³)
73μ OUTER (2.03 g/cm³)

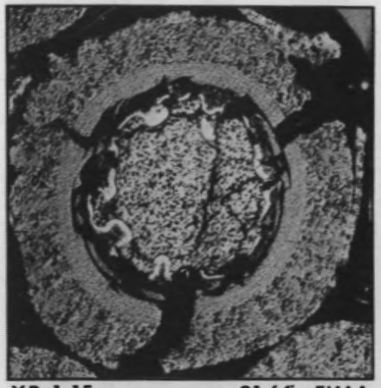

XB-1-15 21.6% FIMA
87% FAILURE AT 1020°C

SOL-GEL UO_2 FUEL

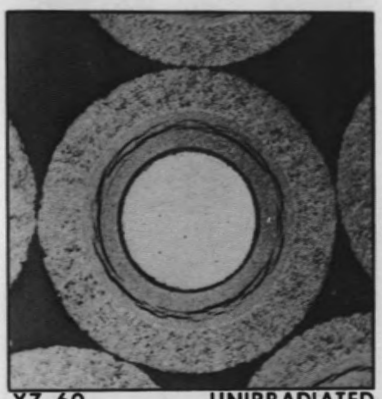

YZ-60 UNIRRADIATED

51μ INNER (2.16 g/cm³)
74μ OUTER (2.05 g/cm³)

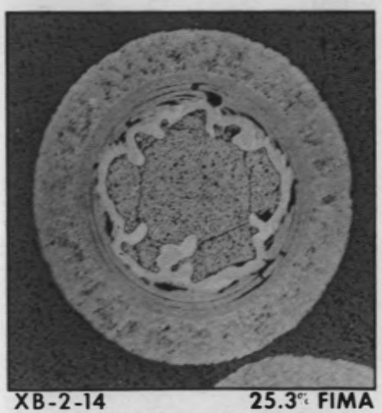

XB-2-14 25.3% FIMA
1% FAILURE AT 1400°C

Fig. 5.7. Comparison of Irradiation Performance of Particles with High-Density Laminar Inner Coatings and Granular Outer Coatings.

Reactor Program,[10] in which sol-gel-fueled coated particles survived to burnup levels of 35 to 50% FIMA in instrumented capsules at temperatures between 1000 and 1300°C.

Summary of Irradiation Tests on Sol-Gel-Derived Fuels as Coated Particles

The irradiation tests discussed here represent only a few of the tests on coated particles with sol-gel-derived fuel kernels. Most have been conducted as part of the Gas-Cooled Reactor Program. Since these tests are reported by that program, they are not discussed in detail here. However, since they are complementary tests used to evaluate the various parameters included in the mathematical model, it is appropriate that we refer to the sources of information on these tests. Table 5.2 lists all the irradiation tests that have contained sol-gel-derived fuel kernels. Details of the tests can be found in the appropriate Gas-Cooled Reactor Program progress reports.[11-18]

---

[10] J. A. Conlin *et al.*, "High Burnup Coated-Particle Irradiation Experiments in ORR Position F-9," GCR Program Semiann. Progr. Rept. March 31, 1967, ORNL-4133, pp. 66–67.

[11] D. B. Trauger *et al.*, GCR Program Semiann. Progr. Rept. Sept. 30, 1966, ORNL-4036.

[12] D. B. Trauger *et al.*, GCR Program Semiann. Progr. Rept. March 31, 1968, ORNL-4266.

[13] D. B. Trauger *et al.*, GCR Program Semiann. Progr. Rept. Sept. 30, 1965, ORNL-3885.

[14] D. B. Trauger *et al.*, GCR Program Semiann. Progr. Rept. Sept. 30, 1964, ORNL-3731.

[15] D. B. Trauger *et al.*, GCR Program Semiann. Progr. Rept. March 31, 1965, ORNL-3807.

[16] D. B. Trauger *et al.*, GCR Program Semiann. Progr. Rept. March 31, 1967, ORNL-4133.

[17] D. B. Trauger *et al.*, GCR Program Semiann. Progr. Rept. Sept. 30, 1967, ORNL-4200.

[18] D. B. Trauger *et al.*, GCR Program Semiann. Progr. Rept. Sept. 30, 1968, ORNL-4353.

Table 5.2. Summary of Irradiation Tests on Coated-Particle Sol-Gel Fuels

Experiment	Fuel Varieties	Fuel Kernel Size (μ)	Coated Particle Variations[a]	Type of Experiment[b]	Fuel Irradiation Temperature (°C)	Fission-Gas Release Rate[c] (R/B)	Peak Burnup (% FIMA)[d]	Status	Objective	Reference
X-basket No. 1 43-89	Sintered UO_2 and bed-melted UC_2	220	12	1	400; 1000		25	Examined	Compare coated-particle model performance characteristics with fuel performance	11
X-basket No. 2 43-97	Sol-gel and sintered UO_2	210	13	1	400; 1400		27	Examined	Compare sol-gel microsphere performance with sintered spheroids	12
X-basket No. 4 43-98	Sol-gel $(Th,U)O_2$	280	15	1	400; 1400		20	Being examined	Test fuel particles prepared for irradiation in Dragon; investigate coating optimization and fast-flux effects on particle performance	
X-basket No. 3 43-104	Sol-gel $(Th,U)O_2$ and sol-gel UO_2	230	10	1	400; 1400		25	Being examined	Determine the effects of the Th/U ratio on fuels with a constant fissile content	
X-basket No. 5 43-105	Sol-gel $(Th,U)O_2$	450	11	1	400; 1400		25	In-reactor	Evaluate the performance of fertile fuels and fast-flux effects, including radiation creep on coated-particle behavior	
Loop 1-14	Sol-gel ThO_2 and $(Th,U)O_2$	240; 210	2	4	1350; 675	4.2×10^{-5}	2.7	Examined	Evaluate the performance of large beds of loose coated particles and the performance and fission-gas retention of coated sol-gel oxide kernels	13
Loop 1-15	Sol-gel ThO_2 and $(Th,U)O_2$ Bed-melted UC_2 and $(Th,U)C_2$	230; 340 380; 180	4	4	1400; 675	2×10^{-6} to 2×10^{-4}	12	Being examined	Same as Loop 1-14, with controlled coolant purity and a preliminary test of a lightly bonded bed of coated particles	11
B9-19	Sol-gel $(Th,U)O_2$	210	1	3	1200	2×10^{-6}	0.7	Examined	Test stability of sol-gel oxide as a coated particle	14
O1-8	Sol-gel $(Th,U)O_2$ and bed-melted $(Th,U)C_2$	210	1	2	1130		0.03	Examined	Test fueled graphite sphere containing loose coated particles within an array of machined holes	15
F-9 HIBUP	Sol-gel UO_2 Bed-melted UC_2	150 125	2	3	1400–1100	10^{-6} to 10^{-4}	50	Examined	Evaluate the fission-product retention and irradiation stability of coated particles at extended burnup levels	16
F-9 HIBUP-2	Sol-gel UO_2 Bed-melted UC_2	265–150 190	9	3	1400	2×10^{-4}	20	Examined	Same as F-9 HIBUP, including some SiC coatings	12
B9-31	Sol-gel UO_2	210	1	3	1400	10^{-6} to 6×10^{-4}	23	Being examined	Test of mathematical model failure predictions under monitored gas-release conditions	11
B9-32	Sol-gel UO_2	280	1	3	1400	1×10^{-4}	25	In-reactor	Evaluate performance of low-temperature pyrolytic carbon coatings	16
A9-8	Sol-gel UO_2	270	2	3	1400	1×10^{-7}	15	In-reactor	Same as B9-32	16

Table 5.2. (Continued)

Experiment	Fuel Varieties	Fuel Kernel Size (μ)	Coated Particle Variations[a]	Type of Experiment[b]	Fuel Irradiation Temperature (°C)	Fission-Gas Release Rate[c] (R/B)	Peak Burnup (% FIMA)[d]	Status	Objective	Reference
A9-9	Sol-gel UO_2 Bed-melted UC_2	240 210	8	3	1000			In preparation	Test retention of solid fission products	16
Dragon	Sol-gel $(Th,U)O_2$	280	2	5	700–1100			In-reactor Dec. 1966 to Sept. 1969	Evaluate sol-gel oxide fuels as coated particles in a fuel element of an operating High-Temperature Gas-Cooled Test Reactor	11
A9-10	Sol-gel UO_2	200	1	3	1000–1500	1.0×10^{-7}	8.9	Examined	Mechanisms of fission-product release	17
A9-12	Sol-gel UO_2	270	1	3	1650	$> 10^{-3}$	12.3	Examined	Performance at high temp	17
A9-13	Sol-gel UO_2	240; 270	2	3	700–1200	1×10^{-3}	2.0	Examined	Release rate from uncoated UO_2	17
A9-14	Sol-gel $(Th,U)O_2$	430	1	3	1250	9×10^{-8}	2.0	Examined	Test engineering-scale coatings	12
A9-15	Sol-gel UO_2 Sol-gel ThO_2 bonded	230; 400	1	3	1250	4×10^{-8}	35	Examined	Bonded bed to high burnup	18
B9-33	Sol-gel UO_2	270	1	3	1250	1×10^{-5}	6.0	Examined	Test Butadiene-derived coating	16
B9-35	Sol-gel UO_2	240	1	3	1250	1.8×10^{-8}	10.7	Examined	Barrier coating at reference temp	17
B9-36	Sol-gel UO_2 Melted UC_2	270	1	3	800–1300	$> 10^{-3}$	5.0	Examined	Release rate from uncoated UC_2	17
B9-37	Sol-gel UO_2	240	1	3	1700	3×10^{-4}	7.7	Examined	Performance of barrier coating at high temp	12
B9-39	Sol-gel UO_2	240	1	3	900	3×10^{-8}	13.3	Examined	Performance at mean HTGR fuel temp	12, 18
B9-41	Sol-gel UO_2	230; 400	2	3	650	1.7×10^{-7}	27	In-reactor	Fission-product behavior in postirradiation heating experiments	18
B9-42	Sol-gel ThO_2 bonded	230; 400	2	3	650		15	In preparation		18
F-9 HIBUP-3	Sol-gel ThO_2 bonded	230; 400	1	3	1200	2×10^{-6}	38	Examined	Bonded bed to high burnup	18
HFIR-HT-1	Sol-gel ThO_2	275; 425	17	1	700; 1100		5	Examined	Effects of fast neutron fluence on performance	18
DFR-3	Sol-gel ThO_2	275	4	1	1150		0.0	Examined	Effects of fast neutron fluence on performance	12

[a]Coated particle variations include both coating parameter and fuel composition variables to make up the different types of coated particles in a test.
[b]1. Noninstrumented static-atmosphere capsules. 2. Instrumented static-atmosphere capsules. 3. Instrumented sweep-gas capsules. 4. Instrumented circulated gas loop experiments. 5. Test reactor fuel rods.
[c]Release-to-birth rate ratio for ^{88}Kr.
[d]Fissions per initial metal atom.

We are using the mathematical model to design all our irradiation experiments and are using the experimental results to refine the model parameters. The specific performance predictions from the mathematical model will be used together with the process development results to establish optimum economic specifications for coated-particle fuels for use in an operating high-temperature gas-cooled reactor in which both the fuel composition and the irradiation conditions will vary with core position.

6. BULK OXIDE PROCESS DEVELOPMENT

R. B. Fitts

The bulk oxide reactor fuels have exhibited excellent in-reactor performance and are the predominant fuels in today's power reactors. Nevertheless, there is a real incentive to develop more economical fabrication techniques for the bulk oxides. The claylike materials, powders, and microspheres from the sol-gel process lend themselves to the production of extrusions, pellets, and Sphere-Pac fuels. Extrusion work was summarized previously,[1] and further work has been deferred to emphasize work on Sphere-Pac and pellets. All three of these fuel forms, at their present state of development, appear to offer economic and/or technical advantages over the standard oxide pellet fabrication techniques.

Low-Energy Microsphere Packing (Sphere-Pac)

R. B. Fitts A. R. Olsen J. Komatsu[2]

High-density microspheres of $(U,Pu)O_2$ produced by the ORNL sol-gel process are ideally suited for fuel rod fabrication by the Sphere-Pac process. We are developing this fabrication process to produce fuel rod loadings with smear densities in the range 80 to 90% of theoretical.

We have reported on our initial Sphere-Pac development work in the last progress report[3] and elsewhere.[4,5] The Sphere-Pac process at that

---

[1]A. B. Meservey, R. B. Fitts, K. H. McCorkle, J. P. McBride, J. M. Robbins, J. G. Stradley, and R. L. Hamner, Status and Progress Report for Thorium Fuel Cycle Development, Dec. 31, 1966, ORNL-4275, pp. 104–118.

[2]Foreign visitor on leave from the Japanese Power Reactor and Nuclear Fuel Development Corporation, Japan.

[3]A. R. Olsen, Status and Progress Report for Thorium Fuel Cycle Development, Dec. 31, 1966, ORNL-4275, pp. 118–120.

[4]A. R. Olsen, J. D. Sease, R. B. Fitts, and A. L. Lotts, Fabrication and Irradiation Testing of Sol-Gel Fuels at Oak Ridge National Laboratory, ORNL-TM-1971 (September 1967).

[5]F. G. Kitts, R. B. Fitts, and A. R. Olsen, "Sol-Gel Urania-Plutonia Microsphere Preparation and Fabrication in Fuel Rods," pp. 195–210 in Intern. Symp. Plutonium Fuels Technol., Scottsdale, Ariz., 1967, Nucl. Met. 13, American Institute of Mining, Metallurgical and Petroleum Engineers, New York, 1968.

time involved pouring the large microspheres into the cladding tube, vibrating the tube to settle the poured bed, and then infiltrating this bed with the fine microspheres.

These studies of binary packing have verified the results of earlier workers in this field,[6,7] provided practical evidence of the simplicity and reproducibility of the binary Sphere-Pac beds, and yielded 30 samples of 3- to 6-in.-long fuel columns at around 84% volume packing for characterization and irradiation testing.

We have continued to investigate Sphere-Pac, and in particular we are attempting to produce denser beds (88% and higher). We have investigated the effectiveness of blending two sizes of large spheres to form the initial poured bed. We placed about 60 g of coarse and medium size spheres in a 3.5-cm-diam 120-cm^3 bottle, rolled the bottle at 275 rpm for up to 5 min, poured the blended spheres into a 1.07-cm-ID graduated tube, and packed the unrestrained bed by vibrating for from 1 to 120 min. Blending was complete after about 1 min, and the poured bed was settled to maximum density after about 1 min of vibration on a Syntron vibrator. The conditions of vibration were 60 cps with about 7g horizontal and 2g vertical acceleration of the bed.

The first data on blending were obtained with equal weights of coarse and medium spheres to determine the general trend in bed densities and to examine the problem of segregation of the size fractions. Figure 6.1 presents the general trend. A definite increase in bed density is obtained with increasing sphere diameter ratios, and an unrestrained bed will begin to segregate during vibration when the size ratio exceeds about 3.5. The blended bed density lacks reproducibility at higher diameter ratios, probably because of segregation during blending.

Figure 6.2 illustrates our results on blended bed volume packing (P_V) as a function of the volume percentage of coarse and medium spheres.

---

[6]R. K. McGeary, J. Am. Ceram. Soc. 44(10), 513–522 (1961).

[7]J. E. Ayer and F. E. Soppet, J. Am. Ceram. Soc. 48(4), 180–183 (1965).

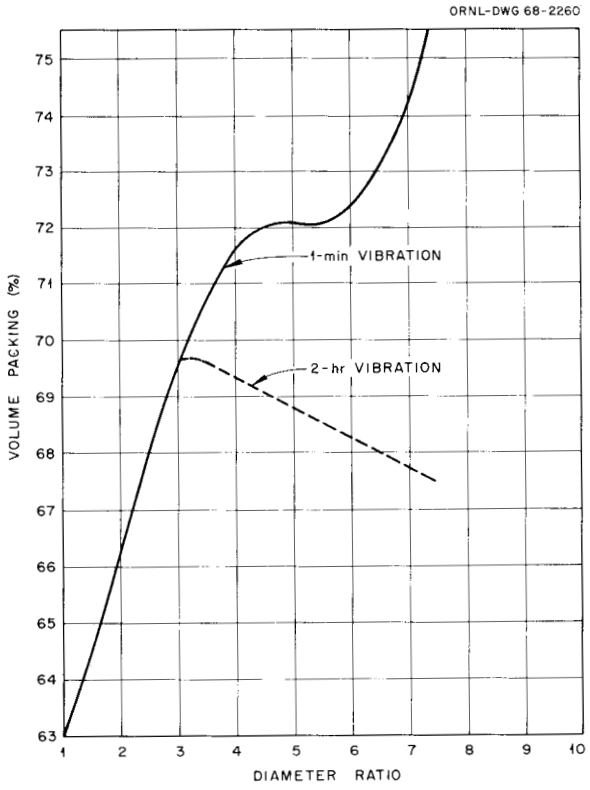

Fig. 6.1. Volume Packing for Unrestrained Equal-Weight Mixture of Two Sizes of Spheres and Effect of Vibration After Mixing.

These results agree well with those obtained by McGeary[6] and extend them to lower diameter ratios and smaller spheres. The data obtained from the maximum density point (about 65% coarse and 35% medium) on these curves may be used to calculate the packing efficiency (P_E) of the medium size spheres in filling the void between the coarse spheres. To calculate this efficiency on a uniform basis, we assume an artificial packing efficiency for the coarse spheres of 63.5%. This is the limit for packing efficiency of a single size sphere in a large tube, as presented by Ayer.[7]

Using this basis for the packing efficiency of smaller spheres in a bed of large spheres, we obtained the values in Fig. 6.3. Some data from McGeary and Ayer are also included. The agreement is excellent for diameter ratios up to 8 or 10. Above this range, Ayer's values deviate significantly from our findings and those of McGeary.

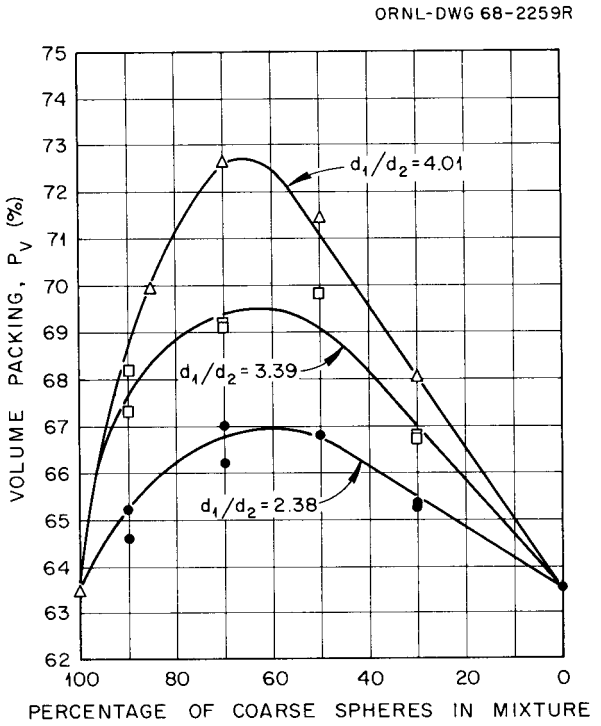

Fig. 6.2. Volume Packing of Blended Spheres of Two Sizes for Various Diameter Ratios.

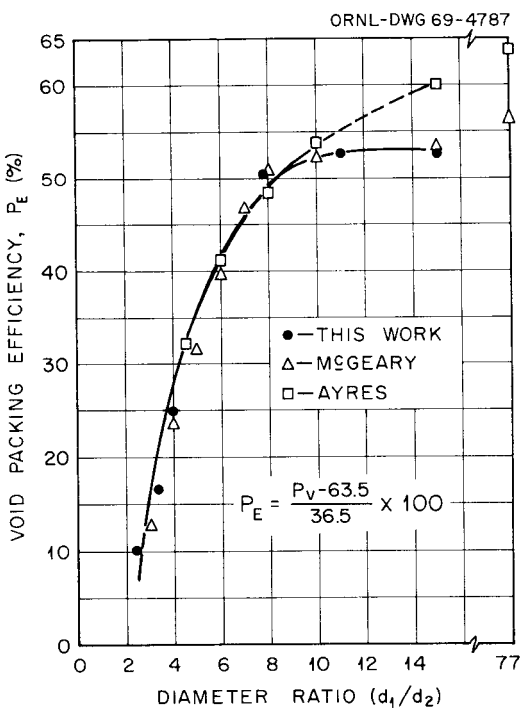

Fig. 6.3. Packing Efficiency of Small Spheres in a Bed of Large Spheres.

Since our objective was to produce a packed bed with a density higher than the 84% obtained from two size fractions, we then tried infiltration of a blended bed with a small size fraction. Based on the data in Fig. 6.3, we used a small size fraction one-tenth the diameter of the medium size in the blended bed. Using a single infiltration of fine spheres into a blended coarse bed, we obtained packing densities exceeding 88%.

A final point to be resolved was the uniformity of Sphere-Pac fuels formed by the blended bed approach. We have prepared four 10-in.-long × 0.345-in.-diam fuel columns by blending ThO_2 microspheres (diameter ratio 4) for the coarse, blended bed and infiltrating fine spheres. We measured the density variation with a gamma-ray absorption densitometer[8] before and after infiltration. One of the coarse beds was uniformly dense (71 ± 1.5% of theoretical) over the entire fuel length. Two had low-density regions (about 66% of theoretical) 2 in. long at the bottom. The other exhibited low density at bottom and top. After the infiltration of small spheres, the low-density regions were gone, and the rods were of uniform density (88 ± 1.5% of theoretical) over the entire length. The density variation in the blended bed before infiltration can probably be eliminated by more sophisticated or better controlled blending techniques. The obliteration of the low-density regions during infiltration is to be expected since the voids in these areas are larger and allow more efficient packing of the fines.

Using the information on blended bed densities and packing efficiencies obtained during this experimental program, we have developed a graphical construction, shown in Fig. 6.4, to correlate and generalize all of our information relating to the Sphere-Pac fabrication procedure. If a 45° operation line is established between the two zero points of the axes, then the void volume associated with any packed volume may be determined by reading up and then across (line ABC). If we now construct a line joining the packing efficiency of a given size sphere (percentage of available void volume filled by spheres) to the void volume zero point,

---

[8] B. E. Foster and S. D. Snyder, Mater. Evaluation 26(2), 27–32 (1968).

ORNL-DWG 68-1631

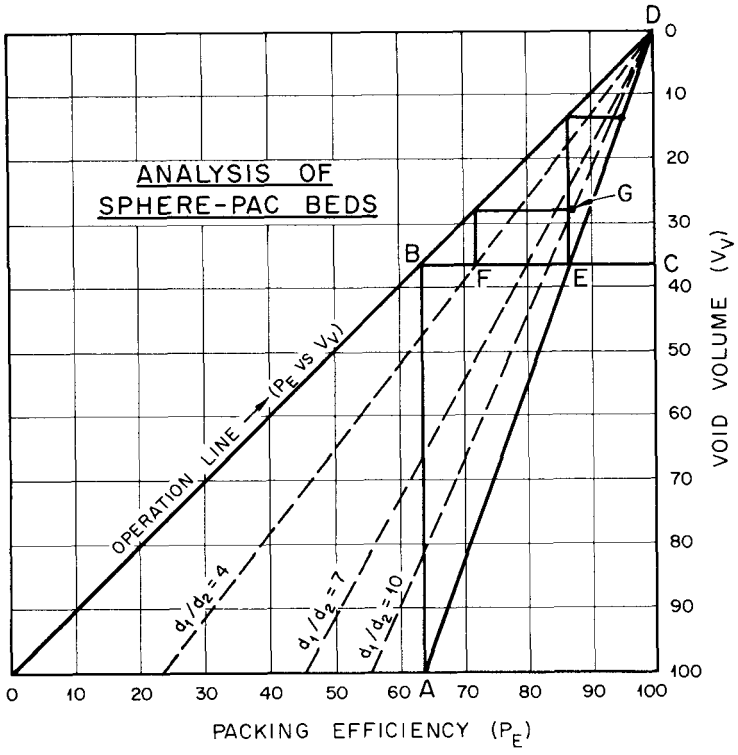

Fig. 6.4. Analysis of Sphere-Pac Beds.

the horizontal distance between this line and the operation line is always proportional to the packing efficiency multiplied by the void volume associated with that packed bed density. Thus, the line AD represents the packing of a single size sphere in a large tube or in a packed bed where the diameter of the sphere is less than approximately 1/25 that of the smallest sphere in the packed bed.

This curve may be used to illustrate the effect of serial infiltrations with spheres with diameter ratios (d_1/d_2) greater than 25. We will obtain 63.5% packing with the coarse spheres. If we then infiltrate a small size sphere at this same efficiency we would obtain, from point E, an 87%-dense bed, and a second infiltration produces a 95%-dense bed. This type of line must also be plotted for the packing of spheres having diameters of various ratios to that of the large spheres in the bed. These data are shown by the dotted lines for spheres of 1/4, 1/7, and 1/10 the size of the spheres in the bed and were obtained from the plot of P_E vs d_1/d_2 in Fig. 6.3.

We may now see the effects of using a blended bed or the effect of infiltration at less than the optimum 63.5% packing efficiency. If a d_1/d_2 ratio of 4.0 is used for a blended bed, the bed density (volume packing) is increased to 72%, point F. Infiltration with spheres one-tenth the size of the medium fraction produces an 88%-dense bed, point G. This is exactly the density that we have obtained and reproduced by this technique. We have also produced 86.5%-dense beds by infiltration of a blended bed ($d_1/d_2 = 3.4$) with the 10/1 size ratio of medium to small. This is the density predicted by the graphical correlation for these conditions.

The above discussion shows that to produce a 90%-dense fuel we must use either a double infiltration with very carefully controlled sphere sizes or a blended bed at d_1/d_2 of about 5.8, followed by a single infiltration. This requires investigation of the behavior of beds blended at this diameter ratio since they tend to segregate, as was shown in Fig. 6.1.

Our work on the Sphere-Pac process has been presented at an American Ceramic Society meeting,[9] and a final report is in preparation. We feel that it is a promising technique for bulk oxide fuel fabrication over the range of 80 to 90% volume fuel loading and that the use of blended beds is the most attractive approach to the formation of fuels with density near 90%.

Pelletizing of Sol-Gel Oxides

R. L. Hamner J. M. Robbins R. A. Bradley

Techniques for making ThO_2–6% UO_2 pellets from sol-gel-derived powders have been investigated by Robbins and Stradley.[10] They studied the effects of sol-gel powder calcination temperature, moisture content, uniaxial and isostatic forming pressure, and sintering atmosphere on the

---

[9]R. B. Fitts, A. R. Olsen, and J. Komatsu, "Sphere-Pac Fabrication of Sol-Gel Nuclear Fuels," Am. Ceram. Soc. Bull. 47(9), 844 (1968).

[10]J. M. Robbins and J. G. Stradley, Fabrication of Sol-Gel-Derived Thoria-Urania by Cold Pressing and Sintering, ORNL-4426 (in preparation).

bulk density of sintered pellets. Differential thermal analysis (DTA), thermogravimetric analysis (TGA), and BET surface area measurements were used to characterize the sol-gel powder. They produced ThO_2–6% UO_2 pellets with shrinkages ranging from 16 to 20%, bulk densities ranging from 78 to 95% of theoretical, and oxygen-to-uranium ratios of 2.67 before hydrogen reduction to 2.00.

We are now investigating the pelletization of sol-gel urania. We produced urania powders from dried microspheres and shards by grinding them to −325 mesh and from a liquid sol by freeze drying.[11] This generally involves freezing the wet material, placing it under vacuum, and supplying enough heat to sublime the frozen moisture out of the structure without melting it. Our source materials are described in Table 6.1. Most of the material was processed in air; however, a portion of the powder produced from shards was processed in argon to provide a comparison of the sintering behavior. We produced 0.2-in. right cylindrical pellets from all of the powders and from whole microspheres by a number of fabrication schemes shown in Fig. 6.5. The selection of a sintering schedule and atmosphere was based on sintering studies of urania microspheres by DTA, chemical analysis, and x-ray crystallite size measurement. The pellets were sintered in Ar–4% H_2 at about 100°C/hr to the temperature indicated in Fig. 6.5. We used a soak period at 150°C to subdue an intense exotherm that occurs just above this temperature because of a nitrate-organic reaction and another soak at 450°C to remove as much of the volatile material as possible before sintering began just above this temperature. In most of our experiments, steam was introduced into the gas stream between room temperature and 1000°C because we had found it to be effective in the removal of carbon.[12] For comparison, we sintered some pellets in a dry atmosphere.

---

[11] E. W. Flosdorf, Freeze-Drying, Reinhold Publishing Corporation, New York, 1949.

[12] H. Beutler and R. L. Hamner, "Drying and Sintering of Sol-Gel Urania Microspheres," Metals and Ceramics Div. Ann. Progr. Rept. June 30, 1967, ORNL-4170, pp. 223–226.

Table 6.1. Description of Sol-Gel Materials Used for Pelletizing

Preparation Variables	Values for Different Physical Forms			
	Gel Spheres	Sol	Gel Shards[a]	Gel Shards[b]
Drying temperature, °C	185		90–95	90–95
Drying atmosphere	Ar-H_2O		Argon	Argon
Sol compositions:				
U, M	~ 0.6	0.71	0.71	0.915
U(IV), mole/mole U	~ 0.89	0.89	0.89	0.896
NO_3^-, mole/mole U	~ 0.18	0.183	0.183	0.093
$HCOO^-$, mole/mole U	~ 0.3	0.38	0.38	0.41

[a]Crystallite size: 55 A.

[b]Crystallite size: 35 A.

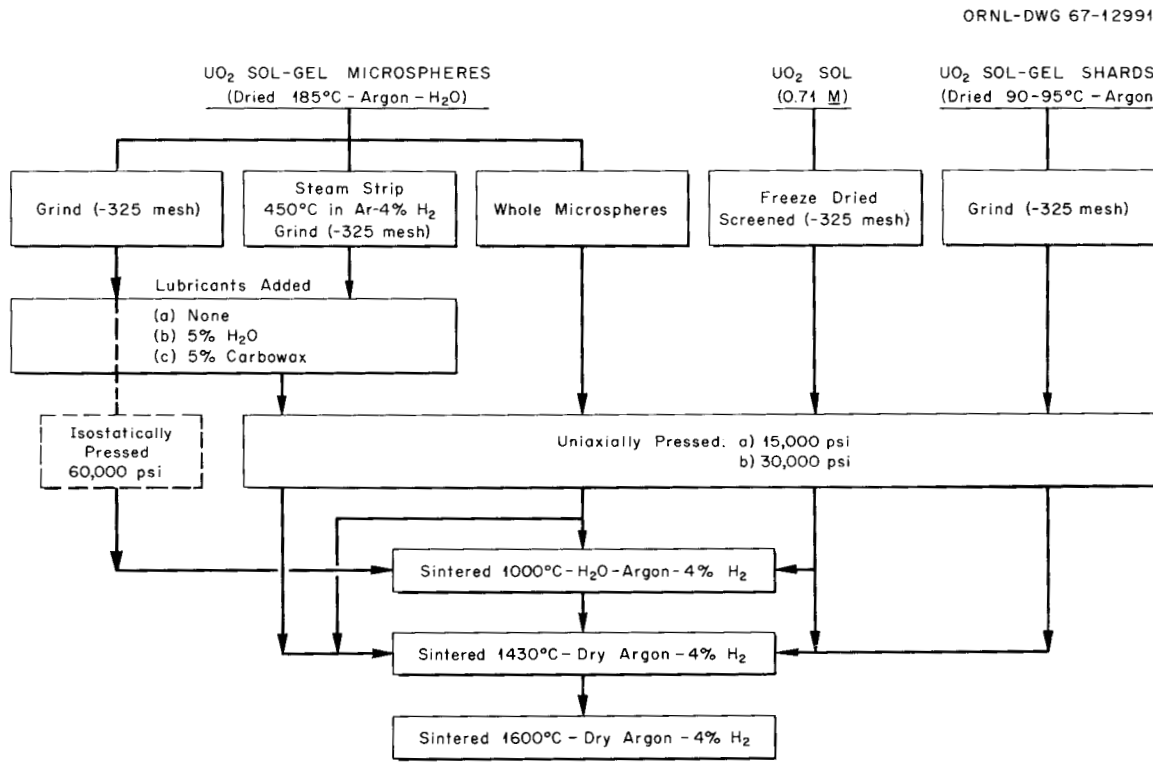

Fig. 6.5. Fabrication of UO_2 Sol-Gel Pellets.

The histories and densities of the pellets obtained by our various fabrication schemes are shown in Table 6.2. The results are not shown for pellets prepared with lubricants, since these had no significant effect on the densities obtained. A summary of our observations and results follows.

We had no difficulty in pelletizing the powders or the whole microspheres, and by various fabrication schemes we produced pellets ranging in density from 68.7 to 92.9% of theoretical after sintering at 1430°C.

We obtained the highest densities from powders derived from the two batches of shards. For each batch of this material, slightly higher densities resulted from the material exposed to air than from the material protected by argon, but densities were not significantly affected by the difference in crystallite sizes of the two batches (55 and 35 A).

Powder obtained by freeze-drying UO_2 was less sinterable than the powdered microspheres. All of the pellets pressed at 30,000 psi from freeze-dried powder cracked during sintering. Calcination of the powder at about 200°C eliminated the cracking. We are studying freeze-drying further to determine how drying conditions affect the powder produced.

Pellets pressed from the whole microspheres were almost as dense as those prepared from powdered microspheres after sintering at 1430°C and had the outward appearance of consolidated microspheres stuck together by a porous matrix.

We obtained the lowest densities on pellets derived from microspheres that had been steam-treated in Ar–4% H_2 at 450°C before being ground to a powder.

Pellets sintered in dry Ar–4% H_2 were about as dense as pellets sintered in a steam-Ar–4% H_2 atmosphere, but the steam treatment will probably be necessary to keep the carbon content low; for example, pellets subjected to the steam treatment retained only 50 ppm C, whereas pellets from the same batch of powder sintered in dry gas retained 380 ppm C after a final sintering at 1430°C.

For the same material, sintered densities increased with increase in uniaxial forming pressure, as expected. Isostatic pressing at 60,000 psi, of course, had a strong influence on density; but we prefer to avoid this operation if possible.

Table 6.2. History and Densities of Pelletized UO_2 Sol-Gel Materials

Material Description[a]	Forming Pressure (psi)	Average Sintered Densities[b] (% of theoretical)		
		1000°C	1430°C	1600°C
	$\times 10^3$			
Dried sol-gel shards[c] ground to −325 mesh	40		92.9	
	30		92.6	
	15		86.8	
Dried sol-gel shards[c] ground to −325 mesh; processed in argon	30		89.8	
	15		81.8	84.4
Dried sol-gel shards[d] ground to −325 mesh	40		92.3	
	30		90.3	
	15		82.5	
Dried sol-gel shards[d] ground to −325 mesh; processed in argon	40		91.5	
	30		88.3	
	15		79.9	80.8
Sol freeze-dried to −325 mesh powder	30		e	
	15	78.7	82.2	84.6
Microspheres, ground to −325 mesh	60[f]	87.5	90.3	
	30	73.5	79.9	82.0
	15	68.1	72.7	
Microspheres, steam-stripped in Ar–4% H_2 at 450°C, ground to −325 mesh	30	70.0	75.7	77.5
	15	64.9	69.4	72.5
Whole microspheres	30	71.1	78.7	
	15	63.1	68.7	70.1

[a]Powder processed in air except where noted otherwise.

[b]Values at more than one sintering temperature were obtained on the same pellet.

[c]Crystallite size, −55 A; oxygen-to-uranium ratio, 2.512 (air), 2.288 (argon).

[d]Crystallite size, −35 A; oxygen-to-uranium ratio, 2.494 (air), 2.470 (argon).

[e]All pellets cracked.

[f]Isostatically pressed.

Lubricants such as Carbowax and water did not significantly affect the density of pellets pressed at 30,000 psi or less, but the use of much higher pressures might require the use of a lubricant to prevent laminations.

We have selected powders derived from dried shards and from freeze-dried sols as being the best candidates for further studies of pelletizing; for reference, however, we shall continue to pelletize powdered microspheres. Our immediate plans are to investigate further means of increasing the densities of the candidate materials.

7. CHARACTERIZATION OF OXIDE FUELS

A. R. Olsen

In evaluating the potential of any fuel process and fabrication technique, it is essential to establish some of the characteristics of the particular material. This information is also invaluable in the interpretation of the results of irradiation test performance.

Thermal Conductivity

D. L. McElroy J. P. Moore
P. H. Spindler

We have measured the thermal conductivity of sol-gel-derived fuels on two types of specimens. In one study,[1] sintered pellets of sol-gel ThO_2 were used to determine the effect of porosity, UO_2 content, and sintering conditions on the thermal conductivity (λ) between 30 and 120°C. A second study involved Sphere-Pac beds of sol-gel thoria to determine the effects of temperature, gas, and gas pressure on thermal conductivity between 50 and 1000°C.

The thermal conductivity of 93.7%-dense ThO_2 was measured from 80 to 1400°K and compared with similar measurements on UO_2. The heat transport in single-crystal and polycrystalline LiF is being studied from 80 to 1100°K to assess the magnitude of radiation conduction, with the hope that such knowledge can be applied to oxide nuclear fuels.

Sintered Specimens[1]

A longitudinal heat flow technique was used to measure thermal conductivity on the nine specimens described in Table 7.1. The two sol-gel ThO_2 samples had equivalent densities and showed little effect of sintering conditions on λ. For the three oxalate ThO_2 specimens λ at 75°C

[1]J. P. Moore, T. G. Kollie, R. S. Graves, and D. L. McElroy, Thermal Conductivity Measurements on Solids Between 20 and 150°C Using a Comparative Longitudinal Apparatus: Results on MgO, BeO, ThO_2, $Th_xU_{1-x}O_{2+y}$ and Al-UO_2 Cermets, ORNL-4121 (June 1967).

Table 7.1. Specimen Description and Thermal Conductivity Data for Thoria and Thoria-Urania

Specimen Description	Density (g/cm^3)	Sintering Conditions	Thermal Conductivity[a] ($w\ cm^{-1}\ °C^{-1}$)		
			30°C	75°C	120°C
Sol-gel thoria	9.046	In hydrogen at 1750°C	0.0828	0.0702	0.0596
Sol-gel thoria	9.046	In air at 1650°C	0.0817	0.0692	0.0509
Oxalate thoria	9.525	In air at 1650°C	0.1260	0.1100	0.0958
Oxalate thoria	8.582	In air at 1650°C	0.0934	0.0800	0.0683
Oxalate thoria	8.116	In air at 1650°C	0.0593	0.0523	0.0480
$Th_{0.953}U_{0.047}O_{2.026}$[b]	9.067	In air at 1650°C	0.0351	0.0347	0.0340
$Th_{0.939}U_{0.061}O_{2.026}$[b]	9.043	In air at 1650°C	0.0245	0.0244	0.0243
$Th_{0.937}U_{0.063}O_{2.000}$	8.796	c	0.0972	0.0832	0.0708
$Th_{0.953}U_{0.047}O_{2.000}$	8.733	In hydrogen at 1750°C	0.0852	0.0769	0.0683

[a]Smoothed values are tabulated here. Measured values were precise to within ±0.25% and have a probable accuracy of ±1.75%. Some of these specimens were ground flat in a solution of ethylene glycol and water. The solution had a noticeable effect on the specimen conductivity when the measurements were made shortly after grinding. It was necessary, therefore, to thoroughly dry the samples by heating to 400 or 500°C in air before making measurements.

[b]Two samples of each material were measured, with similar samples agreeing to within 0.5%.

[c]Sintered in air at 1650°C and then sintered in hydrogen at 1750°C.

is 30% higher than for sol-gel thoria with equivalent densities. The data predict a thermal conductivity of 0.122 $w\ cm^{-1}\ °C^{-1}$ for theoretically dense ThO_2 at 75°C, when corrected for porosity by

$$\lambda = \lambda_{TD}(1 - P)/(1 + \beta P) \ , \qquad (1)$$

where P is the pore volume fraction and β is an empirical parameter describing the effect of porosity. At 75°C, β is 1.2 for oxalate ThO_2

and 6.5 for sol-gel ThO_2, indicating a large effect of porosity and structure.

The effects of oxygen and uranium contents on the thermal conductivity of sol-gel $Th_xU_{1-x}O_{2+y}$ can be compared in Table 7.1. The oxygen-to-metal ratio was maintained at essentially 2.000 when specimens were sintered in hydrogen or sintered in air and then reduced in hydrogen; that is, $y < 0.001$. However, air-sintered materials had significantly higher oxygen-to-metal ratios and y values from 0.028 to 0.026. The significant effect of this change in oxygen-to-metal ratio is that the air-sintered materials have about half the thermal conductivity. Pure thoria showed essentially no difference between the values for air- and hydrogen-sintered material. Therefore, the great difference in the mixed oxide specimens must be attributed to the effect of oxygen-to-metal ratio. If the excess oxygen atoms in the air-sintered materials are interstitials, the thermal conductivity would be reduced by the increase in the number of phonon scatterers. This effect has been shown by Godfrey *et al.*[2] to be large in hyperstoichiometric UO_2.

Sphere-Pac Bed Microspheres

A radial heat flow apparatus similar to one described by Flynn[3] was used, as described elsewhere,[4] to measure the thermal conductivity of two vibratorily compacted beds of thoria microspheres in helium and argon up to 1000°C. The gas pressure ranged from 0.3 to 2 atm. One bed consisted of thoria microspheres less than 44 μ in diameter packed into the measurement chamber to a powder density about 64% of the theoretical density of thoria. The second bed consisted of a typical duplex-particle Sphere-Pac loading with 420-μ and less-than-44-μ microspheres loaded to give a bed density about 84% of theoretical.

---

[2]T. G. Godfrey, W. Fulkerson, T. G. Kollie, J. P. Moore, and D. L. McElroy, Thermal Conductivity of Uranium Dioxide and Armco Iron by an Improved Radial Heat Flow Technique, ORNL-3556 (June 1964).

[3]D. R. Flynn, J. Res. Natl. Bur. Std. C 67(2), 129–137 (1963).

[4]J. P. Moore, D. L. McElroy, and R. S. Graves, "Thermal Conductivity of a 58% Dense MgO Powder in Nitrogen," (Abstract) p. 711 in Thermal Conductivity, Proc. 7th Conf. Gaithersburg, Maryland, Nov. 13–16, 1967, Nat. Bur. Std. Spec. Publ. 302, ed. by D. R. Flynn and B. A. Peavy, Jr., National Bureau of Standards, Washington, D. C., September 1968.

The thermal conductivity as a function of temperature at 1 atm of gas pressure is shown in Fig. 7.1. The results are accurate to better than ±3%. In addition to the packed-bed conductivity, we have included a curve for theoretically dense solid thoria, as recommended by Powell, Ho, and Liley,[5] and high and low thermal conductivity values for helium gas from Massey.[6]

---

[5]R. W. Powell, C. Y. Ho, and P. E. Liley, Thermal Conductivity of Selected Materials, NSRDS-NBS 8 (November 1966).

[6]G. V. Massey, The Thermal Properties of Gases for Use in Reactor Heat-Transfer Calculations, DEG-Report 14(D) (1960).

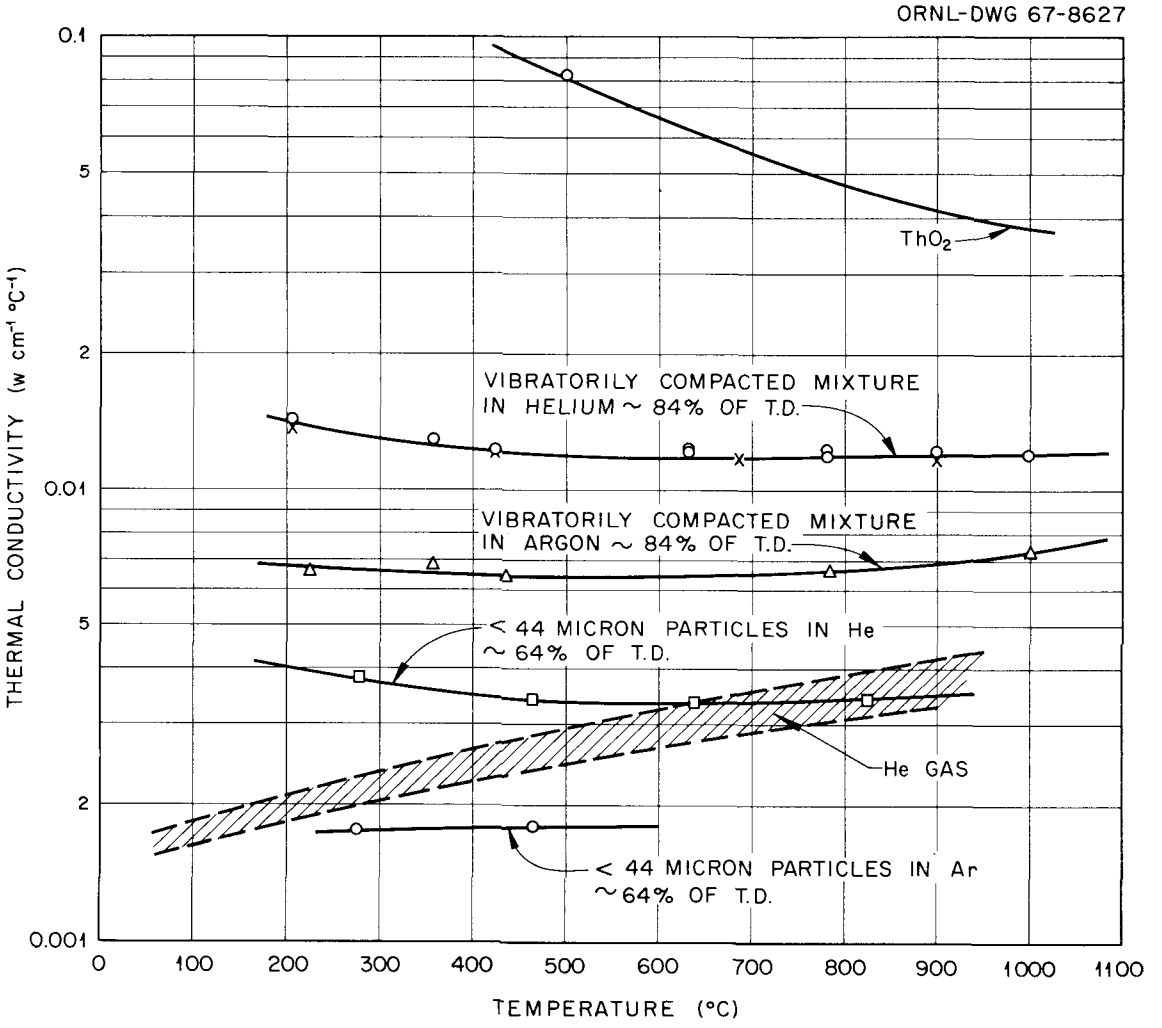

Fig. 7.1. The Effect of Temperature and Gas (at 1 atm) on the Thermal Conductivity of Vibratorily Compacted ThO_2 Microsphere Beds.

The 84%-dense bed had a higher thermal conductivity than the 64%-dense bed. The thermal conductivity in helium for both loadings is substantially greater than that in argon. The temperature independence of thermal conductivity for the powders and the low values of the 64%-dense material in helium when compared to helium gas conductivity indicate that the void size between the particles is limiting the mean free path of the gas molecules. Thus, the conductivity of the gas between the solid microspheres is lowered. For this condition Deissler and Eian[7] showed thermal conductivity to be sensitive to pressure changes. This is because the mean free path varies inversely with pressure. The effect of varying the gas pressure on thermal conductivity of the Sphere-Pac beds is shown in Fig. 7.2. These results are similar to those observed

[7]R. G. Deissler and C. S. Eian, Investigation of Effective Thermal Conductivities of Powders, NACA-RM-E52C05 (June 1952).

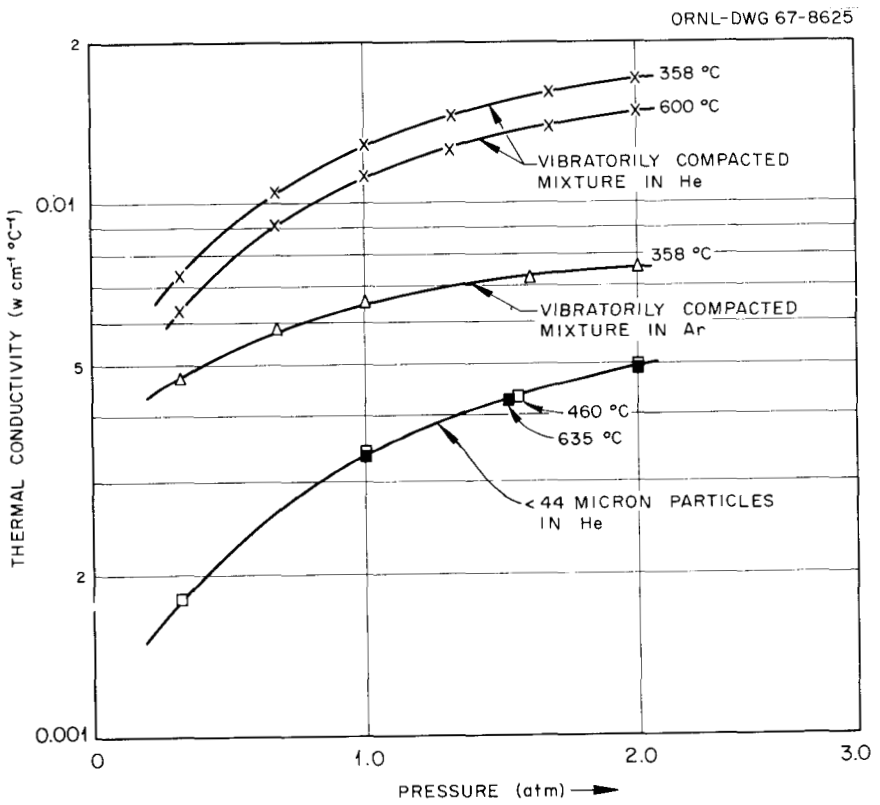

Fig. 7.2. The Effect of Gas Pressure on the Thermal Conductivity of Vibratorily Compacted ThO_2 Microsphere Beds (Bed Density 84% of Theoretical Density for Mixture; 64% of Theoretical Density for 44-μ Particles).

by Deissler and Eian for MgO and by Masamune and Smith[8] for glass beads; small solid particles were used in both.

Similar measurements are planned for UO_2 and $(U,Pu)O_2$ materials derived from the sol-gel process.

ThO_2, 93.7% Dense, Measured to 1400°K

A ThO_2 specimen was supplied by the U.S. Air Force Materials Laboratory for thermal conductivity measurements to assess the applicability of this material as a high-temperature thermal conductivity standard. In brief, our results indicate ThO_2 to be an ideal standard.[9]

The ThO_2 specimen was 93.7% of theoretical density with all pores closed and a grain size of about 18 μ. We measured λ from 80 to 400°K in a guarded longitudinal heat flow apparatus with a most probable accuracy of ±1.2% and from 320 to 1400°K in a radial heat flow apparatus with a most probable accuracy of ±1.5%.

The measured thermal conductivity values from both apparatuses were corrected to theoretical density by Eq. (1) with $\beta = 0.5$. These results in Fig. 7.3 indicate that the thermal conductivity of ThO_2 decreases continuously from 80 to 1400°K. The agreement between the two apparatuses was better than ±1% in their 100°K range of overlap.

A limited analysis of these data has been completed. Figure 7.4 indicates the temperature dependence of the thermal resistivity $(1/\lambda)$ of ThO_2. Two straight lines describe the data:

$$1/\lambda = 0.01935T - 0.1550, \text{ 200 to 400°K ;}$$

$$1/\lambda = 0.02141T - 0.9800, \text{ 400 to 1400°K .}$$

Both apparatuses indicated the slope change that occurs near 400°K. The quality of the data is indicated in Fig. 7.5, where the deviation from the high-temperature equation is plotted against temperature. The results from 400 to 1350°K are within ±1% of this equation. The

---

[8] S. Masamune and J. M. Smith, "Thermal Conductivity of Beds of Spherical Particles," Ind. Eng. Chem. Fundamentals 2, 136–143 (1963).

[9] J. P. Moore, R. S. Graves, and D. L. McElroy, "Thermal Conductivity of ThO_2 and UO_2 from 77 to 1300°K," paper presented at the 1968 Fall Meeting of the American Ceramic Society, Nuclear Division, Oct. 6–9, 1968, Pittsburgh, Pa.

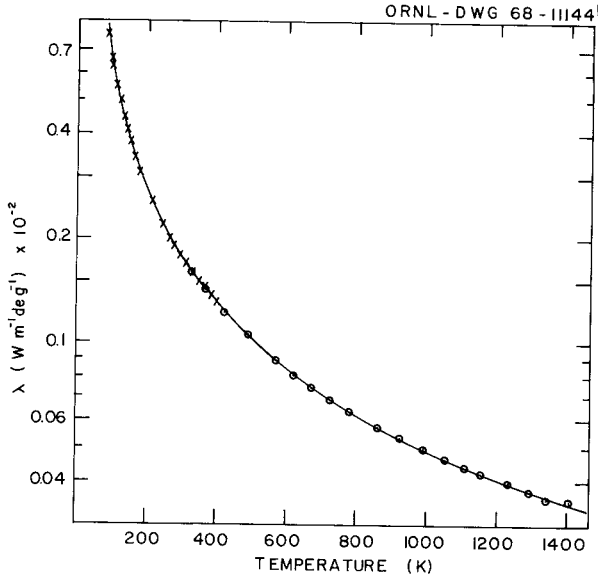

Fig. 7.3. Thermal Conductivity of 93.7%-Dense ThO_2 Corrected to Theoretical Density. Circles denote data from radial apparatus, x's from longitudinal.

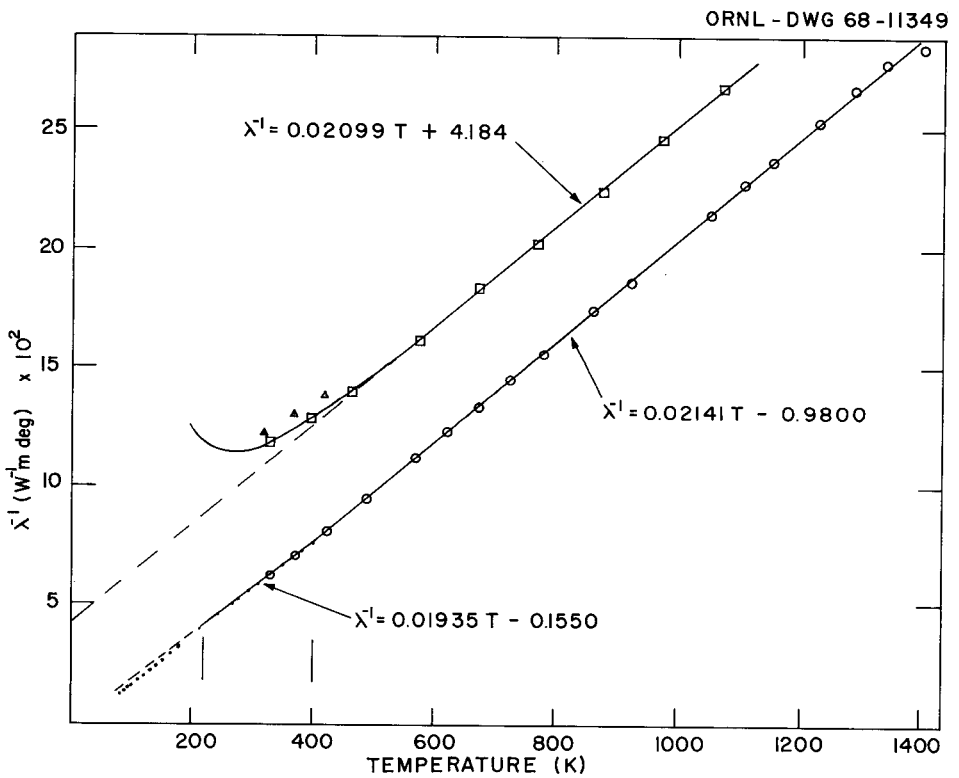

Fig. 7.4. Comparison of Measured Thermal Resistivity for UO_2 (Upper Curve) and ThO_2.

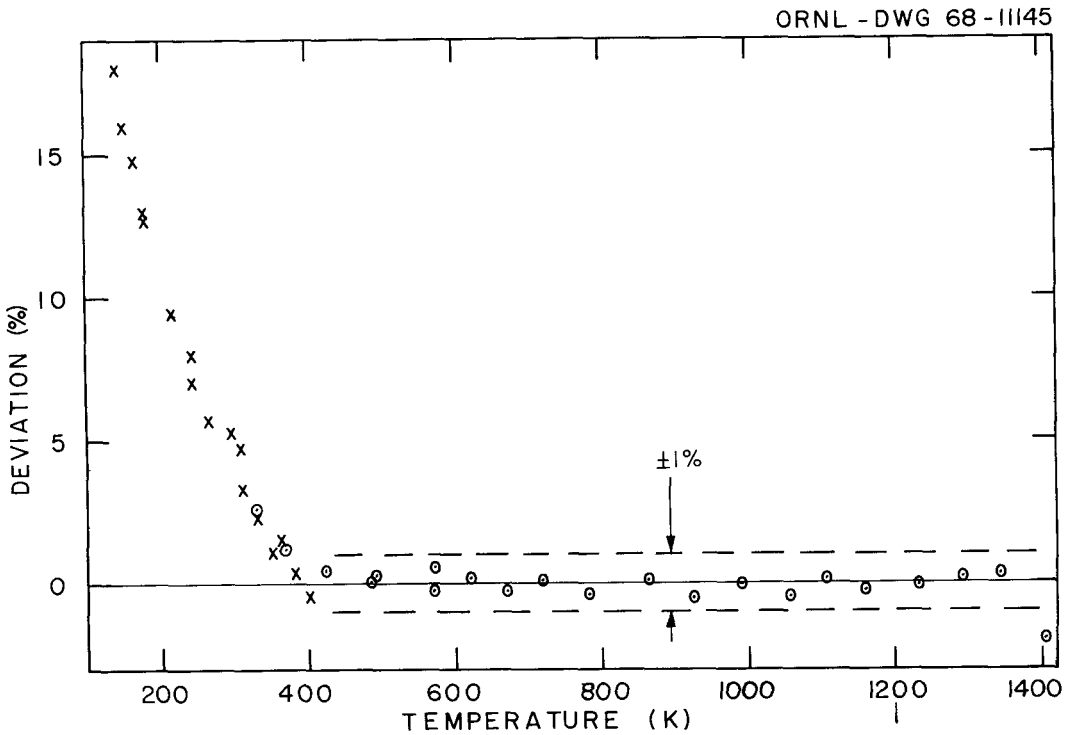

Fig. 7.5. Deviation Analysis of Measured Thermal Resistivity ($1/\lambda$) and Resistivity Calculated by $1/\lambda = 0.02141T - 0.9800$. Point symbols correspond to Fig. 7.3.

deviation at 1400°K may not be real since this is near the upper limit of the present radial apparatus.

The slope of the ThO_2 thermal resistivity temperature relation above 400°K is within 2% of the slope found for UO_2 from 500 to 1200°K and shown as the upper line in Fig. 7.4. If these portions of the curves represent 3-phonon Umklapp scatterings, they indicate that the Debye temperatures of ThO_2 and UO_2 are the same within 7%. This agrees with Debye temperature results from x-ray and elastic constant analyses of ThO_2 and UO_2. The large difference in the constants of the ThO_2 and UO_2 equations and the curvature in the UO_2 thermal resistivity near 300°K are due to phonon scattering by spin disorder. This is the result of the antiferromagnetic-to-paramagnetic transition in UO_2 at 30°K. No such transition exists in ThO_2, so the thermal resistivity of ThO_2 is lower.

Thermal Analysis with ThO_2

Experiments on the mechanisms of material transport in ThO_2 involve imposed thermal transients on powder compacts.[10] These transients have this form: an initial constant rate of change of the surface temperature for a fixed time period, followed by a constant surface temperature for a fixed time period. The resulting temperature gradients in the sample could influence the resulting densification data obtained to examine the mechanism of material transport. A series of calculations were made to assess these temperature gradients for the imposed transients on ThO_2 powder compacts. The governing differential equations were solved for the imposed boundary conditions for three cases: (1) an infinite slab, (2) an infinite cylinder (both with major dimensions of the compact), and (3) a sphere with a volume equal to the compact. These solutions were programmed for computer calculations, and the thermal response of various depths in the bodies was examined. The results indicated that thermal gradients are not important in these densification studies at 1500°C and that center-line temperatures are within 1°C of the surface temperature after a time period in the constant temperature hold that is less than 10% of the period of increasing temperature.

LiF Thermal Conductivity

To assist our understanding of the behavior of oxide nuclear fuels at high temperatures, such as the above-described data on ThO_2, and to obtain useful guidelines on the effects of infrared transmission and vacancy formation on the thermal conductivity, we are studying heat transport in LiF. This optically transparent insulator may allow an evaluation of the magnitude of radiation conduction in other materials where this phenomenon occurs at temperatures where measurement accuracy is poor.

Thermal conductivity measurements on LiF single crystals progressed to 1073°C. Two runs were made, from 343 to 773°K and from 471 to 1073°K, in the radial heat flow apparatus. The high coefficient of thermal

---

[10] C. S. Morgan, "Activation Energy in Sintering," Metals and Ceramics Div. Ann. Progr. Rept. June 30, 1968, ORNL-4370, pp. 33–34.

expansion of LiF ($\alpha = 73 \times 10^{-6}$/deg at 800°C) caused rupture of the core heater potential taps and stopped the first run. The second run was stopped 42° below the melting point, which is 1115°K, because the expansion caused most of the thermocouples to become open circuits.

Figure 7.6 shows the thermal resistivity as a function of temperature for two measuring planes in the LiF single-crystal disks of the second run. Some small difference in the two curves is noted since the top plane disk was used in the first run. The experimental data are plotted onto a network of curves generated by the computer. The straight line of the computer plot is calculated from our low-temperature linear thermal resistivity data. We assume the heat transport at high temperatures is being influenced by radiation transfer, and this accounts for the curved lines. A first estimation for the total thermal conductivity is made as follows

$$\lambda = \lambda_L + 16\sigma n^2 T^3/3k \ , \qquad (2)$$

where

$\sigma = 5.67 \times 10^{-8}$ w m^{-2} °C^{-4}, the Stefan-Boltzmann constant,

n = the index of refraction, taken to be 1.38 for LiF,

T = absolute temperature,

k = the index of absorption, and

λ_L = the lattice conduction part of thermal conductivity.

This relation is an approximation for "gray absorption," which means k is assumed to be independent of wave length and temperature, a suspect assumption at best. The curves in Fig. 7.6 were generated by the computer for k values from 0.5 to 7 in steps of 0.5 and are plotted as the reciprocal of Eq. (2).

The behavior of the experimental data plotted on the computer grid shows that up to about 850°K the nonlinearity of λ^{-1} due to thermal radiation follows the curve with $k \cong 6$. Above 850°K, the experimental data deviates, possibly because of (1) a change of k with temperature, or (2) an error in the temperature gradient measurement due to exposure of the inner thermocouple to a larger space angle of energy radiation.

Experimental difficulties at the high temperatures prohibited demonstration of the influence of thermally produced vacancies and

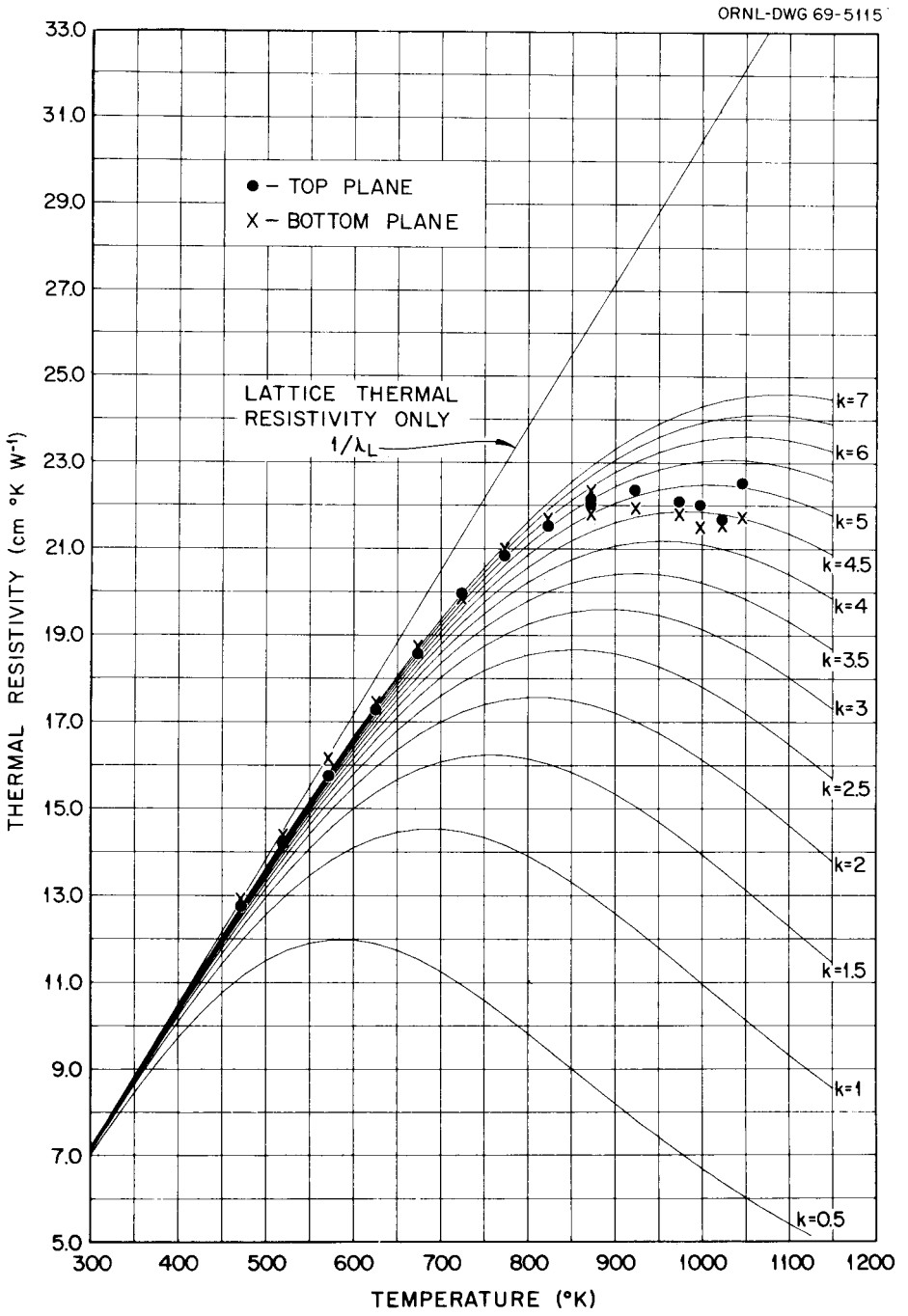

Fig. 7.6. Thermal Resistivity of LiF Single Crystal as a Function of Temperature. Measured values for two planes in the specimen are shown on a computer-derived grid of Eq. (2) plotted as the reciprocal for various values of k.

thermal diffusion on thermal conductivity. Consequently, a third test is under way, using a theoretically dense polycrystalline LiF specimen. The assembly for this run was made to allow for the LiF thermal expansion, and hopefully this will allow data to be obtained to the melting point. Calculations are in progress to include a wave-length and temperature dependency in the absorption term for a more complete interpretation of the data.

Mechanical Properties of Sol-Gel-Derived Fuel Bodies

C. S. Morgan L. L. Hall A. R. Olsen

The ability of a fuel to deform plastically at various temperatures and to support loads is an important influence on the irradiation performance of a metal-clad fuel body. The strength of the material may influence the formation of fission-gas bubbles, and the ability to plastically deform may influence the utilization of included porosity to accommodate solid fission product swelling. The creep of thoria from standard fabrication processes has been investigated at ORNL.[11,12] More recently, we have begun the investigation of the compressive creep of sol-gel-derived thoria pellets. The pellets were fabricated from 400°C-calcined powder with isostatic pressing at 60,000 psi. They were sintered in air for 2 hr at 1450°C and then in hydrogen for 0.7 hr at 1750°C. The resulting density of the pellets was 8.8 g/cm^3 as determined by mercury porosimetry and 9.1 g/cm^3 by water immersion.

Although the studies of compressive creep performance on these pellets were limited, some of the findings are of interest. To obtain some information on the compressive strength and plastic deformation characteristics of this material in a relatively short period of time, we used an Instron machine with a constant head speed. The ends of the specimen were ground flat and parallel and were supported by thoria

---

[11] C. S. Morgan and L. L. Hall, "The Creep of ThO_2 and ThO_2-CaO Solid Solutions," Proc. Brit. Ceram. Soc. 6, 233–238 (1966).

[12] L. E. Poteat and C. S. Yust, "Creep of Polycrystalline Thorium Dioxide," J. Am. Ceram. Soc. 49(8), 410–414 (1966).

disks with tungsten shims to protect the ends and keep the specimen and disks from sintering together. This assembly was placed in the center of a tube furnace, and the load was applied through alumina rods and graphite supporting members. Figure 7.7 shows the effect of temperature on the mechanical strength and plastic deformation of the sol-gel-derived pellet. Of particular importance is the high degree of plastic deformation sustained at the relatively low temperature of 650°C. Figure 7.8 compares pellets from both oxalate-precipitated powder and sol-gel powder; the effect of pellet density is clearly shown by the variation in plastic deformation and strength. We believe that the difference in the shape of the curves for sol-gel pellets at 9.1 g/cm^3 and the sintered oxalate powders at 8.87 g/cm^3 may result from the porosity distribution established by the fabrication procedure. The low-density oxalate powders were formed by uniaxial pressing, whereas

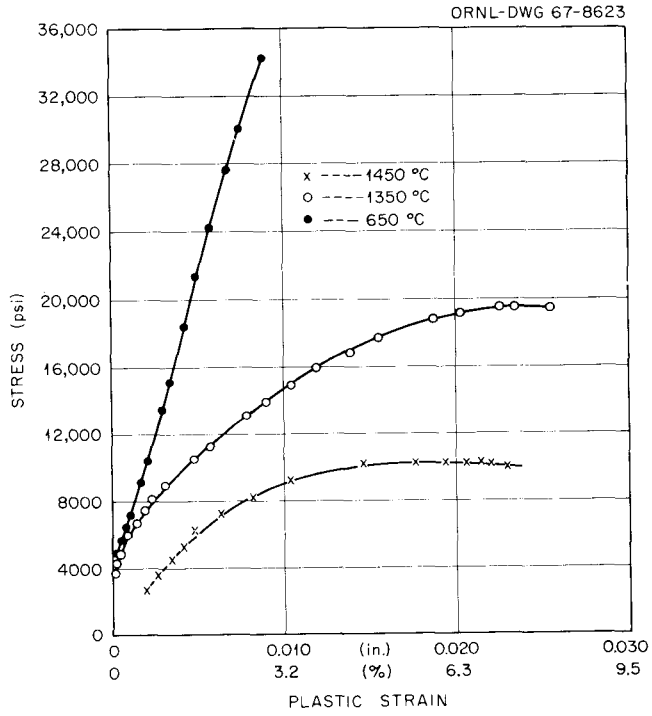

Fig. 7.7. Effect of Temperature on Stress-Strain Relationship for Sol-Gel ThO_2 Pellets of 9.1 g/cm^3 Density Tested at a Constant Compressive Strain Rate of 0.0007/min.

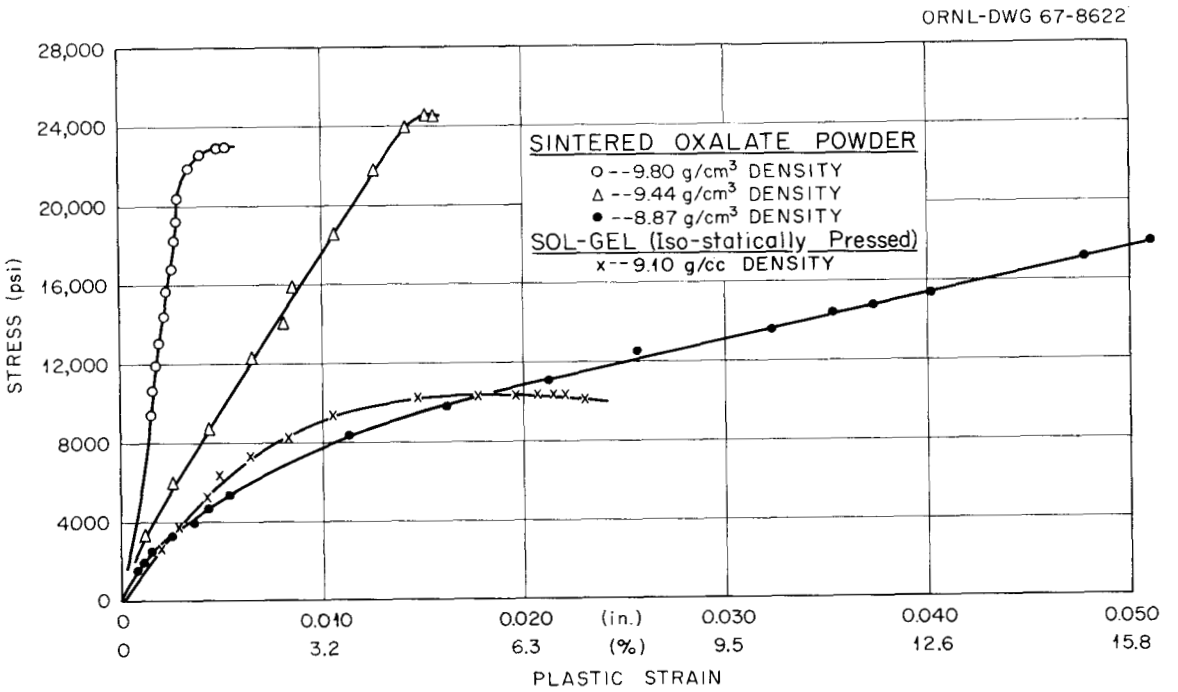

Fig. 7.8. Effect of Density on Stress-Strain Relationship for ThO_2 Pellets Tested at 1450°C with a Constant Compressive Strain Rate.

the sol-gel product had been isostatically pressed. Poteat and Yust[12] in the previous study of high-density thoria pellets prepared from oxalate powder showed that with significant strain the density of the pellets decreased. We suspected that the increased porosity in the lower density pellets might lead first to an increase in density followed by a decrease with increasing strain. And indeed, as we see in Fig. 7.9, in the one test conducted to date this was observed; although this pellet did not fail in test, the final point, with the density below that of the original pellet, was obtained when the pellet showed a significant number of microscopic cracks aligned vertically.

We have conducted only one typical creep test on sol-gel ThO_2 in which creep was measured under constant load. The results of this test on the 9.1-g/cm^3-dense pellet are compared in Fig. 7.10 with a high-density thoria pellet fabricated from oxalate-derived powders. Although the load in these tests was significantly different, our preliminary conclusions indicate that the effect is principally one of density difference rather than a material difference from processing. This is

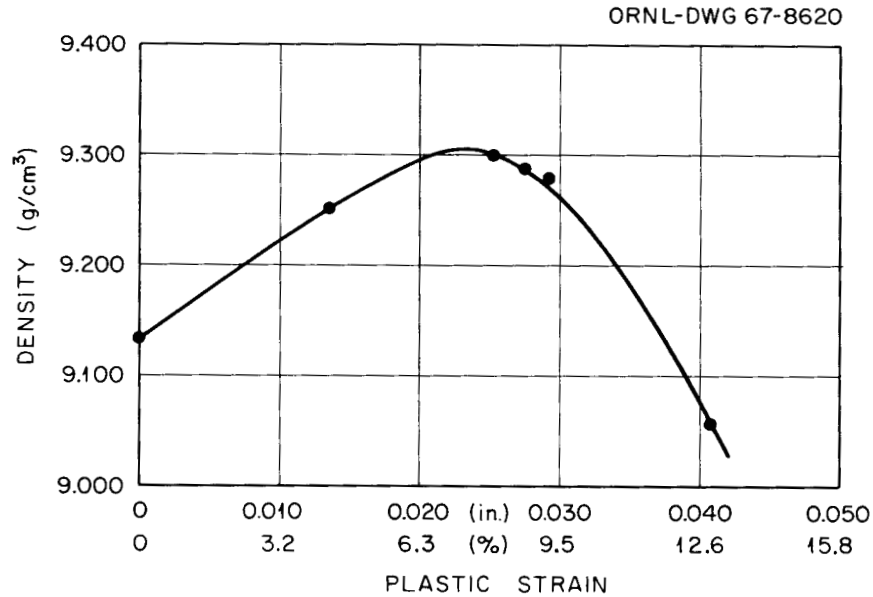

Fig. 7.9. Change in Density of a Sol-Gel ThO_2 Pellet as a Function of Uniaxial Plastic Strain.

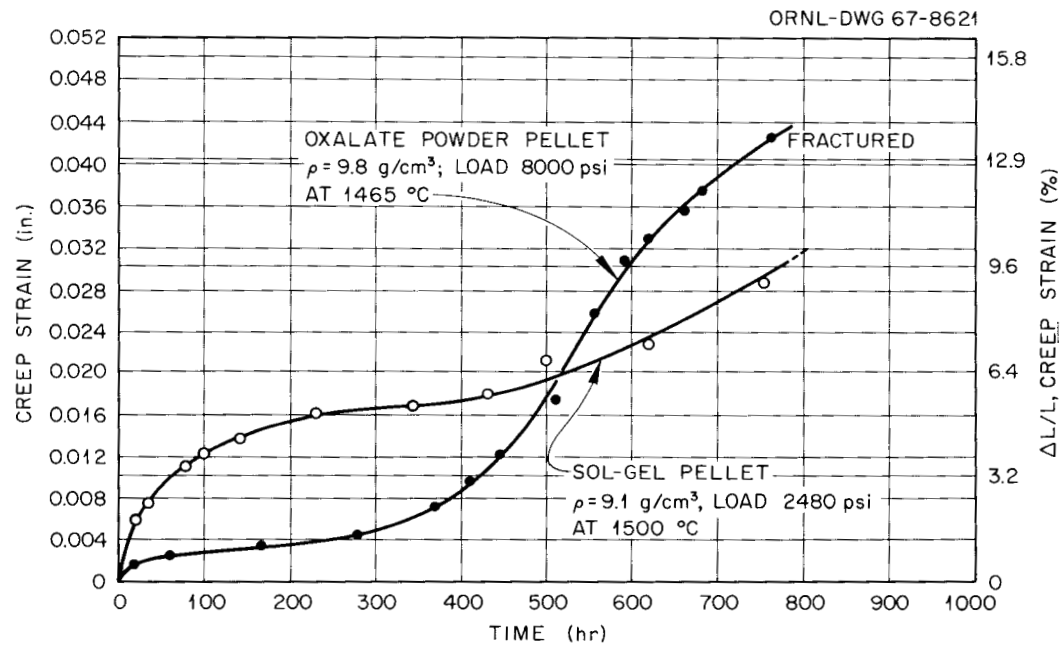

Fig. 7.10. Creep Curves for ThO_2 Pellets with Constant Compressive Loading.

borne out by the difference in the initial strain rate of the two samples, with the low-density material showing a high strain rate during what we had previously shown to be a densification period, while the final creep rates are quite similar. The test of the low-density pellet was terminated before failure.

Additional work on the investigation of the mechanical properties of sol-gel-derived materials, both UO_2 and $(U,Pu)O_2$, is planned.

8. IRRADIATION OF BULK OXIDE FUELS

A. R. Olsen

As part of the evaluation of processes under development for preparing nuclear fuels and fabricating fuel elements, a program for testing the irradiation performance is essential. The irradiation test program in the Thorium Fuel Cycle Development includes the testing of coated particle fuels reported in Chapter 5 of this report and the continuation of irradiation tests[1,2] on bulk thoria-base fuel rods fabricated by loading tubes with pellets, by Vi-Pac with angular particles, or by Sphere-Pac with sol-gel microspheres. Additional work on non-thorium fuels fabricated by similar processes is reported elsewhere.[3,4]

During the past two years the irradiation testing of bulk thoria-base fuels has been restricted by reduced funding and the increased emphasis on coated particle fuels. Consequently, some of the tests have been terminated before they achieved their design burnup levels, and others have had the irradiation stopped at least temporarily. Since July 1968 no bulk thoria fuels have been under irradiation. Table 8.1 lists the tests under irradiation or being examined at the time of the last status report[2] and the current status of these tests. Table 8.2 lists the individual test rod status as of December 31, 1968.

---

[1]A. R. Olsen, J. W. Ullmann, and E. J. Manthos, Status and Progress Report for Thorium Fuel Cycle Development Dec. 31, 1965, ORNL-4001, pp. 102–112.

[2]A. R. Olsen and R. B. Fitts, Status and Progress Report for Thorium Fuel Cycle Development Dec. 31, 1966, ORNL-4275, pp. 121–134.

[3]A. R. Olsen, Fuels and Materials Development Program Quart. Progr. Rept. June 30, 1968, ORNL-4330, pp. 17–25.

[4]A. R. Olsen, Fuels and Materials Development Program Quart. Progr. Rept. Sept. 30, 1968, ORNL-4350, pp. 21–32.

Table 8.1. Thoria-Base Fuel Rods Currently Being Irradiated or Examined[a]

Designation	Number of Rods	Type of Oxide	Density (% of Theoretical)	Fuel Rod Dimensions (cm)			Linear Heat Rating (w/cm)	Peak Burnup (Mwd/MT metal)	Objective	Status
				Length	OD	Wall				
MTR-II	2	Sol-Gel S $ThO_2-4.5\%\ UO_2$ Vi-Pac	88 to 89	57	0.8	0.06	600	100,000	Obtain higher heat rating by increasing enrichment	Being examined
MTR-III	6	Sol-Gel 35 $ThO_2-4.5\%\ UO_2$ Vi-Pac	86 to 89	30	1.1	0.06	820	100,000	Compare oxide calcining atmospheres and higher heat ratings obtained by increasing diameter	Being examined
ETR-II	6	BNL Sol-Gel $ThO_2-4\%\ ^{233}UO_2$ Vi-Pac	90	48	1.3	0.09	630	30,000 to 100,000	Study effects of remote fabrication and oxide recalcining	2 being examined. 4 stored in ETR canal since June 20, 1968
ETR-III	7	Sol-Gel ThO_2 Vi-Pac	88	48	1.3	0.09	770	10,000 to 70,000	Study ThO_2 blanket material with gradually increasing heat rating and provide high-protactinium low-fission-product material for chemical processing	3 rods processed 2 rods being examined 2 rods stored at ORNL
ETR-IV	6	Sol-Gel $ThO_2-5\%\ PuO_2$ Sphere Pac	84	24	1.3	0.09	650 to 1000	20,000 to 100,000	Study sol-gel ThO_2-PuO_2 microsphere performance as vibratorily compacted beds at various heat ratings and burnup levels	1 rod being examined 5 rods stored in ETR canal since June 20, 1968
Sphere-Pac	4	Sol-Gel $ThO_2-5\%\ PuO_2$ Sphere-Pac	84	19	0.64	0.025	650 to 1000	10,000	Test sol-gel ThO_2-PuO_2 microspheres with high cladding temperatures	Being examined
Pellet Rods	3	$ThO_2-4.5\%\ UO_2$	91	11.4	0.79	0.06	400	150,000	Investigate swelling and gas release of ThO_2-base fuels at very high burnup	Being examined

[a]ETR-II, ETR-III, and ETR-IV rods are clad with Zircaloy-2; all other fuel rods are clad with type 304 stainless steel.

[b]The linear heat rating listed here is the peak linear heat rating proposed for test operation.

Table 8.2. Operating Conditions and Current Status of Individual Test Rods in the Bulk Thoria Fuels Irradiation Program

Test Identification	Test Group	Date Removed From Reactor	Peak Burnup (% FIMA)	Peak Cladding Temperature[a] (°C)	Peak Linear Heat Rating (kw/ft)	Fission Gas Release (% ^{85}Kr)	Current Status
43-43	Pellet	12-19-66	10.2	100	6.9	7	Examined
43-45		12-19-66	12.2	100	8.2	Lost	Examined
43-46		12-19-66	11.2	100	7.5	20	Examined
43-75	MTR-II	11-7-66	11.4	100	11.7	30	Examined
43-76		12-19-66	12.5	100	12.9	24	Examined
43-77-14	MTR-III	10-1-67	8.1	110	14.1	42	Examined
43-77-9		10-1-67	9.6	110	16.9	26	Examined
43-78-17		6-20-68	10[a]	110	25		To be examined
43-78-5		6-20-68	10[a]	110	25		To be examined
43-79-11		6-20-68	10[a]	110	25		To be examined
43-79-7		6-20-68	10[a]	110	25		To be examined
43-83	ETR-II	3-13-66	2.2	200	20.4	Lost	Examined
43-84		10-1-67	2.9	200	13.6	47	Being examined
43-85		6-20-68	4[a]	200	20		Stored at ETR
43-86		6-20-68	4[a]	200	20		Stored at ETR
43-87		6-20-68	4[a]	200	20		Stored at ETR
43-88		6-20-68	4[a]	200	20		Stored at ETR
43-90	ETR-III		0.6[a]	210	10	b	Used in ^{233}Pa process studies
43-91			0.6[a]	210	10	b	Used in ^{233}Pa process studies
43-92			0.6[a]	210	10	b	Used in ^{233}Pa process studies
43-93		10-1-67	2.8	240	30	35	Being examined
43-94		10-1-67	3.1	240	30	38	Being examined
43-95		6-20-68	4.5[a]	240	30[a]		Stored at ORNL
43-96		6-20-68	4.5[a]	240	30[a]		Stored at ORNL
43-106	ETR-IV	6-20-68	1.6[a]	250	20[a]		Stored at ETR
43-107		6-20-68	2.1[a]	272	30[a]		Stored at ETR
43-108		6-20-68	2.0[a]	260	26[a]		Stored at ETR
43-109		6-20-68	2.5[a]	272	30[a]		To be examined
43-110		6-20-68	2.0[a]	260	26[a]		Stored at ETR
43-111		6-20-68	1.6[a]	250	20[a]		Stored at ETR
43-99-2	Sphere-Pac	12-13-66	0.5	325	13	13	Examined
43-99-4		12-13-66	0.3	280	11	3	Examined
43-100-2		12-13-66	0.4	305	12	10	Examined
43-100-4		12-13-66	0.3	270	10	2	Examined

[a]Estimated from exposure history.

[b]Not measured.

Effect of Intermediate Heat Rating at High Burnup Levels

A. R. Olsen J. Komatsu[5] E. L. Long, Jr.

The two fuel rods in the MTR-II group were inserted into the MTR in January 1963 in a peak unperturbed flux of 1×10^{14} neutrons cm^{-2} sec^{-1}. During the two years of exposure the test capsules were periodically moved to higher flux positions to maintain a linear heat rating of approximately 600 w/cm (18 kw/ft). Experiment 43-75 was removed from the reactor on November 7, 1966 and Experiment 43-76 on December 19, 1966. When these experiments were removed from the X-baskets, we found that rod 43-76 had inadvertently been irradiated with the Fiberfrax-filled fission gas plenum at the bottom. This inversion probably occurred when the rod was transferred to a new flow holder after reaching an estimated burnup level of 60,000 Mwd/MT. Both rods contained vibratorily compacted sol-gel $(Th-5.9\%\ U)O_2$ powder. The fuel column length was 54 cm and the gas plenum length approximately 1 cm. The smear density of the fuel was 88% of theoretical. The stainless steel cladding on both rods was covered with an oxide film that showed interference colors. After irradiation both rods, as shown in Fig. 8.1, showed a distinct bulge starting at the bottom end cap and extending approximately 5 cm up the rod. In 43-75, in which the fuel contacted the bottom end plug, the maximum change in diameter was 1.22 mm, equivalent to a plastic cladding strain of 15.4%. In 43-76 the fuel was separated from the bottom end plug by 1 cm of Fiberfrax, and the maximum change in diameter was only 0.74 mm, equivalent to a plastic cladding strain of 9.3%. The maximum strain occurred approximately 1 cm from the bottom of the fuel column in both rods. Outside the bulge area the diametral change in both rods was essentially uniform and represented a plastic strain of 0.9% for 43-75 and 1.0% for 43-76. The gamma scans show no significant change in fuel column length or position. Examination of these rods is essentially complete. The peak burnup was 114,000 Mwd/MT(U + Th) for Experiment 43-75 and 125,000 Mwd/MT(U + Th) for 43-76. Metallographic sections from similar axial positions for

[5]Foreign visitor on leave from the Japanese Power Reactor and Nuclear Fuel Development Corporation, Japan.

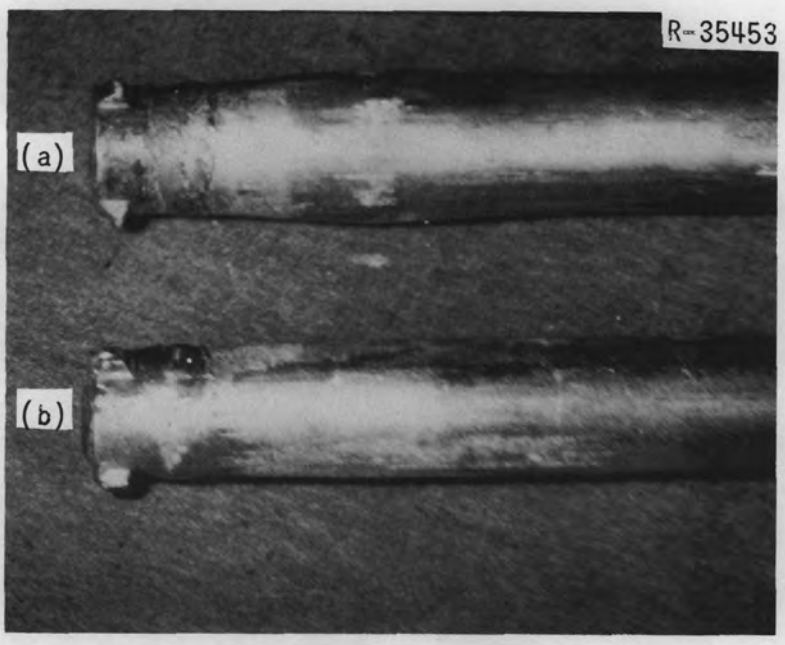

Fig. 8.1. Bottoms of Fuel Rods (a) 43-75 and (b) 43-76 as Removed From the Reactor.

these rods are shown in Fig. 8.2. Although the detailed interpretation of the microstructures is incomplete, there are some obvious comparisons. Comparison of the peak burnup region shows that a higher time-averaged linear heat rating for 43-76 has led to greater grain growth and central void formation. Similar power differences in the regions of peak cladding strain have produced an even greater difference in structure. The internal void volume arising from the cladding expansion of 15% for 43-75 has remained as an annular gap between the densified Vi-Pac fuel and the cladding, but the voids associated with the 9% cladding expansion in 43-76 have redistributed to a central void and circumferential cracks at the fuel midradius. We have not yet explained the unusual localized cladding strain. We are reviewing the adjacent experimental facility loadings for the latter stages of these irradiations to see if a temporary localized overpower condition might have caused the phenomenon. The effects of burnup on fuel swelling in the regions away from the unusual bulged areas are discussed in the next section.

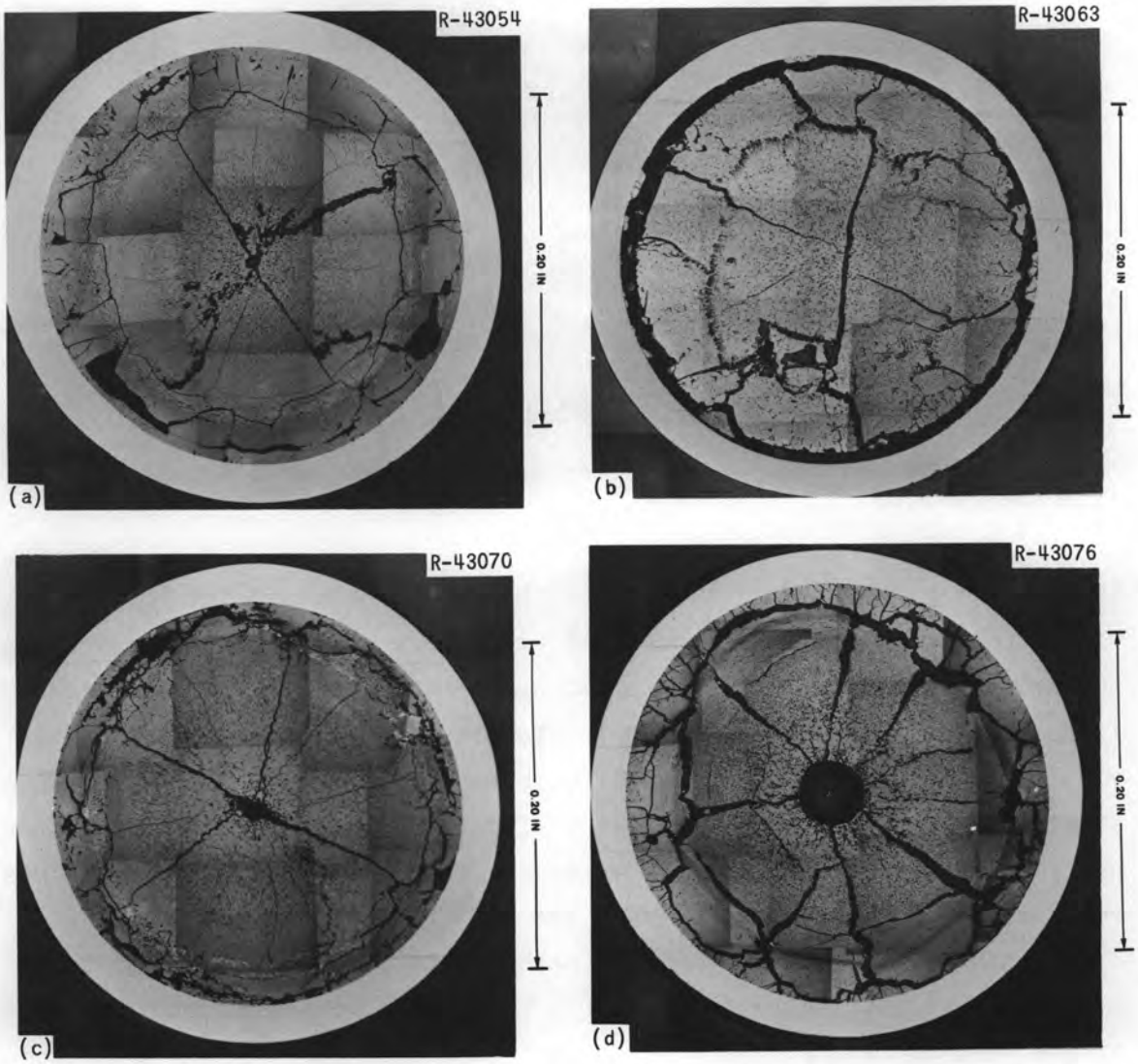

Fig. 8.2. Transverse Sections of (Th–4.5% U)O_2 Test Rods. (a) 43-75 near fuel center, 11.4% FIMA. (b) 43-75 at region of maximum cladding strain, 6.8% FIMA. (c) 43-76 near fuel center 12.5% FIMA. (d) 43-76 at region of maximum cladding strain, 7.7% FIMA.

Effects of Extended Burnup

A. R. Olsen J. Komatsu[6] E. L. Long, Jr.

Previously we reported[7] that three of the rods in the pellet group had been removed after exposure to an estimated 150,000 Mwd/MT(Th + U) (15% FIMA). Subsequent burnup analysis indicates that these rods had achieved only about 120,000 Mwd/MT. Since the objective of extending the exposure was to better define swelling as a function of burnup at very high burnup, this underexposure is unfortunate. Valuable data were nevertheless obtained.

The postirradiation gamma scans and typical microstructures for these test rods (43-43, 43-45, and 43-46) are shown in Figs. 8.3, 8.4, and 8.5. At the very low fuel temperatures associated with the low linear heat ratings achieved (approximately 6 to 8 kw/ft), the primary microstructural change has been extensive sintering. With one exception, all evidence of the original pellet interfaces has disappeared. The exception is shown in longitudinal Section A of Fig. 8.3 and the associated area of the gamma scan. The abrupt dip in gamma activity delineates the void between the first two pellets at the bottom of this test rod. The structure of the end pellet was damaged during postirradiation examination by the puncture made for fission gas sampling; however, there is evidence of gas bubble migration to the hotter central region in the gap between the two pellets. There is no evidence of similar incipient central void formation in any of the other sections. The gross swelling rates and fission-gas release data for these three pellet rods and a similar rod (43-39) reported previously[7] are compared in Table 8.3 with sol-gel Vi-Pac fuels of similar composition and burnup. The gross swelling rates as determined by cladding dimensional changes for the small-diameter, low-linear-heat-rating rods agree quite well with the

---

[6] Foreign visitor on leave from the Japanese Power Reactor and Nuclear Fuel Development Corporation, Japan.

[7] A. R. Olsen and R. B. Fitts, Status and Progress Report for Thorium Fuel Cycle Development Dec. 31, 1966, ORNL-4275, pp. 121–134.

ORNL-DWG 69-2530

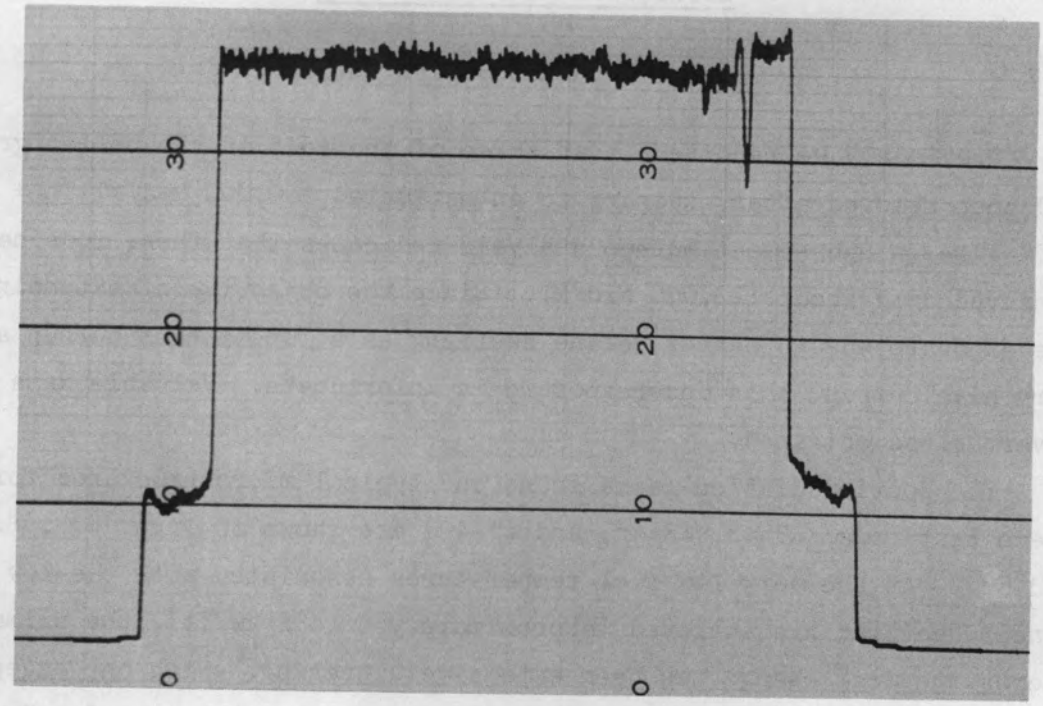

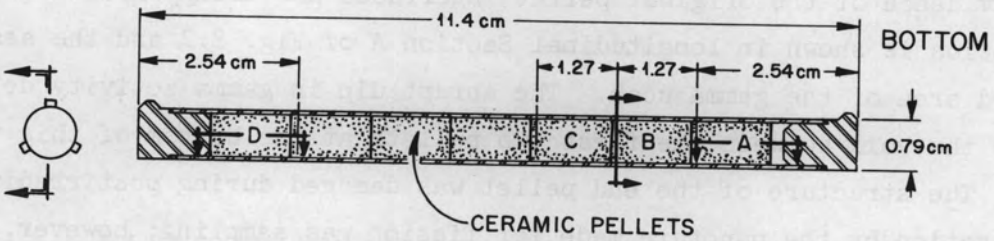

A - METALLOGRAPHY SECTION
B - METALLOGRAPHY SECTION
C - BURNUP ANALYSIS
D - METALLOGRAPHY SECTION

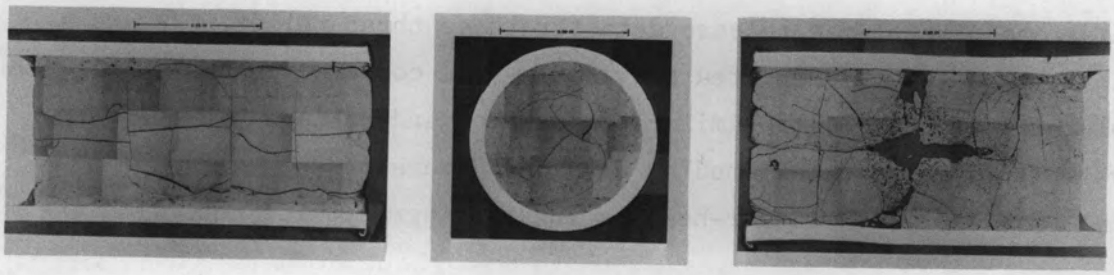

D B A

Fig. 8.3. Postirradiation Gamma Scan and Microstructure of ThO_2–4.5% UO_2 Pellet Fuel Rod 43-43 (10.2% FIMA Burnup). The scales on the photomicrographs denote 0.20 in.

ORNL-DWG 69-2532

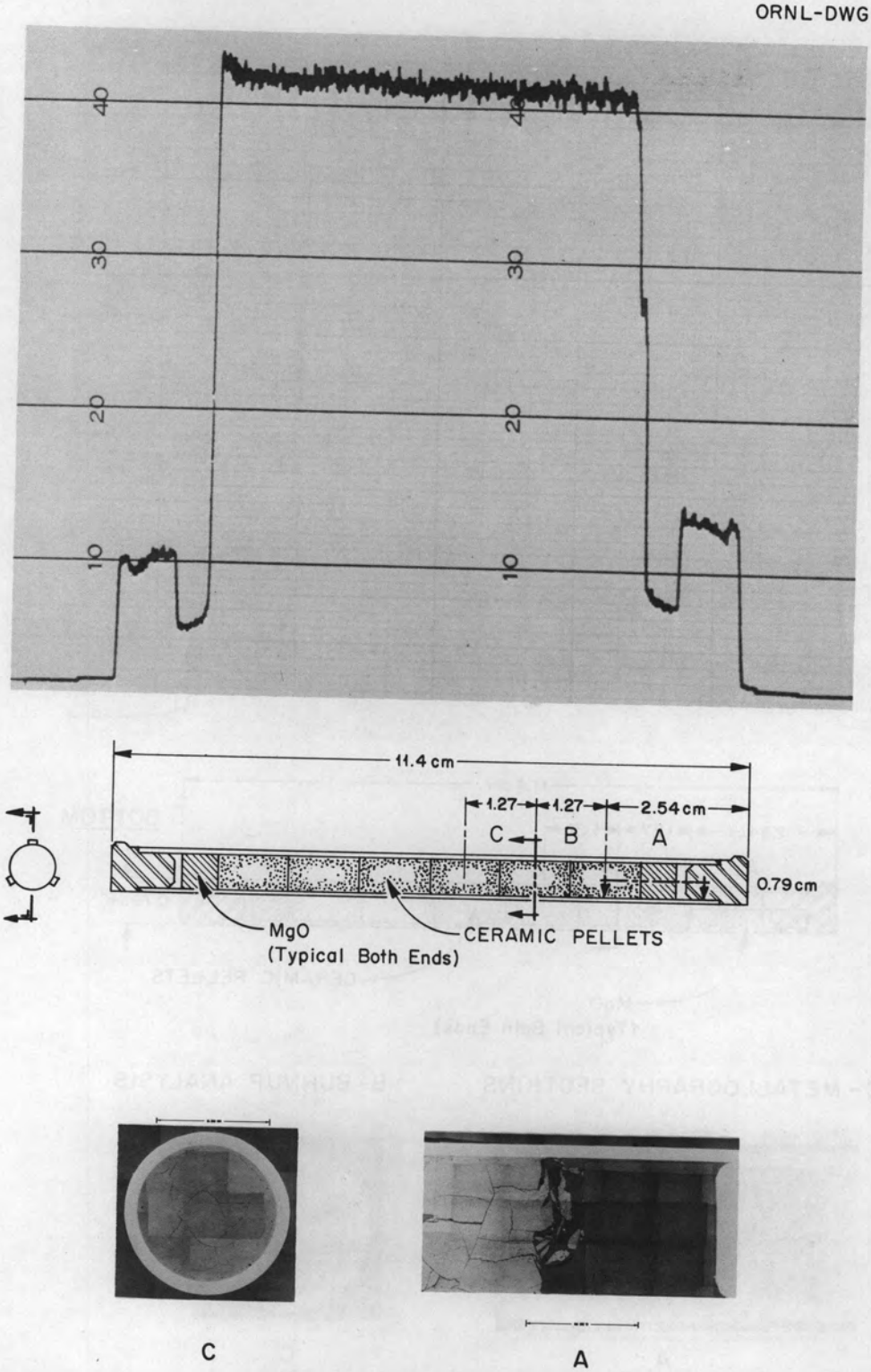

Fig. 8.4. Postirradiation Gamma Scan and Microstructure of ThO_2–4.5% UO_2 Pellet Fuel Rod 43-45 (12.2% FIMA Burnup). The scales on the photomicrographs denote 0.20 in.

ORNL-DWG 69-2531

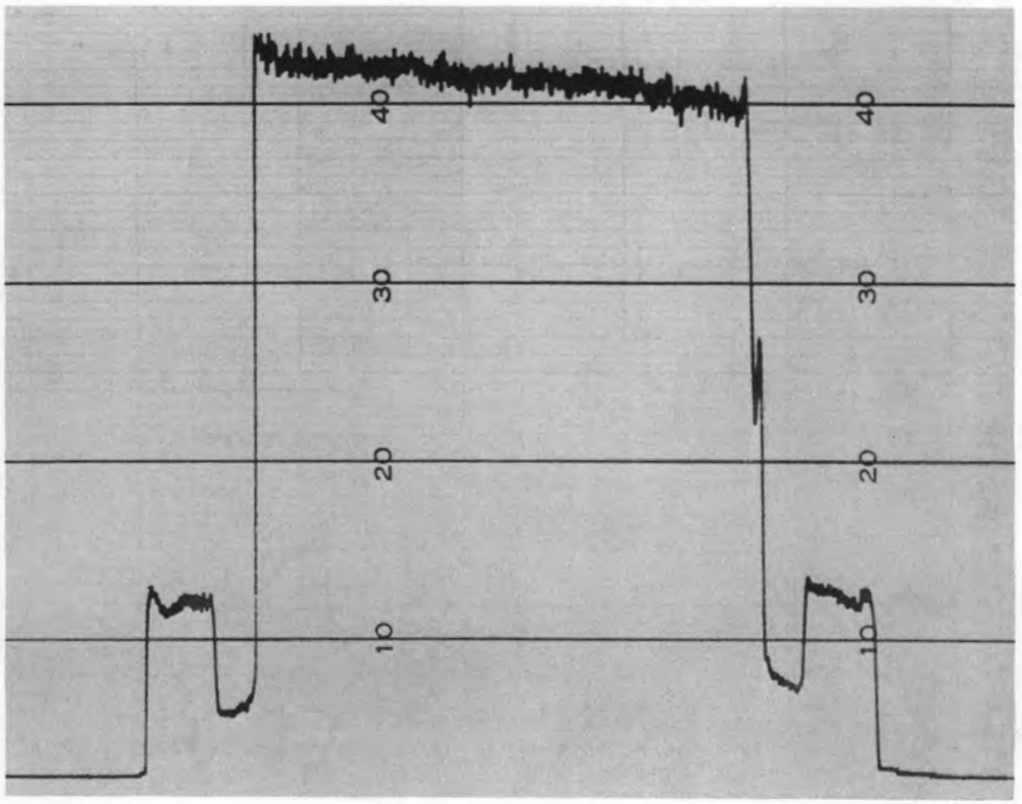

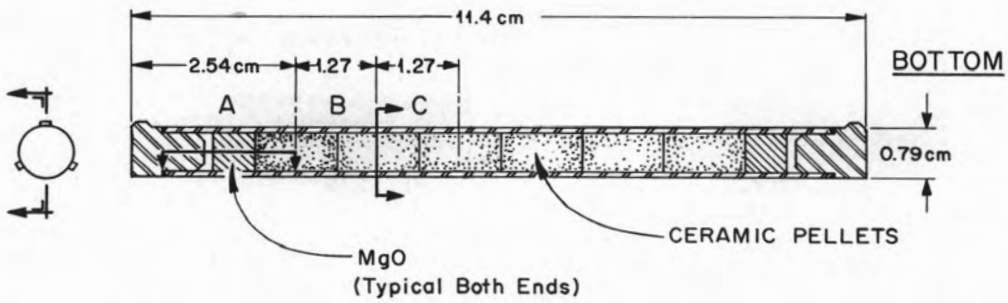

A and C - METALLOGRAPHY SECTIONS

B - BURNUP ANALYSIS

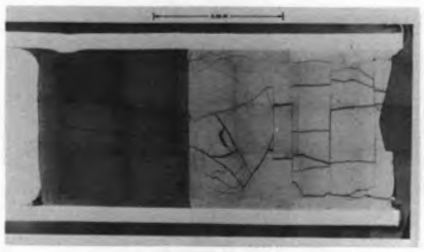

A

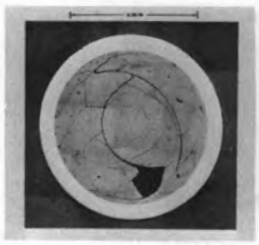

C

Fig. 8.5. Postirradiation Gamma Scan and Microstructure of ThO_2–4.5% UO_2 Pellet Fuel Rod 43-46 (11.2% FIMA Burnup). The scales on the photomicrographs denote 0.20 in.

Table 8.3. Swelling Data on ThO_2–4.5% UO_2 Fuels

Experiment	Fuel		Irradiation Time[a] (days)	Peak Linear Heat Rating[b] (kw/ft)	Peak Burnup (% FIMA)	Fission Gas Release[c] (% ^{85}Kr)	Fuel Swelling (% ΔV/% FIMA)	
	Form	Smear Density (% of theoretical)					Gross at Peak Burnup Region[d]	Minimum Calculated[e]
43-39	Pellet	91.0	905	10.6	12.0	23	1.2	1.07
43-43	Pellet	91.0	1173	6.9	10.2	7	1.3	0.99
43-45	Pellet	91.0	1189	8.2	12.2	Lost	1.1	1.06
43-46	Pellet	91.0	1189	7.5	11.2	20	1.2	1.07
43-62	Vi-Pac	87.0	1107	9.6	12.5	2.6	< 1.04	1.05
43-65	Vi-Pac	85.5	691	8.8	8.1	17	< 1.8	0.98
43-75	Vi-Pac	87.3	745	11.7	11.4	30	1.4	1.05
43-76	Vi-Pac	87.8	746	12.9	12.5	24	1.3	1.05
43-77-9	Vi-Pac	88.4	973	16.9	9.62	26	1.4	1.10
43-77-14	Vi-Pac	87.6	973	14.1	8.1	42	1.8	1.11

[a]Irradiation time is given in effective full power days of reactor operation.

[b]The linear heat ratings are the time-averaged peaks, based on maximum burnup; not necessarily the instantaneous peaks achieved during the irradiation period.

[c]Fission gas release rates are quoted for the average burnup in the test fuel, not for the peak burnup position.

[d]Based on initial fuel void volume and changes in cladding dimensions, if any.

[e]Fuel swelling calculated using volume changes reported by A. R. Olsen et al. in "Properties and Prospects of Thoria-Based Nuclear Fuels," Proc. Brit. Ceram. Soc. 7, 289–310 (1967) and assuming that all of the fission product gases are trapped in the lattice with no gas bubbles formed.

minimum swelling rate calculated by a technique described elsewhere.[8] This calculation technique is based on atomic volumes and lattice accommodation. The measured rates are generally 10% greater and probably result from some fission-gas bubble formation even at these comparatively low fuel temperatures. The effects of higher fuel temperatures on gross swelling rates appear to be evident in the last two tests, which operated at higher linear heat ratings. These two rods (43-77-9 and 43-77-14) have not yet been examined metallographically.

It is apparent that development of a model to describe the swelling of thoria-base fuels will require additional detailed analysis of the available operational histories on these tests and additional information from the other tests in this program.

The postirradiation examination of the test rods from Groups ETR-II and ETR-III has not progressed to the state where information beyond that reported in Table 8.2 is available. The results of processing the first three ETR-III rods have been reported elsewhere.[9]

Performance of Sphere-Pac ThO_2–5% PuO_2 Fuel Rods

A. R. Olsen R. B. Fitts

To date, only the four rods listed in the Sphere-Pac group have been examined after irradiation. The capsule design was discussed previously.[10] Both experiments also contained rods of $(U,Pu)O_2$ fuel. The experiments were withdrawn after one cycle of ETR operation because of failures in the $(U,Pu)O_2$ fuels, which had been operated at very high linear heat ratings (> 50 kw/ft). The data on the $(Th,Pu)O_2$ fuel rods are listed in Table 8.4. These rods operated at their design power levels and performed well. There was no change in fuel length, and gross restructuring

---

[8] A. R. Olsen, D. A. Douglas, Y. Hirose, J. L. Scott, and J. W. Ullmann, "Properties and Prospects of Thoria-Based Nuclear Fuels," Proc. Brit. Ceram. Soc. 7, 289–310 (February 1967).

[9] J. H. Goode and J. G. Moore, Adsorption of Protactinium on Unfired Vycor: Final Hot-Cell Experiments, ORNL-3950 (June 1967).

[10] A. R. Olsen and R. B. Fitts, Status and Progress Report for Thorium Fuel Cycle Development Dec. 31, 1966, ORNL-4275, pp. 121–134.

Table 8.4. Irradiation of ThO_2–5% PuO_2 Sphere Pack Fuels[a]

Fuel Rod	Smeared Fuel Density		Peak Linear Heat Rating (kw/ft)	Peak Burnup (% FIMA)	Fuel Temperature, °C		Fission Gas Release (% ^{85}Kr)
	(g/cm^3)	(% of theoretical)			Avg	Center line	
43-99-2	8.40	83.4	13	0.52	1250	2170	13.2
43-99-4	8.38	83.2	11	0.30	1200	1930	3.3
43-100-2	8.45	83.9	12	0.41	1220	2030	9.9
43-100-4	8.39	83.3	10	0.31	1150	1820	1.6

[a]Irradiated 18.9 days.

occurred only at the centers of the rods with the higher linear heat ratings. Figure 8.6 shows the typical appearance of the fuel for Rod 43-99-2. The spheres in the cooler peripheral regions were loose and lost in polishing. However, radial restructuring to form a dense annular fuel body with a central void is apparent.

The test of the performance of these fuels to higher burnup levels and at higher linear heat ratings depends on the continuation of the ETR-IV group irradiation tests, which are currently stored in the ETR canal.

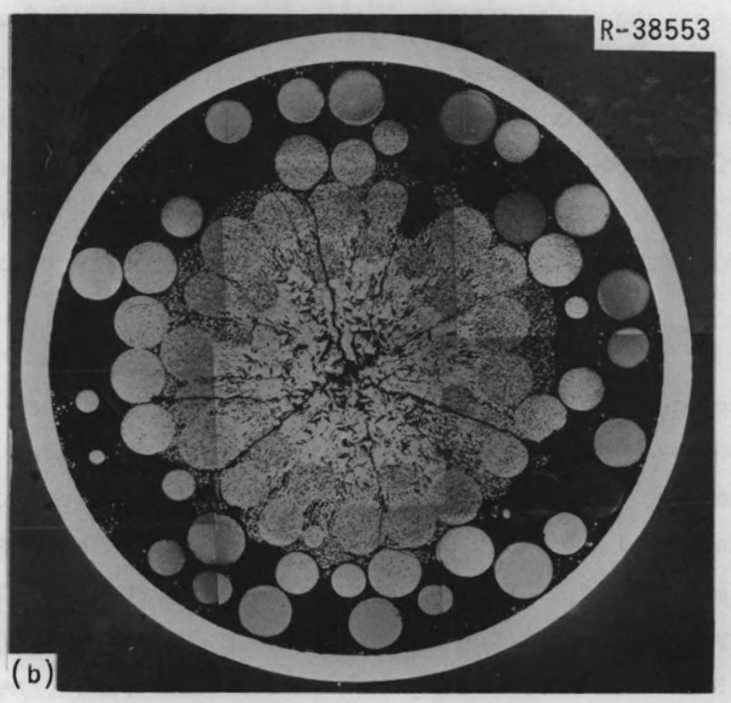

Fig. 8.6. ThO_2–5% PuO_2 Fuel Rod 43-99-2 Fabricated by Sphere-Pac and Irradiated to 0.5% FIMA at 13 kw/ft with a Cladding Temperature of 450°C. (a) Section as cut. (b) As polished. The overall diameter is 0.25 in.

9. ADVANCED STUDIES

Conversion of Oxide-Carbon Gels to Carbides and to Porous Oxides

K. J. Notz

We are concerned with the preparation of more advanced nuclear fuels. Work thus far has been centered on the laboratory-scale preparation of carbides, nitrides, carbonitrides, and porous oxides of interest as nuclear fuels. Sol-gel methods for carrying out these processes are being investigated. In these methods, mixed hydrosols are prepared by ultrasonically dispersing carbon black in the oxide sol. The mixed sol is then converted to gel shards or gel microspheres by suitable means. The oxide-carbon gel is heated in a vacuum or in an inert atmosphere, such as argon, to convert to the carbide or is heated in nitrogen under the appropriate conditions, to form either carbonitrides or nitrides. Temperatures of 1700 to 2100°C are required to obtain dense products. Metal oxide-carbon gels also appear to provide a general route to the preparation of porous oxides. After the oxide matrix is set by heating the gel to 1200 to 1400°C, the carbon is removed by reaction with air at 800°C, CO_2 at 1000°C, or H_2O at 1000°C. The volume of porosity introduced is approximately the volume of carbon originally present in the oxide.

Aside from the inherent simplicity of operations and the remote fabrication advantages of sol-gel methods, we believe that the conversion of oxide-carbon gels to carbides, carbonitrides, nitrides, or porous oxides will have advantages that conventional methods employing blending of oxide powders and carbon blacks do not have. The main advantage involves the extremely intimate mixing and association of the oxides and carbon crystallites on the angstrom scale in the sols and gels. Conceivably, this intimate mixing and association could lead to better control of conversion conditions and to better distribution of porosity in porous oxides.

Results thus far[1-5] have demonstrated the feasibility of this approach for the preparation of ThC_2, UC, $(Th,U)C_2$, and U(C,N). These products were made by starting with oxide sols that were prepared by standard methods used at ORNL.[4,6] The preparation and characterization of the oxide-carbon sols and the conversion of ThO_2-C gels to ThC_2 or porous ThO_2 have been studied extensively. Laboratory-scale demonstrations have shown the technical feasibility of the preparation of $Th_{0.78}U_{0.22}C_2$, UC, and UC-UN microspheres and of porous $Th_{0.78}U_{0.22}O_2$ and UO_2. We believe that similar sol-gel processes will be applicable to the preparation of pure nitrides, PuC, UC-PuC, and solid solutions of uranium and plutonium carbonitrides.

Preparation and Properties of Oxide-Carbon Sols

The preparation of oxide-carbon sols is being studied since fluid, stable hydrosols containing the required amounts of carbon are essential to the process. In addition, an understanding of the interactions between the oxides and carbon in our presently used oxide-carbon sols will be useful in the preparation of other sols such as PuO_2-C, UO_2-PuO_2-C, and UO_2-ZrO_2-C, which will be of future interest.

---

[1] Chem. Technol. Div. Ann. Progr. Rept. May 31, 1967, ORNL-4145, pp. 159–162.

[2] Chem. Technol. Div. Ann. Progr. Rept. May 31, 1966, ORNL-3945, pp. 157–160.

[3] J. L. Kelly, A. T. Kleinsteuber, S. D. Clinton, and O. C. Dean, "Sol-Gel Process for Preparing Spheroidal Particles of the Dicarbides of Thorium and Thorium-Uranium Mixtures," Ind. Eng. Chem. Process Design Develop. 4, 212–216 (1965).

[4] J. P. McBride (Compiler), Laboratory Studies of Sol-Gel Processes at Oak Ridge National Laboratory, ORNL-TM-1980 (September 1967); paper presented at the symposium on Sol-Gel Processes for the Production of Ceramic Nuclear Fuels, Turin, Italy, Oct. 2–3, 1967.

[5] T. A. Gens, D. M. Helton, and S. D. Clinton, Laboratory Preparation of Uranium Nitride Microspheres by a Sol-Gel Technique, ORNL-3879 (November 1965).

[6] P. A. Haas et al., Engineering Development of Sol-Gel Processes at the Oak Ridge National Laboratory, ORNL-TM-1978 (January 1968); paper presented at the symposium on Sol-Gel Processes for the Production of Ceramic Nuclear Fuels, Turin, Italy, Oct. 2–3, 1967.

We are continuing fundamental studies of the interaction of oxides with carbon. Results to date have shown that the oxide crystallites in our ThO_2, UO_2, or ThO_2-UO_3 sols disperse carbon aggregates by a strong interaction with them. In this interaction, the oxide crystallites are sorbed on the surface of the carbon aggregates, and the oxide apparently acts as a protective colloid. The extent of sorption of the oxide depends primarily on the relative surface areas of the oxides and the carbon. As yet, we have not determined the roles of surface charge and the nature of the surface groups of the oxides in the sorption process. We know that many colloidal oxides do not show this type of interaction, and we have found other oxide sols that do.

Viscosity measurements[7] continue to be a very useful tool for determining whether or not a specific interaction occurs between carbon black and an oxide sol. Figure 9.1 shows three types of interactions with 2 M oxide sols. (1) With UO_2 the same stabilized protective colloid interaction described above occurs, where the colloidal oxide consists of small (< 100 A), positively charged particles.[7] This type of interaction also occurs with ThO_2, ThO_2-UO_3, small-particle, high-nitrate ZrO_2, and probably PuO_2 sols. (2) With a large-particle, low-nitrate form of ZrO_2 the interaction is nonprotective and does not have long-term stability, but fairly large amounts of carbon can be added and thixotropy is rather slow to set in. Other large-particle positively charged sols such as Baymal[8] and $Eu(OH)_3$ behave similarly. (3) With SiO_2 (Ludox[9]) the mixture is unstable and highly thixotropic, with a small-particle, negatively charged sol. In at least one instance, with a TiO_2 sol of the above properties, we have been able to obtain a stable, codisperse sol with carbon black by using a proprietary compound (Marasperse CB,[10] a sulfonated lignon) to disperse and stabilize the carbon in a negatively charged state.

---

[7] K. J. Notz, Status and Progress Report for Thorium Fuel Cycle Development Dec. 31, 1966, ORNL-4275, pp. 152–154.

[8] Trade name for AlOOH. Product of E. I. duPont de Memours and Co.

[9] Product of E. I. duPont de Nemours and Co.

[10] Product of American Can Co.

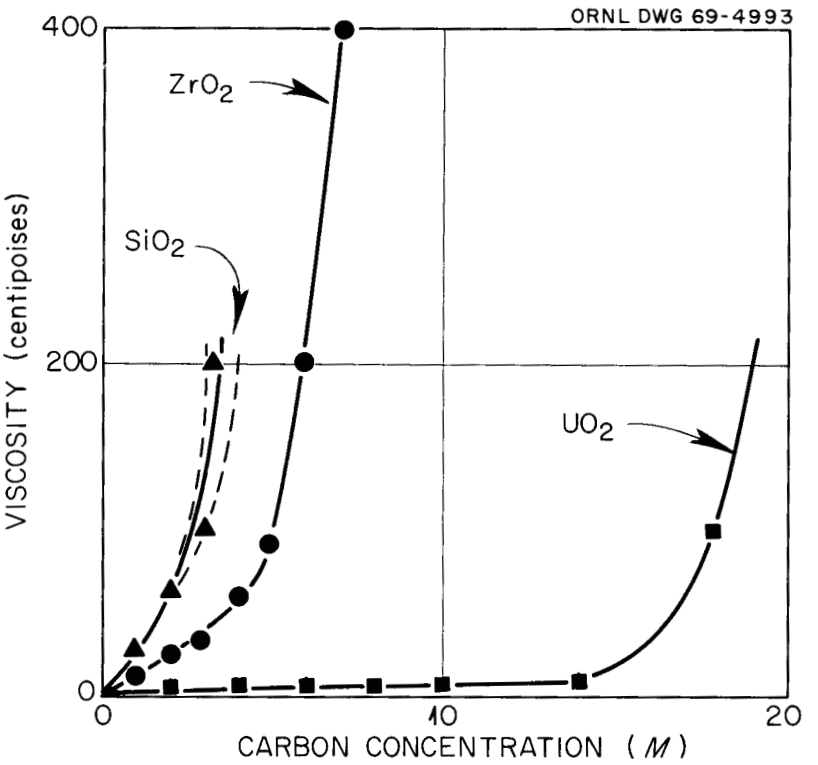

Fig. 9.1. Viscosity of 2 M Oxide Sols with Added Carbon Black (Spheron-9).

Stable, fluid sols containing sufficient carbon to produce mono- or dicarbides or to produce porous oxides could be prepared from UO_2, ThO_2, ThO_2-UO_3, PuO_2, and ZrO_2 sols made at ORNL. The amounts of dispersed carbon required to produce mono- and dicarbides from these oxides are approximately 3 and 4 moles per mole of oxide, respectively. The amount of carbon required to produce oxides with porosity over the range of 10 to 60% is 0.5 to 6 moles per mole of oxide.

Conversion of Oxide-Carbon Gels to Carbides and Carbonitrides

Studies of process variables that affect the conversion of ThO_2-C gel to ThC_2 were extended. The technical feasibility of converting UO_2-C gels to UC and ThO_2-UO_3-C gels to $Th_{0.78}U_{0.22}C_2$ was demonstrated. Initial work on conversion of UO_2-C gels to U(C,N) was promising.

The most important variables in the sol-gel method for preparing ThC_2 are the firing conditions during conversion and the carbon content

in the ThO_2-C gel. To obtain densities greater than 90% of theoretical, the conversion must be effected under a controlled CO overpressure at temperatures such that a critical balance among the rates of chemical conversion, grain growth, and sintering is maintained. If porous carbides are the desired product, the reactions can be carried out under vacuum at lower temperatures. Products having densities of 91 to 93% were obtained when the reaction was carried out at a controlled rate under argon until nearly complete and then completed under vacuum. The argon sweep gas after passage over the sample contained about 4000 ppm of CO, which was maintained by diffusion out of the sample crucible. An infrared in-line CO analyzer (Beckman model 315) monitored the progress of the reactions. This conversion technique also produced 90- to 93%-dense $Th_{0.78}U_{0.22}C_2$ and UC microspheres.

Control of the mole ratio of carbon to metal oxide in the gel starting material is important for efficient conversion to the carbide and preparation of a high-density product. When the initial carbon-to-ThO_2 mole ratio was too low, objectionable amounts of monocarbide were formed; when it was too high, a highly porous product containing excessive free carbon was obtained. For example, excess carbon contents of 0.5 to 2.5% in ThC_2 resulted in highly porous products. A carbon-to-oxide mole ratio of 3.9 appears optimum for preparing dense ThC_2. In practice, the carbon-to-oxide ratio must be adjusted empirically, because additional carbon is acquired by the sorption of organic materials during sphere forming and carbon is lost by reaction with nitric acid (present in the oxide sol) during firing of the gel. We tried to remove the additional carbon imbibed during sphere formation by oxidizing it with air on a thermogravimetric balance, where the rate of reaction could be carefully monitored; however, the degree of oxidation was difficult to control.

The conversion of ThO_2-UO_3-C gel spheres to $Th_{0.78}U_{0.22}C_2$ gave a dense product when the carbon content was not too high (Table 9.1). The products were solid solutions having the monoclinic ThC_2 structure with parameters slightly contracted by the uranium content. A reaction temperature of 1900°C was sufficient for complete reaction, although approximately 2000°C is necessary for ThC_2. The presence of the uranium permitted

Table 9.1. Preparation of $Th_{0.78}U_{0.22}C_2$ Microspheres by Sol-Gel Process[a]

Property of Products	Value for Various Carbon-to-Metal Mole Ratios of Reactants		
	4.00	4.06	4.15
Composition, %			
Thorium	70.3	69.7	69.4
Uranium	20.4	20.2	20.0
Carbon	8.87	9.02	9.37
Oxygen	0.081	0.127	0.173
Free carbon	0.097	0.264	0.146
Material balance	99.65	99.05	98.94
Mercury density, g/cm^3			
1 atm	9.45	8.92	7.75
10,000 psi	9.56	9.09	8.65

[a]Conversions in argon at 1900°C.

conversion at a lower temperature and also seemed to promote a desirable sintering pattern. Densities were 76 to 94% of the calculated value (10.05 g/cm^3, based on the weighted average of ThC_2 and UC_2), depending on the original carbon content. Even at higher porosities, the spheres had a uniform cross section, and the pores were about 1 μ in diameter.

Equally good results to those obtained in preparing $(Th,U)C_2$ were obtained in converting UO_2-C gel spheres to UC (Table 9.2). Three of the products were denser than 90% of theoretical, including two prepared under vacuum. Dense UC is thus easier to prepare by this general method than dense ThC_2. All of the products contained some UC_2 resulting, at least in part, from precipitation during cooling. The lattice parameters, determined by x-ray diffraction of the best crystallized sample (IV-112), was 4.960 A, in agreement with the literature value of 4.9605 A.

Several tests for the preparation of UN and U(C,N) by firing of UO_2-C gels in nitrogen have been conducted. The basic approach is

Table 9.2. Preparation of Uranium Monocarbide Microspheres by the Sol-Gel Process

Conditions and Properties	Values for Various Experiments				
	IV-110	IV-112	IV-114	IV-116	IV-118
C/UO_2 ratio	2.94	2.94	2.94	2.85	3.00
Atmosphere	vacuum	argon	vacuum	vacuum	vacuum
Time, hr	2.5	4	1	4.3	5
Max temp, °C	1810	2180	1730	1600	2100[b]
Final vacuum, torr	0.006	0.008	0.012	0.005	0.005
weight loss, % [a]					18.4
Mercury density, g/cm^3					
1 atm	10.19	12.34		12.86	12.67
10,000 psi	10.39	12.47		12.94	12.69
Metallographic appearance	porous	dense	porous	dense	dense
Free carbon, ppm		280			290
Oxygen, ppm		130			90

[a]Theoretical weight loss for the reaction, $UO_2 + 3C \rightarrow UC + 2CO$, is 18.3%.

[b]Conversion occurred with maximum temperature of 1650°C; the sample was then allowed to heat to 2100°C.

similar to that of Gens.[11] Dense product was obtained, but the phases present have not yet been fully characterized.

By rapid heating of sol-gel UO_2-C mixtures containing excess carbon in a nitrogen atmosphere, rapid conversion to U(C,N) can be obtained.[12] The product can subsequently be densified by compaction-sintering. This

[11]T. A. Gens, D. M. Helton, and S. D. Clinton, Laboratory Preparation of Uranium Nitride Microspheres by a Sol-Gel Technique, ORNL-3879 (November 1965).

[12]J. M. Leitnaker, R. L. Beatty, K. Notz, K. E. Spear, and T. B. Lindemer, Fuels and Materials Development Program Quart. Progr. Rept. June 30, 1968, ORNL-4330, pp. 28–31.

technique is applicable to other actinides, including Th, Pu, and mixed U-Pu. A patent application on this process has been filed.[13]

Conversion of Oxide Gels to Porous Oxides

We have shown previously[14-17] that ThO_2 microspheres or shards of controlled porosity can be prepared from ThO_2-C gels by removing the carbon by oxidation with air after the oxide structure has been preset by firing to 1400°C in argon. The amount of porosity can be controlled by varying the amount of carbon added (i.e., the volume of porosity introduced is nearly equal to the volume of carbon added). Now the technical feasibility of preparing porous ThO_2-UO_2 and UO_2 by this approach has been demonstrated. For the ThO_2-UO_2 preparations, ThO_2-UO_3-C gels were employed, and air oxidation was used to volatilize the carbon. However, in the porous UO_2 preparations, CO_2 or H_2O was necessary for removing the carbon because air caused oxidation to U_3O_8.

In the preparation of 60%-porous ThO_2–22% UO_2, we obtained higher porosities with ThO_2-UO_3-C gel shards than would have been expected by analogy with ThO_2-C gel shards of the same oxygen-to-carbon atom ratio. The amount of carbon that produced 47% porosity in ThO_2 produced 59% porosity in ThO_2-UO_2. Also, the pores in the ThO_2-UO_2 were 400 to 800 A in diameter whereas those in the ThO_2 were about 400 A. The final product was a solid solution of $Th_{0.78}U_{0.22}O_2$.

Trying to prepare porous UO_2 without excessive air oxidation of the UO_2, we tested two methods for removing carbon from the prefired UO_2-C,

---

[13] R. L. Beatty, J. M. Leitnaker, and K. J. Notz, Method for Preparation of Carbonitride Nuclear Fuel Materials, patent applied for.

[14] Chem. Technol. Div. Ann. Progr. Rept. May 31, 1967, ORNL-4145, pp. 159–162.

[15] Chem. Technol. Div. Ann. Progr. Rept. May 31, 1966, ORNL-3945, pp. 157–160.

[16] J. P. McBride (Compiler), Laboratory Studies of Sol-Gel Processes at Oak Ridge National Laboratory, ORNL-TM-1980 (September 1967); paper presented at the symposium on Sol-Gel Processes for the Production of Ceramic Nuclear Fuels, Turin, Italy, Oct. 2–3, 1967.

[17] K. J. Notz, Preparation of Porous Thoria by Incorporation of Carbon in Sols, ORNL-TM-1780 (December 1968).

the water-gas reaction ($H_2O + C \rightleftharpoons CO + H_2$) and the reaction $CO_2 + C \rightleftharpoons 2\ CO$. Both require a temperature of about 1000°C to remove the carbon at a practical rate. We demonstrated the technical feasibility of preparing porous UO_2 by this approach by removing carbon from a sample of gel shards containing 6 moles of carbon per mole of urania. Heating in CO_2 for 2 hr at 900°C and then 2 hr at 1000°C removed 95% of the original carbon. The final porosity of 48% was about 25% less than obtained with ThO_2 at the same carbon content.

Kinetics of the Graphite-UO_2 Reaction[18]

T. B. Lindemer M. D. Allen J. M. Leitnaker

The reaction of microspheres of UO_2 with graphite was studied from 1400 to 1756°C. When a spherically symmetrical layer of carbide was produced around the UO_2 core, only UC_2 was formed and the diffusion of oxygen through this layer was rate-controlling. The Arrhenius relation for this system is

$$k_D = 21.0 \exp(-90{,}000/RT)\ cm^2/sec\ .$$

The reaction of a geometrically nonsymmetrical configuration of UO_2 and UC_2 was also studied. The kinetic behavior was quite different in the symmetrical and nonsymmetrical systems and the conversion in the nonsymmetrical system was 2 to 5 times faster. The importance of these observations to kinetic results reported in the literature for analogous systems is discussed.

Drying and Sintering Studies on Urania Gel Microspheres

W. D. Bond

We are continuing studies of the optimum firing conditions for producing UO_2 microspheres of low carbon content (< 50 ppm) and high density

[18]Summarized from paper accepted for publication in the Journal of the American Ceramic Society.

(> 95% of theoretical). To obtain the desired product properties, the sorbed organic compounds must be removed before sintering and densification of the gel.[16,19] The sorbed organic compounds come from the drying solvent that is used in the sphere forming process. Products having the desired properties can be obtained by firing the gels to 1000°C in steam and reducing the UO_{2+x} in Ar–4% H_2. A small volume of argon or Ar–4% H_2 is used with the steam to prevent back diffusion of oxygen when the steam flow is stopped.

Sorbed organics are more difficult to remove from UO_2 microspheres before densification than from other types of sol-gel spheres, such as ThO_2, PuO_2, PuO_2-UO_2, and UO_2-ThO_2. This is because pure UO_2 begins to sinter fairly rapidly at only 400 to 500°C and the removal of the sorbed organics is slow at such low temperatures.

In our previous studies,[16,19] firing in other atmospheres – such as CO_2, air and argon, and Ar–3% H_2O – did not reproducibly yield UO_2 products with the desired properties. Also, adjustment of the oxidizing potential of CO_2 by the introduction of controlled amounts of CO did not produce reproducible results. Firing in air to 200°C to remove the sorbed organics was very effective for removing carbon; however, it was difficult to prevent overoxidation of the UO_2. Because the reaction of the sorbed organics with air was very rapid and produced excessive temperature rises, the temperature of oxidation could not be controlled. A mixture of 3% H_2O in argon was not sufficient to remove the organics before the start of sintering.

The removal of sorbed organics with steam before sintering is slow, and moderately long heating cycles are required to effectively carry out the firings. Different rates of removal are observed for the different gel preparations. This may be due to small differences in the crystallite

---

[19]W. D. Bond, Status and Progress Report for Thorium Fuel Cycle Development Dec. 31, 1966, ORNL-4275, pp. 157–177.

size, nitric acid content, viscosity, and oxygen-to-uranium atom ratio of the sol or to differences in the sphere forming process. We find that an in-line hydrocarbon analyzer (for carbon-hydrogen bonds) for the effluent gas is helpful in conducting the firings so that desired product properties are achieved. A typical curve of hydrocarbon removal as a function of time and temperature is shown in Fig. 9.2. Rise rates and soaking times in the steam atmosphere were selected so that the hydrocarbons are removed at a temperature as low as practical. The peaks of maximum evolution of hydrocarbons correspond to those previously observed for maximum weight loss in thermogravimetric studies.[16] On heating the gel in argon, the sorbed 2EH was evolved; the evolution increased with increasing temperature (Fig. 9.2). When steam was introduced, the rate of removal increased dramatically and reached a maximum during the 175°C hold period. The evolution continued in steadily decreasing amounts to about 350°C and then began to increase. Another maximum was reached at about 400°C. Two smaller gas evolution peaks occurred between 450 and 500°C. The evolution then steadily decreased from 500 to about 600°C; at 600°C, it was complete. The largest peak occurred at 150 to 200°C, as expected since the boiling point of 2EH is 183 to 185°C. However, significant amounts of alcohol remained after steam treatment to 200°C, indicating that the alcohol is strongly sorbed. Heating the gel too rapidly to permit removal of the sorbed alcohol (Fig. 9.3) (temperature rise rates of 300°C/hr) resulted in hydrocarbon evolution up to 950°C and also during cooldown of the sample in argon.

Firing in steam to 1000°C consistently produced good results when organic materials were removed before sintering (Table 9.3). Products had a uniform black color, a density that was 95 to 99% of theoretical, a carbon content less than 50 ppm, and an oxygen-to-uranium atom ratio less than 2.005. X-ray diffraction measurements showed that crystallite sizes were 500 to 800 A; 400-μ-diam spheres resisted crushing loads of 1500 to 2000 g.

The soaking conditions used for most of the firings are given in Fig. 9.4. The flow rates used were: steam, 5 to 10 scfh; Ar–4% H_2 or argon, 0.5 scfh. The hydrocarbon analyzer monitored most of the firings.

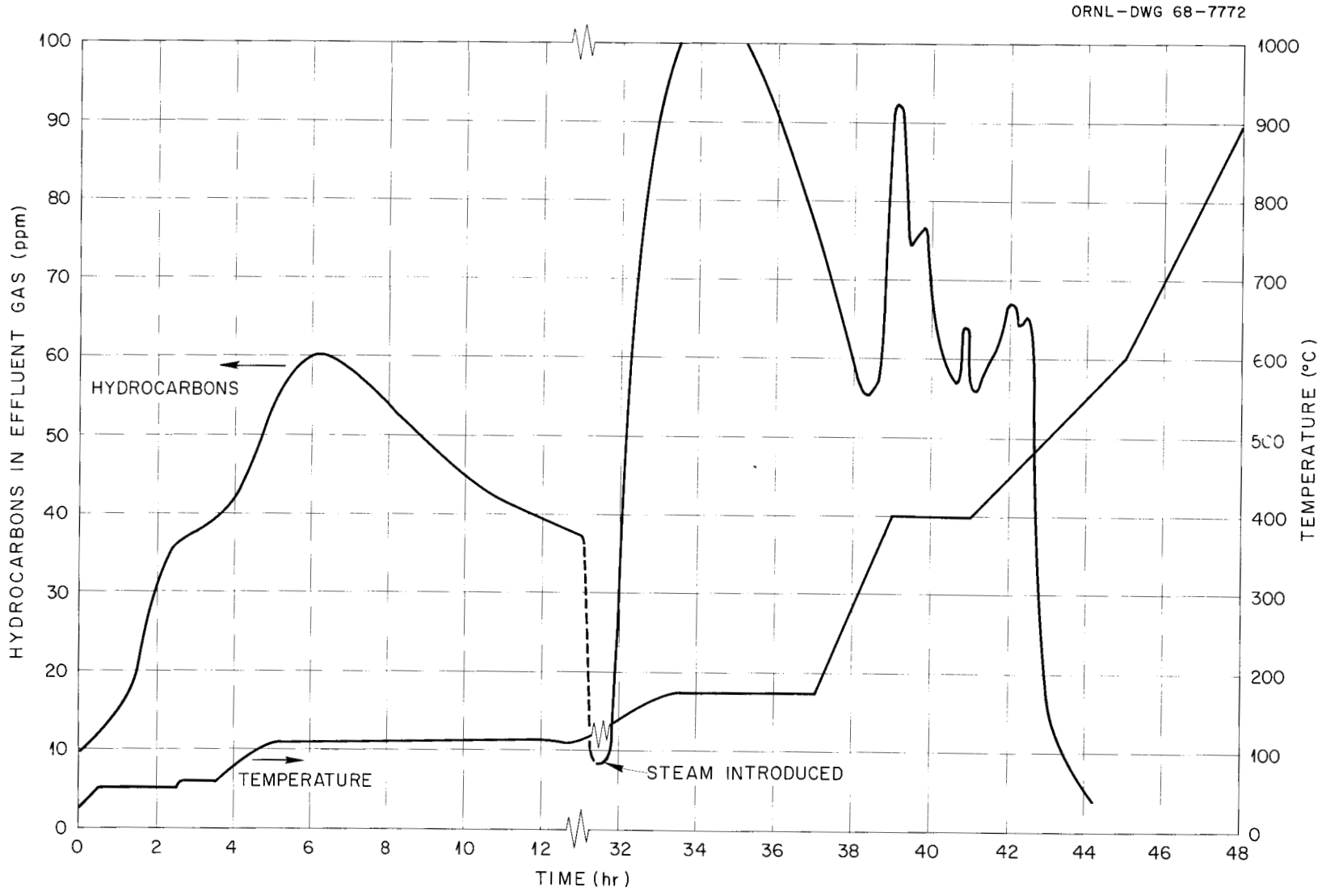

Fig. 9.2. Hydrocarbon Content in Off-Gas from UO_2 Gel Microspheres as a Function of Firing Time and Temperature During Firing. Slow schedule. Conditions: 30 g of UO_2; 1 scfh Ar to 110°C and hold overnight; 5 scfh steam and 0.5 scfh Ar to 900°C.

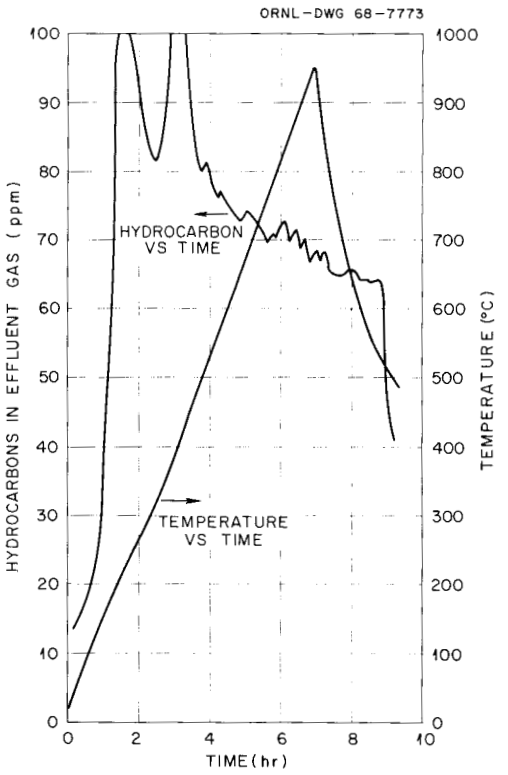

Fig. 9.3. Hydrocarbon Content in Off-Gas from UO_2 Gel Microspheres as a Function of Firing Time and Temperature. Fast schedule. Conditions: 10 g UO_2 microspheres; 1 scfh Ar to 110°C; 5 scfh steam and 0.5 scfh Ar to 950°C; cool in argon.

Table 9.3. Properties of UO_2 Gel Microspheres Fired in a Steam Atmosphere at 1000°C

Sol Preparation Method	Gel Preparation	Amount Fired (g)	Density by Mercury Intrusion at 210 psi (% theoretical)[a]	Carbon (ppm)
Precipitation	P-11-2-1504	130	97.5	< 20
	P-6-16-1545	65	96.7	10
	P-9-11-1545	82	97.2	< 20
Amine Extraction	P-7-27-1408	40	99.3	30
	P-9-8-1049	55	97.3	< 20
	P-7-31-1040	65	100.1	30
	P-219-1310	30	97.7	20
	P-2-20-1107	15	95.6	30
	P-2-12-1248	45	97.9	< 20

[a]Calculated by using 10.97 g/cm^3 as the density of UO_2.

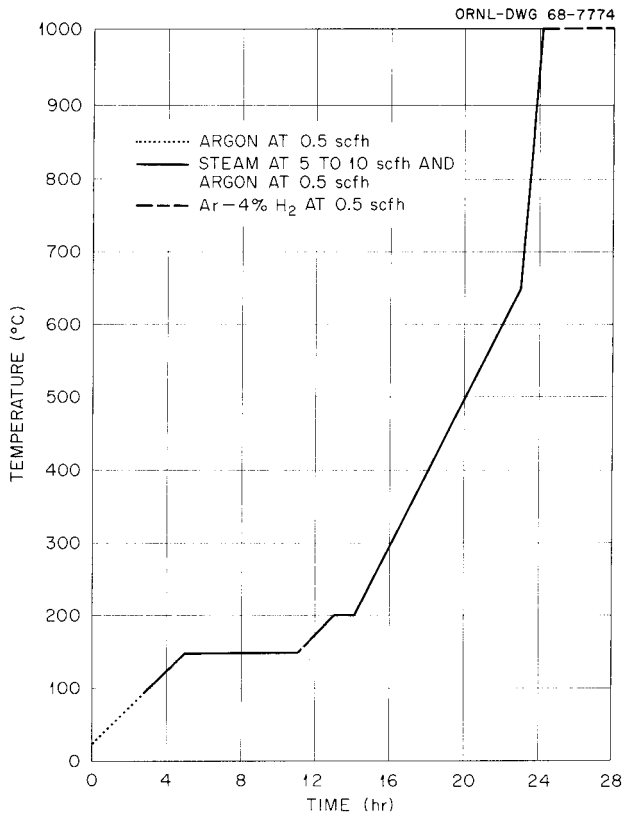

Fig. 9.4. Soaking Conditions for the Firing of UO_2 Gel Microspheres.

Shorter soaking times could be used with some but not all of the preparations shown in Table 9.3. A few of the preparations were heated to 1000°C at the rate of 300°C/hr after the usual soaking to 200°C. The desired product properties were obtained; however, the faster rise generally resulted in a low-density product. A few of the gel preparations could be fired to high density at 850°C, but most required firing at 1000°C.

Except for cracking of the spheres, no apparent differences were observed in the firing characteristics of UO_2 gel spheres that were formed from sol prepared by amine extraction and those formed from sol prepared by precipitation. A few of the products from sols that had been prepared by amine extraction cracked badly when fired at temperature rise rates as low as 25°C/hr; however, most of these gel products could be dried and fired without cracking. We believe that the cracking was the result of insufficient crystallite growth in the sol preparations.

ORNL-4429
UC-25 — Metals, Ceramics, and Materials

INTERNAL DISTRIBUTION

1-3. Central Research Library
4-5. ORNL — Y-12 Technical Library
Document Reference Section
6-50. Laboratory Records Department
51. Laboratory Records, ORNL R.C.
52. ORNL Patent Office
53. MIT Practice School
54. R. E. Adams
55. G. M. Adamson
56. L. G. Alexander
57. M. D. Allen
58. J. W. Anderson
59. S. E. Beall
60. R. E. Blanco
61. J. O. Blomeke
62. S. E. Bolt
63. E. S. Bomar
64. W. D. Bond
65. R. A. Bowman
66. G. E. Boyd
67. R. A. Bradley
68. R. E. Brooksbank
69. K. B. Brown
70. F. R. Bruce
71. W. L. Carter
72. J. M. Chandler
73. S. D. Clinton
74. C. F. Coleman
75. J. H. Coobs
76. L. T. Corbin
77. C. M. Cox
78. D. J. Crouse
79. F. L. Culler
80. J. E. Cunningham
81. F. L. Daley
82. D. E. Ferguson
83. L. M. Ferris
84. B. C. Finney
85. R. B. Fitts
86. J. H Frye, Jr.
87. F. J. Furman
88. H. E. Goeller
89. J. H. Goode
90. A. T. Gresky
91. W. R. Grimes
92. P. A. Haas
93. R. G. Haire
94. L. C. Hall
95. J. P. Hammond
96. R. L. Hamner
97. W. O. Harms
98. F. E. Harrington
99. C. C. Haws, Jr.
100-102. M. R. Hill
103. A. R. Irvine
104. J. P. Jarvis
105. P. R. Kasten
106. F. J. Kitts
107. N. A. Krohn
108. J. A. Lane
109. C. E. Larson
110. J. M. Leitnaker
111. T. B. Lindemer
112. C. S. Lisser
113. R. E. Leuze
114. M. H. Lloyd
115. J. T. Long
116-125. A. L. Lotts
126. R. S. Lowrie
127. H. G. MacPherson
128. S. Mann
129. J. P. McBride
130. R. W. McClung
131. K. H. McCorkle
132. W. T. McDuffee
133. D. L. McElroy
134. J. T. Meador
135. A. B. Meservey
136. J. G. Moore
137. J. P. Moore
138. W. L. Moore
139. C. S. Morgan
140. L. E. Morse
141. J. P. Nichols
142. R. G. Nicol
143. E. L. Nicholson
144. K. J. Notz
145. A. R. Olsen
146. J. R. Parrott
147. W. A. Pate
148. P. Patriarca
149. W. L. Pattison
150. W. H. Pechin
151. S. Peterson

152. J. W. Prados
153. R. B. Pratt
154. J M Robbins
155. J. T. Roberts
156. A. D. Ryon
157. C. F. Sanders
158. J. L. Scott
159. J. D. Sease
160. R. J. Shannon
161. W. A. Shannon
162. D. M. Shepherd
163. J. W. Snider
164. P. H. Spindler
165. D. A. Sundberg
166. O. K. Tallent
167. E. H. Taylor
168. R. E. Thoma
169-217. D. B. Trauger
218. W. E. Unger
219. J. E. Van Cleve
220. V. C. A. Vaughen
221. T. N. Washburn
222. C. D. Watson
223. G. M. Watson
224. A. M. Weinberg
225. J. R. Weir
226. M. E. Whatley
227-236. R. G. Wymer
237. C. M. Adams, Jr. (consultant)
238. L. Brewer (consultant)
239. L. S. Darken (consultant)
240. J. A. Krumhansl (consultant)
241. P. H. Emmett (consultant)
242. J. J. Katz (consultant)
243. J. L. Margraves (consultant)
244. E. A. Mason (consultant)
245. R. B. Richards (consultant)

EXTERNAL DISTRIBUTION

246. A. Amorosi, Argonne National Laboratory, LMFBR Program Office
247. R. H. Ball, RDT-OSR, P.O. Box 2325, San Diego, California
248. J. E. Ayer, Argonne National Laboratory
249. E. E. Bain, Nuclear Fuel Service, Erwin, Tennessee
250. J. A. Buckham, Manager, Chemical Technology Branch, Idaho Nuclear Corporation, P.O. Box 1845, Idaho Falls, Idaho
251. J. Crawford, AEC, Washington, D.C.
252. P. Clark, AEC, Washington, D.C.
253. D. F. Cope, RDT Site Office, ORNL
254. G. W. Cunningham, AEC, Washington, D.C.
255. C. B. Deering, RDT Site Office, ORNL
256. Donald de Halas, Pacific-Northwest Laboratory
257. W. Devine, Jr., Production Reactor Division, P.O. Box 550, Richland, Washington
258. E. W. Dewell, Babcock and Wilcox Co., Lynchburg, Virginia
259-268. T. D. Edwards, Gulf General Atomic, San Diego, California
269. R. Fryar, Kerr-McGee Corp., Oklahoma City, Oklahoma
270. J. Giambusso, AEC, Washington, D.C.
271-272. R. H. Graham, Gulf General Atomic, San Diego, California
273. J. S. Griffo, AEC, Washington, D.C.
274. N. Haberman, RDT, AEC, Washington
275. C. J. Hardy, AERE, Harwell, England
276. P. G. Holstead, RDT, OSR, P.O. Box 550, Richland, Washington
277-278. S. Jaye, Gulf General Atomic, San Diego, California
279. Donald Keller, Battelle Memorial Institute, Columbus, Ohio
280. W. J. Larkin, AEC, ORO
281. K. Laughan, RDT Site Office, AEC, ORO
282. S. Marshall, National Lead Company of Ohio
283. C. L. Matthews, RDT, OSR, AEC, ORO
284. G. L. Mercer, Division of International Affairs, AEC, Washington, D.C.

285. E. R. Merz, Director, Institute of Chemical Technology, KFA, Julich, West Germany
286. T. McIntosh, AEC, Washington, D.C.
287. W. H. McVey, AEC, Washington, D.C.
288. E. C. Moncrief, Babcock and Wilcox Co., Lynchburg, Virginia
289. R. L. Morgan, AEC, Savannah River Operations Office, Aiken, S.C.
290. Peter Murray, Westinghouse Atomic Power Division, P.O. Box 355, Pittsburgh, Pennsylvania
291. M. V. Nevitt, Argonne National Laboratory, Argonne, Illinois
292. R. I. Newman, Nuclear Fuels Department, Allied Chemical Co., P.O. Box 70, Morristown, New Jersey
293. R. E. Norman, Gulf General Atomic, San Diego, California
294. R. E. Pahler, AEC, Washington, D.C.
295. R. L. Philippone, RDT, OSR, AEC, ORO
296. R. A. Proebstle, General Electric Co., KAPL, Schenectady, N.Y.
297. C. W. Richards, AEC, Canoga Park, California
298. J. A. Rode, United Nuclear Corp., Hematite, Missouri
299. H. Schneider, AEC, Washington, D.C.
300. Hugo Schumacher, EIR, Ch-5303, Wurenlingen, Switzerland
301. M. Shaw, AEC, Washington, D.C.
302. L. R. Shepherd, Chief Executive, Dragon Project, AEE Winfrith, Dorchester, Dorset, England
303. J. M. Simmons, Division of Reactor Development and Technology, AEC, Washington, D.C.
304. E. E. Sinclair, AEC, Washington, D.C.
305. E. E. Stansbury, University of Tennessee, Knoxville, Tennessee
306. D. K. Stevens, AEC, Washington, D.C.
307. K. G. Steyer, Gulf General Atomic, San Diego, California
308. C. L. Storrs, HPO-A1/CE
309. A. A. Strasser, United Nuclear Corporation, 5 New Street, White Plains, N.Y.
310. J. A. Swartout, Union Carbide Corporation, New York, N.Y.
311. C. A. Trilling, Atomics International
312. Guenther Wirths, NUKEM, Hanau, West Germany
313. R. P. Varnes, Combustion Engineering, Windsor, Connecticut
314. W. R. Voigt, AEC, Washington, D.C.
315. B. L. Vondra, NUMEC, Apollo, Pennsylvania
316. M. J. Whitman, AEC, Washington, D.C.
317. E. L. Zebroski, General Electric Co., 310 DeGuigne Drive, Sunnyvale, California
318. M. Zifferero, CNEN, Instituto di Chemica Farmacentica e Tossicologica dell 'Universita, Piazzale delle Scienze, 5, Rome, Italy
319. M. A. Khan, Division of Nuclear Power and Reactors, International Atomic Energy, Karntner Ring 11, 1010 Vienna, Austria
320. M. E. A. Hermans, KEMA, The Netherlands
321. L. V. Trigianni, W. R. Grace and Company, Washington Research Center, Clarksville, Maryland
322. Laboratory and University Division, AEC, ORO

323-539. Given distribution as shown in TID-4500 under Metals, Ceramics, and Materials category (25 copies — CFSTI)